ABSTRACT

Title of Thesis: NUMERICAL SIMULATION STUDY AND RESILIENCE ASSESSMENT OF STEEL ECCENTRICALLY BRACED FRAMES WITH REPLACEABLE LINKS

Abhilekh Prasai
**Master of Science, 2021**

Thesis directed by: Yunfeng Zhang, Professor
Department of Civil and Environmental Engineering

Earthquake demand parameters, EDP, such as displacement, velocity and acceleration are meaningful to engineers. In general, most decision-makers are non-engineers and do not understand these parameters. This study uses a procedure stipulated in FEMA P-58 to convert the earthquake demand parameters derived from nonlinear time history analysis into performance measures that are more meaningful to the decision-makers. This conversion of EDPs is better known as the performance-based design. In compliance with FEMA P-58, this study performed structural design and nonlinear time history analysis, and then assessed the seismic performance of ten different prototype buildings with K-type steel Eccentrically Braced Frames (EBFs) as primary seismic force resisting system. Among the ten EBFs, nine EBFs are new designs, and one existing 23-story EBF building that underwent a $M_w$6.3 earthquake in Christchurch, New Zealand. Next, an intensity-based assessment using nonlinear response history analysis is carried out in an open-source finite element analysis software - OpenSees. The assessment results help evaluate the building's seismic resilience performance using a FEMA companion tool known as PACT. Ultimately, PACT converts the EDP into performance measures such as repair cost, repair time,

unsafe placarding, and environmental impacts. This study uses the existing EBF building performance assessment to validate the performance assessment of this study. Overall, PACT results predict a 75% probability that both the repair cost and the repair time on average will be less than or equal to 8.0% of the total repair cost and the total repair time, respectively, for the nine EBF design with replaceable link beams. Hence, these results suggest the EBFs design adhering to the current seismic code specifications are resilient if replaceable link beams are used.

# NUMERICAL SIMULATION STUDY OF TEN STEEL ECCENTRICALLY BRACED FRAMES AND EVALUATING ITS RESILIENCE USING FEMA P-58 PROCEDURE

by

Abhilekh Prasai

Thesis submitted to the Faculty of the Graduate School of the
University of Maryland, College Park, in partial fulfillment
of the requirements for the degree of
Master of Science
2021

Advisory Committee:
Professor Yunfeng Zhang, Chair
Professor Amde M. Amde
Professor Michelle Bensi

# Acknowledgements

First and foremost, I am extremely grateful to my supervisor, Prof. Zhang, for his invaluable advice, continuous support, and patience during my thesis. His immense knowledge and ample experience have encouraged me in my academic research. I would also like to thank Prof. Amde and Prof. Bensi for being part of my thesis committee. Last but not the least, I would like to express my gratitude to my parents. Without their tremendous understanding, encouragement, and support throughout my life, it would be impossible for me to complete my study.

# Table of Contents

# List of Tables

# List of Figures

# Chapter 1: Introduction

## *1.1 Background*

At present, earthquakes and possibly a tsunami caused by them are responsible for most fatalities caused by natural hazards. This is likely due to the unpredictability of earthquakes. As earthquakes are spontaneous, people cannot anticipate them. As a result, more deaths are likely to occur during an earthquake. The data for deaths due to natural hazards in the last two decade supports this claim. The data shows that the annual death toll due to natural hazards had crossed 100s of thousands during 2004 and 2010 [1]. Further data reveals that earthquakes were responsible for 93 per cent and 69 per cent of the total annual death toll during 2004 and 2010, respectively. These peaks are attributed to the two deadliest earthquakes of the century, the Sumatra earthquake and tsunami of 2004, and the Port-au-Prince earthquake in 2010 [2]. Further, property damage due to an earthquake is equally devastating. Earthquakes directly or indirectly affect both structural and nonstructural components. Post-earthquakes, either these components need repair or replacement or remain undamaged. The cost of this repair or replacement comprises the property damage associated with earthquakes. For the US, the Northridge quake (1994) was the costliest earthquake, causing $15.3 billion in insured damages equivalent to $26.9 billion in 2019 dollars [1]. Additionally, Table 1.1 displays the top 10 most expensive US Earthquakes by inflation-adjusted insured losses. In summary, earthquakes are responsible for significant property and life losses. Due to the devastating effects of earthquakes on life and property, researchers are focused on improving the performance of structures in seismic regions. These researchers' primary intent is to balance strength, stiffness, and energy dissipation to

enhance structural performance. In general, to prevent significant life and property loss in these regions, different seismic resisting systems have been developed with extensive research. An ideal seismic resisting system should satisfy two criteria:

1. The structure should have adequate stiffness to limit nonstructural damages during a minor earthquake.
2. The structure should possess sufficient ductility to prevent collapse during a major earthquake.

Over the years, Moment Resisting Frames MRFs and Concentrically Braced Frames CBFs have been the most dominant structural systems among the various seismic resisting system. But, neither MRFs nor CBFs satisfies both of these requirements completely. Although MRFs have sufficient energy dissipation capacity to provide the required ductility, they require large member sizes and costly panel zone doubler plates to satisfy the drift requirement. In contrast, CBFs meet the deflection criteria easily attributed to the braces' truss action but fail to accommodate a stable energy dissipation mechanism compared to MRFs. Hence, both these frames have an advantage and a disadvantage over each other. Researchers combined the benefits of both MRFs and CBFs while reducing their weaknesses, resulting in the development of a new lateral resisting frame known as Eccentric Braced Frames EBFs.

In general, EBFs employs eccentricities between the brace connections and beam-column joints, which are chosen to ensure that the beam yields in shear. It is believed that this is the first application of cyclic shear yielding as the primary energy dissipation mechanism of a structure [3]. In 1977, a one third scale model EBF was subjected to severe earthquake loading at the University of California. This study demonstrated the

excellent seismic performance of EBFs [3]. As a result, several EBFs buildings were constructed in 1981, such as the 19-storied Bank of America Building in San Diego [4] and the 47-storied Embarcadero Building in San Francisco [5]. Also, various arrangements of EBFs exist in practice today. The figure below illustrates the different EBFs bracing configurations in practice.

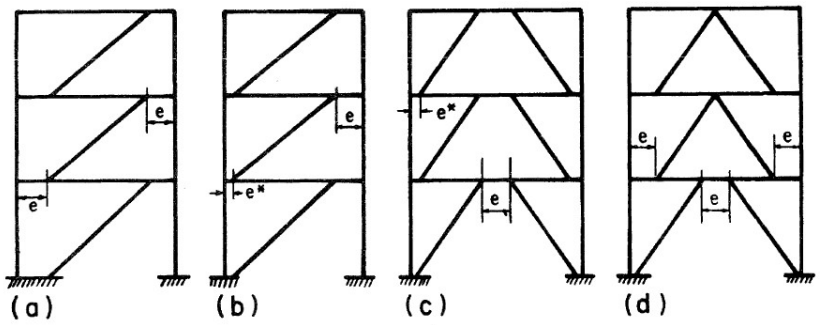


*Figure 1. 1 Some Alternative Bracing Arrangements for EBF's [6]*

This system's inherent feature is that the axial forces induced in the braces are transmitted either to a column or another brace primarily through shear and bending in a segment of a floor beam called the link beam. Hence, the braces must not buckle under extreme loading conditions; otherwise, the loads are not transmitted. It is essential to determine the ultimate capacity of the link beams to avoid the buckling of braces. Researchers have developed an accurate estimation of the maximum capacity of the links. This maximum capacity of the links is used to determine the axial force in the braces. Finally, the brace is sized such that the axial force back calculated using the maximum link capacity is lower than its buckling capacity. Hence, the braces will not buckle until the link beam reaches its total capacity. An EBF is so proportioned that significant inelastic activity occurs in the link under severe loadings. In this manner,

links provide the fuses necessary to prevent buckling of the braces [7]. This process is the essence of the capacity design principle. Here, Links are the deformation-controlled members, whereas all the other elements are force-controlled members. In simpler words, inelastic deformation is limited to the links, whereas the system's remaining elements should remain elastic during a severe earthquake.

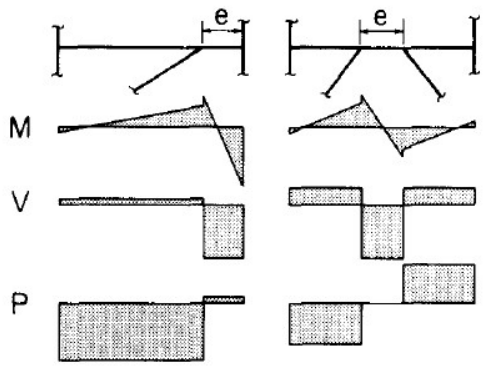


*Figure 1. 2 Typical force distributions in beams and links of EBFs under lateral load [8]*

Next, it is essential to understand the distribution of the internal forces in EBFs. Figure 1.3 illustrates the internal forces, Bending moment M, Shear V and axial force P, in the beams and links of two common EBFs arrangements under lateral load. The figure shows that the link beam is subjected to high shear force along its entire length and high bending moments at its ends. Also, the length of the link beam affects its behavior significantly. If the links are short, the links will likely yield in shear (forming plastic shear hinges) with relatively little moment yielding at its ends. Conversely, if the links are too long, the links will form conventional plastic moment hinges at the ends, with little or no shear yielding. Generally, short links are called shear links as they form shear hinges, and long links are called moment links due to the formation of moment hinges. Additionally, an intermediate link length is also possible where both shear and

moment yielding co-occurs. The energy dissipation and ultimate failure mechanisms for these three classes of links differ substantially.

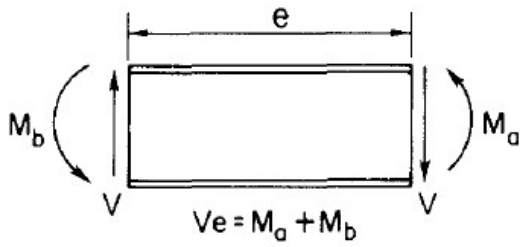


*Figure 1. 3 Static Equilibrium of Link [8]*

The relationship between the link beam's length and energy dissipation is best explained using the link beam's static equilibrium state. Figure 1.4 shows the static equilibrium of the Link element. From Figure, it is simple to derive $e = 2M_p/V_p$ using simple statics. In this equation, $Mp= ZF_y$ is the fully plastic moment of the W section and $V_p = 0.55*F_y*dt_w$ is the fully plastic shear capacity of the section where $F_y$ is the yield strength of the steel, Z is the plastic modulus, d is beam depth, and $t_w$ is the web thickness. This equation is the theoretical dividing line between a link with dominating shear yielding and one with dominating moment yielding. Thus, based on simple plastic theory, if $e < 2M_p/V_p$, the link shear will reach $V_p$ before the end moments reach $M_p$, and the link will yield in shear. In contrast, if the $e>2M_p/V_p$, the link end moments will yield before the link shear yields. This theoretical equation is based on two assumptions, i.e., there is no M-V interaction, and the material is perfectly plastic (no strain hardening). Although experimental results from [9]& [10] show that the first assumption is quite reasonable, the results show that the second assumption is not reasonable. These experiments clearly show that the effect of strain hardening in links is essential and cannot be neglected. Additionally, these experiments studied both

stiffened and unstiffened links and their behavior. In the first series of tests [9], 15 full-sized links were subjected to quasi statically applied cycles of increasing relative end displacement. Figure 1.5 presents the link behavior of both stiffened and unstiffened W18*40 specimens, 28 inches in length (e=1.11 $M_p/V_p$) of A36 steel, in form of the hysteresis loop. As can be seen from the figure, the unstiffened specimen experienced severe web buckling right after shear yielding and lost its load-carrying capacity significantly, which is clear from the hysteresis loop. Additionally, the pinching effect in the hysteresis loop suggests poor energy dissipation and ductility. In contrast, the hysteresis loop for the stiffened link shows excellent energy dissipation and ductility. Hence, a stiffened link beam outperforms an unstiffened link beam. Also, the rotation capacity of the stiffened link from this experiment was 0.1 radian from the experiments. Further, the W18*40 specimens had an ultimate strength of 210 kips which is 1.875 times its nominal shear yield capacity $V_p$ (112 kips). Since the ultimate shear strength is higher, using the theoretical equation $e = 2M_p/V_p$ is no longer valid.

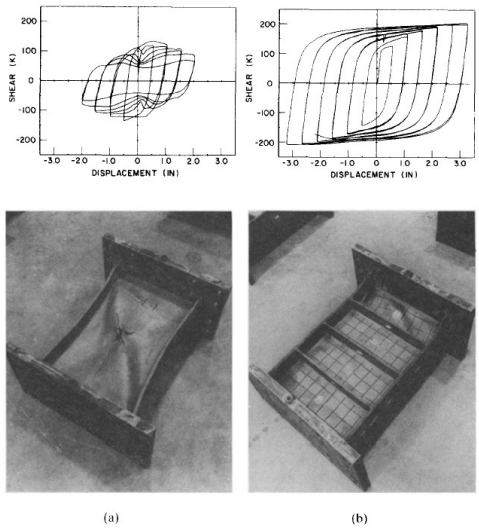


*Figure 1. 4 Hysteretic behavior of (a) unstiffened shear link; (b) stiffened shear link [9]*

Major critical observations from [9]& [10] series of tests are summarized below:

1. Shear links achieve large plastic rotations and energy dissipation than moment links.
2. Inelastic web buckling in shear links leads to a significant loss in load carrying capacity, plastic rotation capacity, and energy dissipation.
3. Adding stiffeners reinforces the link against web buckling. A well-stiffened shear link can achieve plastic rotations up to y = +0.10 radian under cyclic load or y=0.20 radian under monotonic load.
4. Shear links strain-harden, achieving ultimate shear strengths on the order of 40% to 50% or more of the initial shear yield capacity *Vp.*

These experiments conclude that due to significant strain hardening in links, V permitted is 1.4 to 1.5 times of Vp. Also, to prevent excessive flange strains, Kasai and Popov suggest limiting link end moments to 1.2 Mp. Thus, from the link statics of Fig. 4, if the end moments are limited to 1.2 Mp and the link shear is assumed to achieve 1.5 Vp, the limiting link length is e = 2(1.2 Mp)/1.5 Vp = 1.6 Mp/Vp. This equation for link length is more accurate than the theoretical one. Hence, in order to assure the more desirable behavior of links that yield in shear, it is recommended that the link length comply with the following equation:

$$e \leq 1.6\frac{Mp}{Vp} \qquad \text{Eq-1}$$

Next, it is vital to understand the energy dissipation mechanism or collapse mechanism to predict the plastic rotation demands. The members are assumed to exhibit rigid plastic behavior to develop the collapse mechanism. For instance, Figure 1.6 shows collapse mechanisms for an MRF and two types of EBFs. For the MRF in Figure 6, θ

represents both overall frame drift and rotation demand at the beam's plastic hinges. However, for EBFs, the rotation demands on the links are much more significant than θ. From the geometric mechanism, the link rotation is determined as follows:

$$\gamma = \frac{L}{e}\theta \qquad \text{Eq-2}$$

In fact, Link rotation is denoted by $\gamma$ which is hinting to shear yielding. Also, the links are cross hatched in Figure 1.6 to indicate that they have yielded in shear and formed a shear hinge. Additionally, the Link rotation equation changes with the type of EBF arrangements.

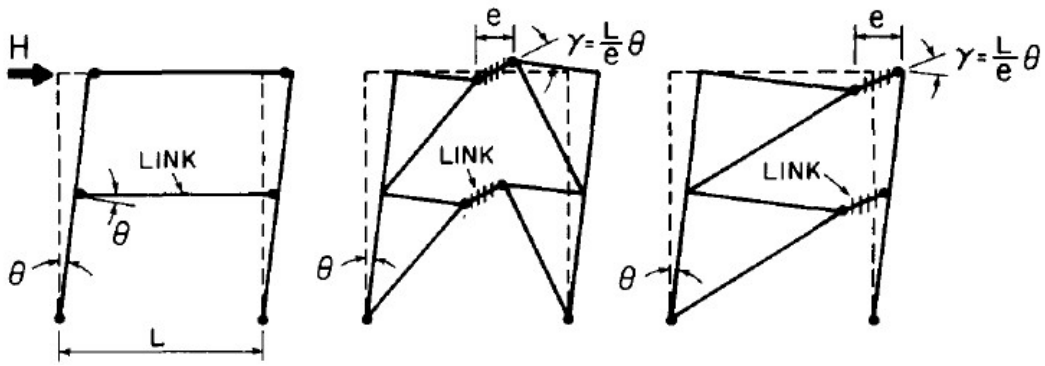


*Figure 1. 5 Energy dissipation mechanisms MRF and EBF [8]*

Overall, now we have some understanding of EBFs behavior when subjected to lateral loads. The structure's response to the earthquake will generate different Earthquake demand parameters EDP such as displacement, floor acceleration, and floor velocity. Generally, most decision-makers are not engineers, hence do not understand these terms. Therefore, the need to convert these parameters into quantities more easily understood by the decision-makers was felt. This need gave birth to the concept of Seismic resilience. The ASCE Committee on Critical Infrastructure [11]states that resilience refers to the capability to mitigate against significant all-hazards risks and

incidents, and to expeditiously recover and reconstitute critical services with minimum damage to public safety and health, the economy, and national security. Also, the resilience of a system is the persistence of its functions and performances under uncertainty in the face of disturbances [12]. From the year 2000, researchers affiliated with the Multidisciplinary Center for Earthquake Engineering Research (MCEER), sponsored by the National Science Foundation, and headquartered at the University at Buffalo, have collaborated on studies to conceptualize, and measure disaster resilience. MCEER researchers defined disaster resilience as the ability of social units (e.g., organizations, communities) to mitigate hazards, contain the effects of disasters when they occur, and carry out recovery activities in ways that minimize social disruption and mitigate the effects of future disasters. In general, resilient systems reduce failure probabilities; failure consequences- such as deaths and injuries, physical damage, and negative economic and social effects; and recovery time. Overall, Resilience of a system can be measured by the residual functionality post disaster and the recovery time to achieve pre-disaster level performance.

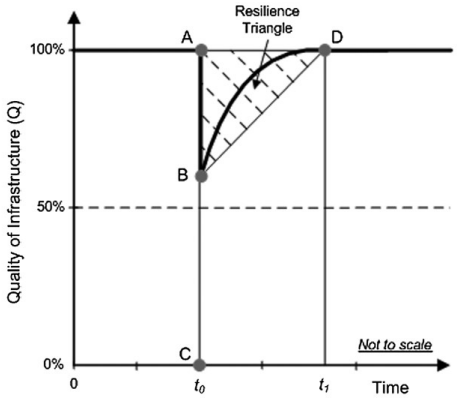


*Figure 1. 6 Resilience properties and triangle [13]*

Generally, resilience is quantified using a time dependent performance function. Attoh-Okine et al [13] developed several possible paths of performance during regular

operation and during cases of unexpected events, for instance, a path demonstrating sudden failure as shown in Figure 1.7, as well as a path demonstrating a decrease in service life, and a path for the regular operation of the system. They used the concept of resilience, as illustrated in Figure 1.7 to define a resilience index as follows:

$$Resilience = \frac{\int_{t_0}^{t_1} Q(t)dt}{100(t_0 - t_1)} \quad \text{Eq 3}$$

where Q = infrastructure quality, or the performance of a system; $t_0$ = time of incident or disturbance occurrence; and $t_1$ = time to full recovery. Additionally, to evaluate the attributes and determinants of resilience, MCEER investigators developed the R4 framework of resilience:

1. Robustness— the residual performance post-disaster or the system's ability to withstand disaster forces without significant loss of performance.
2. Redundancy— alternate paths to avoid any disruption or loss to the system's functionality.
3. Resourcefulness—diagnosing and prioritizing problems and initiating solutions by identifying and mobilizing materials.
4. Rapidity— the speed capacity to restore functionality quickly, minimizing losses and avoiding disruptions.

However, four interrelated dimensions: technical, organizational, social, and economic can also help conceptualize resilience [13]. The technical dimension refers to the physical systems' ability to perform to desired levels when subjected to earthquake forces. The organization dimension relates to capacity of organizations that manage critical facilities and have the responsibility for carrying out essential disaster-related functions to make decisions and take actions that contribute to achieving greater

robustness, redundancy, resourcefulness, and rapidity. The social dimension consists of measures specifically designed to reduce the extent to which earthquake-stricken communities and governmental jurisdictions suffer due to the loss of critical services during an earthquake. Similarly, the economic dimension refers to the capacity to reduce both direct and indirect economic losses resulting from earthquakes.

## *1.2 Scope and Objectives*

This study focuses on EBFs primarily on K-type (b in Figure 1.1). Further, all the links in this study are short/shear links, i.e., shear yielding is the primary energy dissipation mechanism. Short links were selected because of their high link rotation capacity compared to both long and moderate links. Sufficient support against lateral torsional buckling and local web buckling is assumed. Without stiffeners, link beams lose significant load-carrying capacity. A uniform building plan was selected without any torsional, geometric, mass or stiffness irregularity. Therefore, a 2D model of the seismic resisting frame was sufficient for structural analysis. Accidental eccentricity was neglected in this study. A total of 10 buildings were considered in this study, seven new designs using the location for Apple headquarters, California; two new designs using the location for Space Needle, Seattle; and one existing building located in Christchurch, New Zealand. All new designs were designed to satisfy AISC 360 [14] specification. Site specific design response spectrum was developed using ASCE 7-10 [15]. Due to Incremental Dynamic Analysis IDA's complexity, a simpler method was adopted from FEMA P-58 [16]. Since this method does not use a full backbone curve for the materials, the structure's collapse was assumed to occur either when the roof displacement exceeded 4% of the total building's height or when numerical instability

occurred. Hence, material non-linearity was limited to post-yield stiffness reduction and did not include the capping zone. Lean on columns were modelled to incorporate geometric non-linearity to the model. Only far-field ground motions from FEMA P695 [17] were used for time history analysis. Non-structural estimates based on the floor occupancy were generated using Normative Estimation Tool complimentary with FEMA P58 [16].

This research aims to quantify structural resilience for nine new design and one existing K-type EBFs using the procedure in FEMA P-58. The first objective for the new designs is to perform an elastic structural analysis using the site-specific design response spectrum. These buildings are designed using AISC 360 specifications [14]and the Seismic design Manual [18]. After the structural analysis, the members are proportioned such that they satisfy all these requirements. The second objective is to model these proportioned members to include material and geometric non-linearity. A set of 44 far-field ground motions were scaled to match the design response spectrum. After which non-linear time history analysis is performed using each of the 44 ground motions. Average of forces in links, beams, braces, and columns were calculated from this ana. All the elements were rechecked to resist these average forces. The ground motions were further scaled until half of the ground motions caused failure. This data was fed into a Collapse fragility tool complimentary with FEMA to estimate collapse fragility of the system. A site-specific hazard curve was derived using the USGS database. Pre-defined Non-structural fragility is readily available in PACT. PACT stands for Performance assessment calculation tool, which is complimentary with FEMA P-58. Finally, the non-linear time history results, component and system

fragility are fed to PACT for performance assessment. The engineering demand parameters are converted into terms such as repair cost and downtime by PACT. Further, an existing structure's performance is accessed to verify the PACT assessment.

# Chapter 2: Literature Review

Performance based seismic design concept only surfaced during the late 19$^{th}$ century. Ahmed Ghobarah explored the state of development for performance-based design in 2001 [19]. Ghobarah states that the current seismic code standards focus on controlling damage during minor and moderate quakes, and collapse during major ones. The author agrees these standards have helped decrease the number of fatalities but states that they have resulted in unexpectedly high economic losses. Hence, he concludes performance-based design is the future to limit these losses. Further, Ghobarah defines performance-based design as a method in which structural design criteria are expressed to achieve a set of performance objectives. The author claims performance-based design and displacement-based design are analogous because damages can be directly related to displacements. Also, the author accredits SEAOC VISION 2000 [20], ATC 40 [21], and FEMA 273 AND 274 [22] for laying the foundation for the performance-based design. Overall, the author concludes the absence of standard methodology, lack of data and simplification of the design process as the major challenges faced by performance-based design. Next, Priestly explains various force-based (with displacement limit) and displacement-based performance assessment methods [23]. The author acknowledges that seismic design approach is slowly changing its focus from strength to performance. The author claims the onset of performance-based design was marked by the development of the capacity design principle. Capacity design principle improves the structure's performance during an earthquake improves. Further, the author presents the four performance levels defined as per SEAOC VISION 2000 [20]

1. Fully Operational- Continued performance with negligible damage
2. Operational- minor damage and disruption to nonessential services
3. Life Safe- Damage is moderate to extensive but life safety is substantial
4. Near Collapse- life safety at risk, severe damage, collapse prevented.

The author emphasizes that drift capacity is more fundamental to seismic design than strength. Hence, the author strongly recommends the displacement-based approach for the future.

Hamburger discusses the challenges faced by structural engineers to implement the performance-based design in practice [24]. The author believes that most owners do not want to spend on design for earthquakes having higher return period than the intended use of the building. Besides, doing so does not increase the value of the property either. Hence, Hamburger claims that standard performance objectives are required as owners may select lower performance objectives than required. Hamburger states one approach to incorporate performance-based design in practice is to modify the building code requirements. For instance, increasing the Importance factor for buildings like a hospital. In contrast, Hamburger states the main problem with this approach of modifying codes is that the performance provided by the codes are unknown. Next, Hamburger discusses another approach for performance-based design, predicting the behavior by comparing the individual components inelastic response to available data. The author claims inaccurate analytical techniques to predict demands, lack of data to compare with, and design officials' unwillingness to accept design are the major drawbacks of this approach. Further, Hamburger emphasizes the need to change the structural engineers' role in the design process. In summary, both these

papers express a strong need for a standard performance base design process. Therefore, PEER researchers developed a framework for performance-based design. Moehle and Deierlein derived the framework methodology for performance-based design from various works of PEER researchers [25]. The authors attribute the need for performance-based design to convert the earthquake parameters into decision variables which the stakeholders can understand. Moehle and Deierlein suggest that a probabilistic approach by PEER researchers was developed to account for earthquakes' uncertainty. They claim the use of simplified elastic analysis methods to generate engineering demands, the unclear relationship between engineering demands and component performance, and the misrepresentation of system performance using component performance are the main shortcomings of the first-generation performance-based design.

Moehle and Deierlein state that to develop a robust method to performance-based design, PEER researchers broke down the design process into logical elements. These logical elements are Intensity measure (IM), Engineering demand parameter (EDP), Damage measure (DM) and Decision Variable (DV). IM involves a hazard analysis to determine a mean annual probability of exceedance of an intensity measure, such as peak ground acceleration, specific to the location of interest. In the next step EDP, the structure's response to ground motions is recorded. The authors mention Incremental Dynamic Analysis (IDA) as one of the acceptable approaches. Using IDA and IM, mean annual probability of exceeding the EDPs can be generated. DM step evaluates the relationship between the structural and non-structural elements with the EDP exceedance probability. The final step DV is to convert the EDP into decision variables,

such as downtime and casualties, meaningful to the stakeholders. Moehle and Deierlein conclude that there is a tremendous gap in knowledge to categorize DMs and EDP-DMs relation. This gap is due to insufficient attention to damage measures other than strength and ductility, reliance on computer simulation and lab testing data and lack of experimental data for non-structural component damage.

Next, Hamburger describes the development of next-generation performance-based seismic design guidelines developed by the ATC-58 project [26]. The author believes these guidelines will improve the reliability and effectiveness of current building codes. These guidelines are based on the framework developed by PEER researchers. The author illustrates the design process using figure below:

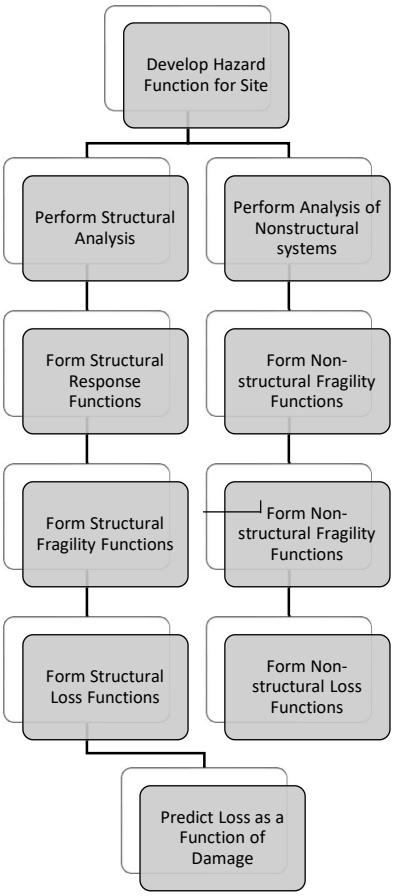


*Figure 2. 1 Performance assessment process adapted from [26]*

The author elaborates the performance assessment process of the ATC-58 project which expresses performance objectives as repair and replacement cost, earthquake casualties, and losing functionality while being repaired. The author concludes that component damage is related to EDPs using fragility functions. Further, Hamburger states that ATC-58 encouraged independent research to develop fragility for non-structural components due to the sheer number of components. Additionally, the author asserts that ATC-58 generated loss functions for repair cost by discussing the level of damage with contractors and estimators and the loss function for life losses based on previous earthquake data. The author believes ATC-58 will revolutionize the practice of performance-based design.

# Chapter 3: EBF Prototype Structure Design

## *3.1 General Features*

This study begins with the seismic design of nine K-type steel EBF buildings with different height. Among the nine EBFs, seven are designed using the location for the Apple headquarters, California, and the remaining two are designed using the location for Space Needle, Seattle. For the seven California location EBF buildings, the number of stories varies from 4 to 10 with a unit increment. Whereas for the two Seattle location buildings, the number of stories is 4 and 5. Additionally, all the EBFs in this study have a typical story height of 14 feet. Further, Soil classification is essential for earthquake design. ASCE 7-10 states that "when the soil properties are not known in sufficient detail to determine the site class, Site Class D can be used unless the authority having jurisdiction or geotechnical data determines Site Class E or F soils are present at the site" [15]. Due to insufficient soil data in this study, both the sites are classified as class D.

A uniform and rectangle building plan was selected for the EBFs design, shown in Figure 3.2. Overall, the building plan has six bays along the E-W and five along the N-S direction. Each bay is 25 feet wide; hence, the building's overall dimension is 150 feet by 125 feet. Since the building plan is rectangular, the total area is 150*125, 18750 sq feet. In general, seismic load resisting systems are required to resist the lateral loads generated by an earthquake. As can be seen in Figure 3.2, Eight peripheral bays have a thicker line weight. These thicker lines denote the EBF bays which comprise the lateral load resisting system in this study. Also, there are 4 EBF bays in each of the orthogonal direction, and all of them are K-type EBFs. Figure 3.1 shows the typical K-type EBFs

arrangement used in this study. In general, the combination of columns, beams and braces constitute this arrangement. Although these members can have different sectional shapes, this study uses HSS sections for braces and W sections for both columns and beams. Both W and HSS sections should comply with the ASTM Specifications. Table 2-4 in AISC Steel Construction Manual [27] lists the applicable ASTM specifications for various structural shapes. As per this table, the W sections preferred material is ASTMS A992 steel. Hence, W sections with A992 steel is selected. A992 steel has a nominal yield stress of 50 ksi and ultimate tensile stress of 65 ksi. Although A500 Grade C is the preferred material as per Table 2-4 AISC Steel construction manual for HSS sections, Grade B is also listed as other applicable material. Here, A500 Grade B material is selected for the HSS sections. A500 Grade B has a nominal yield stress of 46 ksi and ultimate tensile stress of 58 ksi.

This study assumes office occupancy for all the buildings. All loads are calculated based on this assumption. Although other types of loads such as wind, rain, and snow exist, they are not included in the calculation as this study is focused on seismic design. Only dead and live loads are considered in the load combination in addition to seismic loads. ASCE 7-10 defines dead load as, "Dead loads consist of the weight of all materials of construction incorporated into the building including, but not limited to, walls, floors, roofs, ceilings, stairways, built-in partitions, finishes, cladding, and other similarly incorporated architectural and structural items, and fixed service equipment including the weight of cranes" [15]. A uniform dead load of 75 psf is assumed for floors excluding the roof; this load includes the deck with concreting, beams, girders, fireproofing, ceiling, mechanical, electrical plumbing, partitions. For the roof, a

uniform dead load of 55 psf was assumed. Further ASCE 7-10 states, "a load produced by the building's use and occupancy or other structure that does not include construction or environmental loads, such as wind load, snow load, rain load, earthquake load, flood load, or dead load, is called live load" [15]. Here, a uniform live load of 50 psf for floors and 25 psf for the roof were assumed. The following few sections discuss earthquake load generation.

## *3.2 Design Response Spectrum*

After the gravity loads are calculated, the next step is to determine the lateral loads. It is impossible to generate these loads without the design response spectrum. This section gives a basic introduction to the design response spectrum. When a single degree of freedom (SDOF) structure is subjected to an earthquake ground motion, the equation of motion is expressed as:

$$m\ddot{x}(t) + c\dot{x}(t) + kx(t) = -m\ddot{x}_g(t) \qquad \text{Eq-3}$$

The structure's natural period depends on the structure's mass and stiffness for structures with low damping. Hence, we can easily change the period of the SDOF by altering either the mass or the stiffness. After each alteration, we can numerically solve the equation of motion to generate peak responses of displacement, velocity, or acceleration. The plot of these peak values for each alteration is known as the response spectrum. Hence, a specific ground motion will generate a particular response spectrum. Designing the structure using a particular ground motion is not adequate due to the uncertainty of earthquake ground motions. This inadequacy led to the development of the design response spectrum, which combines several elastic response spectra. This study uses the ASCE 7-10 [15] procedure to generate the design response

spectrum. This procedure's first step involves determining the building's risk category based on the risk to human life, health, and welfare associated with their damage or failure by nature of their occupancy or use. Further, this categorization of buildings helps determine earthquake and other loads based on the risk associated with unacceptable performance. This study categorizes all the buildings as category II using Table 3.1. For buildings belonging to risk category II, the seismic importance factor ($I_e$) is 1, Table 3.2. As described earlier, the site classification is Class D- Stiff soil due to insufficient data.

The second step is to determine the mapped spectral acceleration parameters. The mapped spectral acceleration parameters $S_1$ and $S_s$ in this study were determined using the USGS website [28]. Both spectral acceleration parameters need to be modified using site coefficients based on the site class to determine the Maximum considered earthquake ($MCE_R$) spectral acceleration parameters, $S_{ms}$ and $S_{m1}$. $MCE_R$ stands for risk-targeted Maximum Considered Earthquake, based on a 1% risk of structural collapse in 50 years. Site class and mapped spectral acceleration parameters are used to determine the site coefficients. The site coefficients $F_a$ and $F_v$ are determined using Table 3.3 and 3.4, respectively. $F_a$ applies to $S_s$ in the constant acceleration part of the spectrum, whereas $F_v$ applies to $S_1$, which is in the spectrum's constant velocity. After the site coefficients are applied, $S_{ms}$ and $S_{m1}$ are calculated using the following equations:

$$S_{Ms} = F_a * S_S \quad \text{Eq-4}$$

$$S_{M1} = F_v * S_1 \quad \text{Eq-5}$$

For the California location (Lat 37.3348502; Lng -122.0090877), $S_s$ and $S_1$ were 1.52g and 0.616g, respectively. Using Site Class D and both $S_s$ and $S_1$ parameters in Table 3.3 and 3.4, $F_a$ and $F_v$ were found to be 1 and 1.5, respectively. Further, using equation 4 and 5, we get $S_{ms}$= 1.52g and $S_{m1}$=0.924g. Similarly, for the Seattle location (Lat: 47.62050630, Lng: -122.34927740), $S_s$ and $S_1$ were 1.348g and 0.523g, respectively. $F_a$ and $F_v$ were again found to be 1 and 1.5, respectively. Therefore, using equation 4 and 5, we get $S_{ms}$= 1.348g and $S_{m1}$=0.785g.

Finally, to build the design response spectrum, we need to determine the design spectral acceleration parameters. The design spectral acceleration parameters are determined from $S_{MS}$ and $S_{M1}$ using the following equations.

$$S_{DS} = \frac{2}{3} * S_{MS} \quad \text{Eq-6}$$

$$S_{D1} = \frac{2}{3} * S_{M1} \quad \text{Eq-7}$$

Hence replacing $S_{MS}$ and $S_{M1}$ in the above equations, the California location $S_{DS}$ and $S_{D1}$ are 1.01g and 0.349g, respectively. Likewise, for the Seattle location $S_{DS}$=0.899g and $S_{D1}$=0.523g. Further, the design response spectrum needs additional parameters as can be seen in Figure 3.3. All of these parameters are directly related to $S_{DS}$ and $S_{D1}$. The time parameters are related to $S_{DS}$ and $S_{D1}$ as follows:

$$T_0 = 0.2\frac{S_{D1}}{S_{DS}} \quad \text{Eq-8}$$

$$T_S = \frac{S_{D1}}{S_{DS}} \quad \text{Eq-9}$$

$T_L$ = Long- period from Fig 22-12 through 22-16 [15]

In Figure 3.3, the design response spectrum can be easily divided into four different zones based on the type of lines. Linear, constant, parabolic, and cubic lines define the four zones. Hence, each of the zones will have a different equation. In other words, if the fundamental period of a structure is greater than 0 seconds but less than $T_0$, the spectral acceleration value varies linearly from 0.4 $S_{DS}$ at T=0 secs to $S_{DS}$ at T= $T_0$. If the structure's period is in between $T_0$ to $T_S$, then the spectral acceleration is constant, $S_{DS}$. Further, if the period is in between $T_s$ and $T_L$ seconds, then the spectral acceleration is given by

$$S_a = \frac{S_{D1}}{T} \qquad \text{Eq-10}$$

Finally, for periods exceeding $T_L$, $S_a$ shall be taken as

$$S_a = \frac{S_{D1} T_L}{T^2} \qquad \text{Eq 11}$$

Using the above equations, design response spectrum for both California and Seattle location were developed.

## *3.3 Seismic Load Calculation*

This section describes two analytical procedure to determine seismic loads. Both methods require the effective seismic weight and design response spectrum to generate earthquake loads. The seismic weight is calculated based on dead and live loads, whereas the design response spectrum was developed earlier in section 3.2. In this study, the seismic weight comprises of dead loads only. Table 3.5 shows the seismic

mass calculation for the four-story EBFs. Same calculation is repeated to determine the seismic weight for all the remaining EBFs. Table 3.6 tabulates the effective seismic weight for all the EBFs considered in this study. Since there are four bays of identical EBFs resisting lateral forces in each orthogonal direction, the seismic weight is distributed equally on all four frames. After the seismic mass is distributed in each of the frames, one of the analytical procedures is used to generate lateral loads. Although there are three different analytical procedures, equivalent lateral force analysis, modal response spectrum analysis, and seismic response history procedures, to determine seismic load according to ASCE 7-10, only the first two procedures are used in the design study and in later sections nonlinear time history analysis will be performed to get more accurate seismic response to design basis earthquake ground motion records. Not all procedure is acceptable for all structures. To determine which procedure is permitted, it is essential to classify the structure into seismic design categories. As per ASCE 7-10, the structures can be classified into four seismic design categories. These categories are based on $S_{DS}$ and $S_{D1}$ parameters. Using the design spectral parameters and risk category in Table 11.6-1 and 11.6-2 [15], it is evident that all the EBFs in this study belong to seismic design category D. For any structure in seismic design category D, all three analytical procedures are permitted if the building is regular and the total height is less than 140 ft, Table 3.7. Equivalent lateral force analysis is the simplest method for earthquake load generation. Even though the Equivalent lateral force method is permitted, the modal response spectrum was performed for all the structures in this study. Both of these procedures have been described in this section because the

modal response spectrum analysis requires the base shear generated from the equivalent lateral force analysis.

### 3.3.1 Equivalent Lateral Force Method

The equivalent lateral force method is the simplest among the three analytical procedure. This method simplifies the effect of dynamic loading of an expected earthquake by substituting it with a static force distributed laterally on a structure. This procedure assumes that the building's response is directly related to its fundamental mode shape. Additionally, this assumption is only valid for low rise and symmetric buildings. In this method, base shear V is determined using the following equation

$$V = C_S W \qquad \text{Eq 12}$$

Where, $C_S$ is the seismic response coefficient and W is the effective seismic weight. The seismic response coefficient is dependent upon the fundamental period of the structure and design response spectrum. Overall, Natural period T for all EBFs in this study is greater than $T_S$ but less than $T_L$. Hence, only the following equation was used.

$$C_S = \frac{\frac{S_{D1}}{T}}{(\frac{R}{I_e})} \qquad \text{Eq 14}$$

Where, $S_{D1}$ is the design spectral response acceleration parameter at a period of 1.0 s, T is the fundamental period of the structure, R is the response modification factor and $I_e$ is the importance factor. All of these parameters, except R and T, have already been discussed in detail. R for the system accounts primarily for the ductility of the system. In other words, the response modification is used to simplify the structural design process such that a linearly elastic procedure is sufficient for building design. For

EBFs, the response modification factor is 8, Table 3.8 [15]. Further, the table lists overstrength factor $\Omega_0$ and Deflection amplification factor $C_d$ for EBFs. This overstrength factor is used while designing force-controlled members, and the deflection amplification factor is used to predict the inelastic displacement. Additionally, ASCE 7-10 have imposed minimum values for $C_S$. These values are not governing for this study; hence, they have not been discussed here. Next, the fundamental period of the structure, T, in the direction under consideration can only be established using modal analysis. As the design is an iterative process, sectional properties may change at least twice. Subsequently, this change in sectional properties affects modal analysis results. Therefore, as a simpler alternative to performing a modal analysis, ASCE 7-10 permits the approximate building period, Ta. The following equation determines Ta

$$T_a = C_t h_n^x \qquad \text{Eq 15}$$

Where $h_n$ is the structural height, $C_t$ and x are parameters determined using Table 3.10. For EBFs in Table 3.10, Ct and x were 0.03 and 0.75, respectively. Further, ASCE 7-10 limits the maximum value for T to be used for analysis. ASCE 7-10 states that the fundamental period, T, shall not exceed the upper limit coefficient on the calculated period (Cu), Table 3.9, times the approximate fundamental period, Ta. Table 3.9 shows the relationship between the upper limit coefficient and $S_{D1}$. For this study, SD1 exceeds 0.3 for both the locations under consideration. Therefore, from Table 3.9, Cu is 1.4 for both locations. Overall, Table 3.11 shows the approximate and the maximum allowable period for all nine EBFs.

Finally, all the parameters required by equation 12 to determine the total base shear are known. After the base shear is calculated, it is used to generate the lateral forces at each level. First, the base shear is distributed horizontally based on the relative rigidity of EBFs. Since all the lateral resisting frames are identical, the base shear is distributed equally to the four EBFs. Second, this base shear per frame is distributed vertically to determine the lateral loads on each floor. As per ASCE 7-10, this vertical distribution is determined from the following empirical equation

$$F_x = C_{vx}V \quad \text{Eq 15}$$

And

$$C_{vx} = \frac{w_x h_x^k}{\sum_{i=1}^{n} w_i h_i^k} \quad \text{Eq 16}$$

Where $C_{vx}$ is vertical distribution factor, V is the total design base shear, $w_i$ and $w_x$ are the portion of total effective seismic weight of the structure (W) located or assigned to level i or x, $h_i$ and $h_x$ are the height from base to level i or x and k is an exponent related to structure period. Note k is 1 for structures having a period of 0.5 s and 2 for structures having a period of 2.5 s. For T values in between 0.5s and 2.5 s, k is determined using interpolation. Figure 3.4 shows detailed equivalent lateral force calculation for the 4 story EBF in California (Apple headquarters). This procedure was repeated for all the EBFs in this study. Hence, the lateral loads required for structural analysis are determined using equivalent lateral force method.

### 3.3.2 Modal Response Spectrum Method

Modal response spectrum method RSM is another procedure to determine the lateral loads. RSM is based on linear dynamic analysis that considers all the natural vibration

modes. This method provides insight into the dynamic behavior by measuring pseudo-spectral acceleration, velocity, or displacement as a function of the structural modal period and damping. First, Modal analysis was performed using a commercial structural analysis software STAAD Pro [29] student version. This analysis generated modal periods and shapes for all the modes. Each of these modes will have its own effective seismic weight ($\bar{W}$) and base shear ($V_m$). These are calculated for each mode using the following equation

$$V_m = C_{sm}\bar{W} \quad \text{Eq 17}$$

$$\bar{W}_m = \frac{(\sum_{i=1}^{n} w_i \phi_{im})^2}{\sum_{i=1}^{n} w_i (\phi_{im})^2} \quad \text{Eq 18}$$

where $C_{sm}$ is the seismic response coefficient of the $m_{th}$ mode of vibration of the structure in the direction of interest and $\bar{W}_m$ is the effective seismic weight of the $m_{th}$ mode of vibration of the structure. Further, ASCE 7-10 states that the analysis shall include a sufficient number of modes having a combined modal mass participation of at least 90 per cent of the actual mass in each of the orthogonal horizontal directions of response considered by the model. For this study, the first two modes were sufficient to obtain a modal mass participation greater than 90% for all the EBFs. The modal mass participation factor is calculated using the following equation

$$\Gamma_m = \frac{\bar{W}_m}{\sum_{i=1}^{n} w_i \, \phi_{im}} \quad \text{Eq 19}$$

In general, the value for each force-related design parameter of interest, including story drifts, support forces, and individual member forces for each mode of response, shall be computed using each mode's properties and the response spectra defined in Section 3.2 divided by the quantity R/Ie. Each mode generates its own response. To generate

the overall response of the structure, the responses from each mode have to be combined. At present, there are two different methods to combine parameters of interest. In this study, the square root of the sum of the squares (SRSS) method was used to combine the parameters of interest, story shear. Using this combined story shear, the lateral forces in each floor were back calculated. As per ASCE 7-10, the base shear calculated using the RSM method should be scaled to match 85% of the base shear generated using the equivalent lateral force method described earlier. Detailed sample RSM calculation for the 4 story EBF is presented in Figure 3.5.

## *3.3 Structural Analysis for Seismic Design*

Now that all the loads required for seismic analysis are known, structural analysis can be performed. This study uses the Load and Resistance factor design LRFD for structural analysis/design. Since this study involves Dead, Live and Earthquake Loads, the following 6 LRFD load combinations were considered.

1. 1.4 D
2. $1.2D + 1.6L$
3. $1.2D + 1.6L + 0.5L_r$
4. $1.2D + 1.6L_r + 1.0L$
5. $1.2D + 1.0E + 1.0L$
6. $0.9D + 1.0E$

Where D is dead load, L is live load, $L_r$ is roof live load and E stands for earthquake load. Further, E consists of both horizontal and vertical effects of an earthquake. Hence, it can be divided into a vertical component $E_v$ and horizontal component $E_h$. $E_v$ is simply the lateral forces generated from RSM multiplied to a redundancy factor $\rho$. As all the EBFs in this study fall under seismic design Category D, $\rho$ is 1.3 [15]. Whereas, the vertical seismic load effect, $E_v$, is calculated using the design short period spectral acceleration and dead load. $E_v$ and $E_h$ are calculated using the following equations.

$$E_h = \rho Q_E \quad \text{Eq 20}$$

$$E_v = 0.2 S_{DS} D \quad \text{Eq 21}$$

$$E = E_h \pm E_v \quad \text{Eq 22}$$

Where, $Q_E$ represents the lateral seismic force generated using the RSM method. Additionally, the vertical component in Equation 21 is positive for load combination 5 and is negative for load combination 6.

Finally, Structural analysis was performed using a commercial software STAAD.Pro [29] with a student license. STAAD.Pro is one of the most widely used structural analysis and design software products worldwide. STAAD.pro has predefined material properties for both A992 and A500 Grade-B steel. The sectional properties database for American standard steel shapes was also readily available in STAAD.pro. Overall, Structural analysis was an iterative process until all the members were sized to meet the structural design requirements discussed in the next section. A 2-D model of the EBFs frame was modelled in STAAD.pro for structural analysis. Figure 3.6 shows an extruded view of the frame in 4 story EBFs (California). While modelling the EBFs, the braces were pinned and a lean on column with both ends pinned was also introduced. These end releases can be clearly seen in Figure 3.7. The EBFs in addition to resisting lateral loads also take on gravity loads. The gravity loads on the EBF are calculated based on the tributary area. Further, the total gravity load excluding the gravity loads resisted by the EBFs is lumped on the lean on column. Detailed calculations for gravity loads are presented in Table 3.12 and 3.13.

Figure 3.8 to 3.11 shows the application of the calculated loads in STAAD.pro. As can be seen from the figure, there are no gravity loads applied to the links. This is to

facilitate removal of the link beams without disturbing any gravity load paths. Finally, the internal forces such as bending moment, shear force and axial forces are generated. Figure 3.12 and 3.13 show combined bending moment diagram BMD and shear force diagram SFD for all the load combinations, envelope. Additionally, Figure 3.14 displays the internal forces developed in a link beam for an earthquake load case. This figure exactly resembles the force distribution from Figure 1.3.

## *3.4 Seismic Design*

After structural analysis, the final step in this chapter is seismic structural design. The basic concept of seismic design is to proportion and detail the structure such that it can withstand large deformation demands through the inelastic behavior of structural elements. These elements are specially designed to withstand the inelastic behavior acceptably. Further, the structures' ability to deform inelastically permits them to be designed for lower seismic forces. In this study, seismic design is facilitated by standard provisions in AISC Seismic Provisions for structural steel buildings [18]. The AISC Seismic Provisions for Structural steel buildings intends to provide a means of designing structures to respond to maximum considered earthquake ground shaking. The structures designed using this provision is expected to have a low probability of collapse but may sustain significant inelastic behavior and structural damage.

In case of EBFs under design level seismic loading, inelastic deformation is restricted primarily to the links. AISC provisions for EBFs ensure that cyclic yielding and energy dissipation occurs primarily in the link while the diagonal braces, columns, and outside beam link remain elastic. Further, columns in EBFs are designed as per the capacity design principle to ensure the frame's full strength and deformation capacity is

maintained without failure of any column or by soft-story formation. Similar to columns, diagonal braces and outside beams must be designed to resist the loads developed by the fully yielded and strain-hardened link.

AISC Seismic Provisions classify sections for ductility into highly ductile or moderately ductile sections. This classification is based on the width-to-thickness ratio of compression elements. As per Seismic provision, Links in EBFs should satisfy the requirements for highly ductile members. An exception to this provision is for the link flanges of short links where a moderately ductile member is allowed. As all the links in this study are short, the link flanges can satisfy moderately ductile members. Next, the columns in EBF should satisfy the requirements for highly ductile members. Also, the provision allows both the brace and the outside beam to satisfy the moderately ductile requirements. All the sections used in this study adhere to the above requirements. Equation 23 to 26 present the limiting width-to-thickness ratio for members of both W section and HSS section.

| For W sections | Width to thickness ratio | |
|---|---|---|
| Highly Ductile | $0.32\sqrt{\frac{E}{R_y F_y}}$ | Eq 23 |
| Moderately Ductile | $0.4\sqrt{\frac{E}{R_y F_y}}$ | Eq 24 |
| For HSS sections | | |
| Highly Ductile (brace) | $0.65\sqrt{\frac{E}{R_y F_y}}$ | Eq 25 |

Moderately Ductile (brace) $0.76\sqrt{\frac{E}{R_y F_y}}$ Eq 26

For shear links, the links have high shear demand. This is clearly seen in Figure 3.14. As per the AISC Seismic Provisions, design shear strength of the, $\phi_v V_n$, is given by:

$V_n = V_p$ Eq 27

$\phi_v = 0.75$ Eq 28

Here $V_p$ depends upon the ratio of required axial strength to axial yield strength. In all the links for this study this ratio is less than 0.15. Therefore, as per the specification $V_p$ is given by

$V_p = 0.6 F_y A_{lw}$ Eq 29

Where Fy is the yield strength of the material and $A_{lw}$ is (d- $2t_f$) tw for a W section. The required strength of columns, beams and outside links are determined using the capacity-limited seismic load effect $E_{cl}$. This effect determines the forces developed in the members assuming an adjusted link shear strength at the link ends. The adjusted link shear strength is taken as Ry times the nominal shear strength of the link, Vn, multiplied by 1.25 for W-sections. For the beams outside the link, using 88% of this force is permitted as per the specification. As all the links in this study are short links, a link rotation angle is limited to 0.08 radians. Figure 3.15 to 3.18 show the sample calculation for links, braces, outside beams and columns. Hence, all the buildings were designed using the procedure described above. The section sizes for all these buildings are presented in Table 3.14 to 3.17.

*Table 3. 1 Risk Category of Buildings for Earthquake and Other loads Adapted from ASCE 7-10* [15]

| Use or Occupancy of Buildings and Structures | Risk Category |
|---|---|
| Buildings and other structures that represent a low risk to human life in the event of failure | I |
| All buildings and other structures except those listed in Risk Categories I,III and IV | II |
| Buildings and other structures, the failure of which could pose a substantial risk to human life | III |
| Buildings and other structures not included in Risk Category IV (including, but not limited to, facilities that manufacture, process, handle,store,use or dispose of such substances where their quantity exceeds a threshold quantity established by the authority having jurisdiction and is sufficient to pose a threat to the public if released. | |
| Buildings and other structures designated as essential facilities | IV |
| Buildings and other structures, the failure of which could pose a substantial hazard to the community. | |
| Buildings and other structures (including, but not limited to, facilities that manufacture, process, handle, store, use or dispose of such substances as hazardous fuels, hazardous chemicals, or hazardous waste) containing sufficient quantities of highly toxic substances where the quantity exceeds a threshold quantity established by the authority having jurisdiction to be dangerous to the public if released and is sufficient to pose a threat to the public if released.<br>Buildings and other structures required to maintain the functionality of other Risk Category IV structures. | |

*Table 3. 2 Importance Factors by Risk Category of Buildings for Earthquake and Other Loads Adapted from ASCE 7-10* [15]

| Risk Category from Table 1.5-1 | Snow Importance Factor $I_s$ | Ice Importance Factor- Thickness, $I_i$ | Ice Importance Factor- Wind, $I_w$ | Seismic Importance Factor, $I_e$ |
|---|---|---|---|---|
| I | 0.80 | 0.80 | 1.00 | 1.00 |
| II | 1.00 | 1.00 | 1.00 | 1.00 |
| III | 1.10 | 1.25 | 1.00 | 1.25 |
| IV | 1.20 | 1.25 | 1.00 | 1.50 |

*Table 3. 3 Site Coefficient Fa Adapted from ASCE 7-10* [15]

| | Mapped Risk-Targeted Maximum Considered Earthquake ($MCE_r$) Spectral Response Acceleration Parameter at Short Period | | | | |
|---|---|---|---|---|---|
| Site Class | $S_s \leq 0.25$ | $S_s=0.5$ | $S_s=0.75$ | $S_s=1.0$ | $S_s \geq 1.25$ |
| A | 0.8 | 0.8 | 0.8 | 0.8 | 0.8 |
| B | 1.0 | 1.0 | 1.0 | 1.0 | 1.0 |
| C | 1.2 | 1.2 | 1.1 | 1.0 | 1.0 |
| D | 1.6 | 1.4 | 1.2 | 1.1 | 1.0 |
| E | 2.5 | 1.7 | 1.2 | 0.9 | 0.9 |
| F | See section 11.4.7 | | | | |

*Table 3. 4 Site Coefficient Fv Adapted from ASCE 7-10* [15]

| Site Class | Mapped Risk-Targeted Maximum Considered Earthquake ($MCE_r$) Spectral Response Acceleration Parameter at 1-s Period | | | | |
|---|---|---|---|---|---|
| | $S_s \leq 0.25$ | $S_s=0.5$ | $S_s=0.75$ | $S_s=1.0$ | $S_s \geq 1.25$ |
| A | 0.8 | 0.8 | 0.8 | 0.8 | 0.8 |
| B | 1.0 | 1.0 | 1.0 | 1.0 | 1.0 |
| C | 1.7 | 1.6 | 1.5 | 1.4 | 1.3 |
| D | 2.4 | 2.0 | 1.8 | 1.6 | 1.5 |
| E | 3.5 | 3.2 | 2.8 | 2.4 | 2.4 |
| F | See section 11.4.7 | | | | |

*Table 3. 5 Effective Seismic Mass Calculation (4 story EBFs)*

Total Seismic Mass (Including the Exterior Walls)

| | Level | Weight | Mass(slug) | Mass (per frame) |
|---|---|---|---|---|
| 1 | Roof | 1127.50 | 35015.53 | 8753.881988 |
| 2 | 3F | 1598.75 | 49650.62 | 12412.65528 |
| 3 | 2F | 1598.75 | 49650.62 | 12412.65528 |
| 4 | 1F | 1598.75 | 49650.62 | 12412.65528 |
| | | **5923.75** | **183967.39** | |
| | Effective Seismic Weight(lbf) | | | **5923.75** |

*Table 3. 6 Effective seismic mass summary*

| SN | Name | Location | Effective Seismic Weight (kips) |
|---|---|---|---|
| 1 | 4EBF-AH | California | 5923.75 |
| 2 | 5EBF-AH | California | 7522.50 |
| 3 | 6EBF-AH | California | 9121.25 |
| 4 | 7EBF-AH | California | 10720.00 |
| 5 | 8EBF-AH | California | 12318.75 |
| 6 | 9EBF-AH | California | 13917.50 |
| 7 | 10EBF-AH | California | 15516.25 |
| 8 | 4EBF-SN | space needle | 5923.75 |
| 9 | 5EBF-SN | space needle | 7522.50 |

*Table 3. 7 Permitted Analytical Procedures Adapted from ASCE 7-10* [15]

| Seismic Design Category | $S_s \leq 0.25$ | Equivalent Lateral Force Analysis, Section 12.8 | Modal Response Spectrum Anlaysis, Section 12.9 | Seismic Reponse History Procedures, Chapter 16 |
|---|---|---|---|---|
| B,C | All structures | P | P | P |
| D,E,F | Risk Category I or II buildings not exceeding 2 stories above the base | P | P | P |
| | Structures of light frame construction | P | P | P |
| | Structures with no structural irregularities and not exceeding 160 ft in structural height | P | P | P |
| | Structures exceeding 160 ft in structural height with no structural irregularities and with T < 3.5 Ts | P | P | P |
| | Structures not exceeding 160 ft in structural height and having only horizontal irregularities of Type 2,3,4,or 5 in Table 12.3-1 or vertical irregulatities of Type 4, 5a, or 5b in Table 12.3-2 | P | P | P |
| | All other structures. | NP | P | P |
| *P: Permitted; NP: Not Permitted; Ts= $S_{D1}/S_{DS}$ | | | | |

*Table 3. 8 Design Coefficients and Factors for Seismic Force Resisting Systems Adapted from ASCE 7-10* [15]

| | Seismic Force- Resisting System | ASCE 7 Section Where Detailing Requirements Are Specified | Response Modification Coefficient, R | Overstrength Factor, $\Omega_o$ | Deflection Amplification Factor, $C_d$ | Structural System Limitations Including Structural Height, h (ft) Limits — Seismic Design Category B | C | D | E | F |
|---|---|---|---|---|---|---|---|---|---|---|
| B | BUILDING FRAME SYSTEMS | | | | | | | | | |
| 1 | Steel eccentrically braced frames | 14.1 | 8 | 2 | 4 | NL | NL | 160 | 160 | 100 |
| 2 | Steel special concentrically braced frames | 14.1 | 6 | 2 | 5 | NL | NL | 160 | 160 | 100 |
| 3 | Steel ordinary concentrically braced frames | 14.1 | $3\frac{1}{4}$ | 2 | $3\frac{1}{4}$ | NL | NL | 35 | 35 | NP |

*Table 3. 9 Coefficient for Upper Limit on Calculated Period Adapted from ASCE 7-10* [15]

**Table 12.8-1 Coefficient for Upper Limit on Calculated Period**

| Design Spectral Response Acceleration Paramter at 1 s, $S_{D1}$ | Coefficient $C_u$ |
|---|---|
| ≥0.4 | 1.4 |
| 0.3 | 1.4 |
| 0.2 | 1.5 |
| 0.15 | 1.6 |
| ≤0.1 | 1.7 |

*Table 3. 10 Values of Approximate Period Parameters Ct and x Adapted from ASCE 7-10* [15]

| Structure Type | $C_t$ | x |
|---|---|---|
| Moment resisting frame systems in which the frames resist 100% of the required seismic force and are not enclosed or adjoined by coponents that are more rigid and will prevent the frames from deflecting where subjected to seismic forces: | | 0.8 |
| Steel moment- resisting frames | 0.028(0.0724) | 0.9 |
| Concrete moment-resisting frames | 0.016(0.0466) | 0.75 |
| Steel eccentrically braced frames in accordance with Table 12.2-1 lines B1 or D1 | 0.03(0.0731) | 0.75 |
| Steel buckling-restrained braced frames | 0.03(0.0731) | 0.75 |
| All other structural systems | 0.02(0.0488) | 0.75 |
| *Metric Equivalents are shown in parentheses | | |

*Table 3. 11 Approximate time period and Maximum time period allowed for all nine EBFs*

| | | | | | |
|---|---|---|---|---|---|
| **$C_t$** | 0.03 | x | 0.75 | | |
| **$C_u$** | 1.4 | | | | |
| | | | | | |
| SN | **Name** | **Location** | **Str Ht(hn)** | **$T_a$** | **$T_U$** |
| 1 | 4EBF-AH | California | 56 | 0.614 | 0.860 |
| 2 | 5EBF-AH | California | 70 | 0.726 | 1.016 |
| 3 | 6EBF-AH | California | 84 | 0.832 | 1.165 |
| 4 | 7EBF-AH | California | 98 | 0.934 | 1.308 |
| 5 | 8EBF-AH | California | 112 | 1.033 | 1.446 |
| 6 | 9EBF-AH | California | 126 | 1.128 | 1.580 |
| 7 | 10EBF-AH | California | 140 | 1.221 | 1.709 |
| 8 | 4EBF-SN | space needle | 56 | 0.614 | 0.860 |
| 9 | 5EBF-SN | space needle | 70 | 0.726 | 1.016 |

*Table 3. 12 Typical gravity Loads on EBFs*

| DEAD LOAD | | | | | | | |
|---|---|---|---|---|---|---|---|
| **Tributary Loads on Beams (One way slab)** | | | | | | | |
| | DL | Length | Breadth | Load(kips) | Load/ft(21ft) | divided equally in the beams and not the link beam. | |
| **Roof** | 55 | 25 | 4.17 | 5.73 | 0.27 | | |
| **3F** | 75 | 25 | 4.17 | 7.81 | 0.37 | | |
| **2F** | 75 | 25 | 4.17 | 7.81 | 0.37 | FRAME LOADS | |
| **1F** | 75 | 25 | 4.17 | 7.81 | 0.37 | | |
| | | | | | | | |
| **Tributary Loads on Columns** | | | | | | | |
| | DL | Length | Breadth | Half Beam Tri Area | Load(kips) | | |
| **Roof** | 55 | 25 | 12.5 | -2.86 | 14.32 | | |
| **3F** | 75 | 25 | 12.5 | -3.91 | 19.53 | | |
| **2F** | 75 | 25 | 12.5 | -3.91 | 19.53 | POINT LOADS | |
| **1F** | 75 | 25 | 12.5 | -3.91 | 19.53 | | |
| **LIVE LOAD** | | | | | | | |
| **Tributary Loads on Beams (One way slab)** | | | | | | | |
| | LL | Length | Breadth | Load(kips) | Load/ft(21ft) | divided equally in the beams and not the link beam. | |
| **Roof** | 25 | 25 | 4.17 | 2.60 | 0.12 | | |
| **3F** | 50 | 25 | 4.17 | 5.21 | 0.25 | | |
| **2F** | 50 | 25 | 4.17 | 5.21 | 0.25 | FRAME LOAD | |
| **1F** | 50 | 25 | 4.17 | 5.21 | 0.25 | | |
| | | | | | | | |
| **Tributary Loads on Columns** | | | | | | | |
| | LL | Length | Breadth | Half Beam Tri Area | Load(kips) | | |
| **Roof** | 25 | 25 | 12.5 | -1.30 | 6.51 | Roof Live Load | |
| **3F** | 50 | 25 | 12.5 | -2.60 | 13.02 | POINT LOADS | |
| **2F** | 50 | 25 | 12.5 | -2.60 | 13.02 | | |
| **1F** | 50 | 25 | 12.5 | -2.60 | 13.02 | | |

*Table 3. 13 Typical gravity loads on Lean on Column*

| Dead Load and Live Load Calculations | | | | | |
|---|---|---|---|---|---|
| **Tributary Loads on Columns** | | | | | |
| | DL | Area | | Load(kips) | |
| **Roof** | 55 | 18125 | 996875.00 | 996.88 | |
| **3F** | 75 | 18125 | 1359375.00 | 1359.38 | |
| **2F** | 75 | 18125 | 1359375.00 | 1359.38 | POINT LOADS |
| **1F** | 75 | 18125 | 1359375.00 | 1359.38 | |
| | | | | | |
| | LL | Area | | Load(kips) | |
| **Roof** | 25 | 18125 | 453125.00 | 453.13 | Roof Live Load |
| **3F** | 50 | 18125 | 906250.00 | 906.25 | |
| **2F** | 50 | 18125 | 906250.00 | 906.25 | POINT LOADS |
| **1F** | 50 | 18125 | 906250.00 | 906.25 | |

*Table 3. 14 Link Sectional properties for all EBFs*

| Link Beam | | | | | | | | | |
|---|---|---|---|---|---|---|---|---|---|
| Story No | 4EBF-AH | 5EBF-AH | 6EBF-AH | 7EBF-AH | 8EBF-AH | 9EBF-AH | 10EBF-AH | 4EBF-SN | 5EBF-SN |
| 1 | W10*88 | W12*120 | W12*170 | W12*152 | W12*170 | W12*210 | W12*210 | W10*88 | W12*120 |
| 2 | W10*88 | W12*120 | W12*170 | W12*152 | W12*170 | W12*210 | W12*210 | W10*88 | W12*120 |
| 3 | W10*68 | W10*112 | W12*120 | W10*112 | W12*152 | W12*152 | W12*152 | W10*68 | W10*112 |
| 4 | W10*68 | W10*112 | W12*120 | W10*112 | W12*152 | W12*152 | W12*152 | W10*68 | W10*112 |
| 5 | | W10*68 | W10*112 | W10*68 | W10*112 | W10*112 | W10*112 | | W10*68 |
| 6 | | | W10*112 | W10*68 | W10*112 | W10*112 | W10*112 | | |
| 7 | | | | W10*68 | W10*112 | W10*112 | W10*112 | | |
| 8 | | | | | W10*112 | W10*112 | W10*112 | | |
| 9 | | | | | | W10*112 | W10*112 | | |
| 10 | | | | | | | W10*113 | | |

*Table 3. 15 Brace Sectional properties for all EBFs*

| Braces | | | | | | | | | |
|---|---|---|---|---|---|---|---|---|---|
| Story No | 4EBF-AH | 5EBF-AH | 6EBF-AH | 7EBF-AH | 8EBF-AH | 9EBF-AH | 10EBF-AH | 4EBF-SN | 5EBF-SN |
| 1 | HSS 7*7*0.625 | HSS 8*8*0.625 | HSS 8*8*0.625 | HSS 9*9*0.625 | HSS 9*9*0.625 | HSS 9*9*0.625 | HSS 9*9*0.625 | HSS 7*7*0.625 | HSS 8*8*0.625 |
| 2 | HSS 7*7*0.626 | HSS 8*8*0.625 | HSS 8*8*0.625 | HSS 9*9*0.626 | HSS 9*9*0.625 | HSS 9*9*0.625 | HSS 9*9*0.625 | HSS 7*7*0.626 | HSS 8*8*0.625 |
| 3 | HSS 7*7*0.627 | HSS 7*7*0.626 | HSS 7*7*0.626 | HSS 8*8*0.625 | HSS 9*9*0.625 | HSS 9*9*0.625 | HSS 9*9*0.625 | HSS 7*7*0.627 | HSS 7*7*0.626 |
| 4 | HSS 7*7*0.628 | HSS 7*7*0.626 | HSS 7*7*0.626 | HSS 8*8*0.625 | HSS 9*9*0.625 | HSS 9*9*0.625 | HSS 9*9*0.625 | HSS 7*7*0.628 | HSS 7*7*0.626 |
| 5 | | HSS 7*7*0.626 | HSS 7*7*0.626 | HSS 8*8*0.625 | HSS 8*8*0.625 | HSS 9*9*0.625 | HSS 9*9*0.625 | | HSS 7*7*0.626 |
| 6 | | | HSS 7*7*0.626 | HSS 8*8*0.625 | HSS 8*8*0.625 | HSS 9*9*0.625 | HSS 9*9*0.625 | | |
| 7 | | | | HSS 8*8*0.625 | HSS 8*8*0.625 | HSS 8*8*0.625 | HSS 9*9*0.625 | | |
| 8 | | | | | HSS 8*8*0.625 | HSS 8*8*0.625 | HSS 9*9*0.625 | | |
| 9 | | | | | | HSS 8*8*0.625 | HSS 9*9*0.625 | | |
| 10 | | | | | | | HSS 9*9*0.626 | | |

*Table 3. 16 Outside Beam Sectional properties for all EBFs*

| Outside Beam | | | | | | | | | |
|---|---|---|---|---|---|---|---|---|---|
| Story No | 4EBF-AH | 5EBF-AH | 6EBF-AH | 7EBF-AH | 8EBF-AH | 9EBF-AH | 10EBF-AH | 4EBF-SN | 5EBF-SN |
| 1 | W18*97 | W18*97 | W18*97 | W18*97 | W21*147 | W21*147 | W21*147 | W18*97 | W18*97 |
| 2 | W18*97 | W18*97 | W18*97 | W18*97 | W21*147 | W21*147 | W21*147 | W18*97 | W18*97 |
| 3 | W18*97 | W18*97 | W18*97 | W18*97 | W21*147 | W21*147 | W21*147 | W18*97 | W18*97 |
| 4 | W18*97 | W18*97 | W18*97 | W18*97 | W21*147 | W21*147 | W21*147 | W18*97 | W18*97 |
| 5 | | W18*97 | W18*97 | W18*97 | W21*147 | W21*147 | W21*147 | | W18*97 |
| 6 | | | W18*97 | W18*97 | W21*147 | W21*147 | W21*147 | | |
| 7 | | | | W18*97 | W21*147 | W21*147 | W21*147 | | |
| 8 | | | | | W21*147 | W21*147 | W21*147 | | |
| 9 | | | | | | W21*147 | W21*147 | | |
| 10 | | | | | | | W21*147 | | |

*Table 3. 17 Column Sectional properties for all EBFs*

| Column | | | | | | | | | |
|---|---|---|---|---|---|---|---|---|---|
| Story No | 4EBF-AH | 5EBF-AH | 6EBF-AH | 7EBF-AH | 8EBF-AH | 9EBF-AH | 10EBF-AH | 4EBF-SN | 5EBF-SN |
| 1 | W14*132 | W14*145 | W14*176 | W14*211 | W14*283 | W14*257 | W14*132 | W14*132 | W14*145 |
| 2 | W14*132 | W14*145 | W14*176 | W14*211 | W14*283 | W14*257 | W14*132 | W14*132 | W14*145 |
| 3 | W14*74 | W14*132 | W14*132 | W14*211 | W14*211 | W14*257 | W14*257 | W14*74 | W14*132 |
| 4 | W14*74 | W14*132 | W14*132 | W14*211 | W14*211 | W14*257 | W14*257 | W14*74 | W14*132 |
| 5 | | W14*132 | W14*132 | W14*132 | W14*211 | W14*211 | W14*257 | | W14*132 |
| 6 | | | W14*132 | W14*132 | W14*211 | W14*211 | W14*257 | | |
| 7 | | | | W14*132 | W14*211 | W14*211 | W14*257 | | |
| 8 | | | | | W14*211 | W14*211 | W14*257 | | |
| 9 | | | | | | W14*211 | W14*257 | | |
| 10 | | | | | | | W14*257 | | |

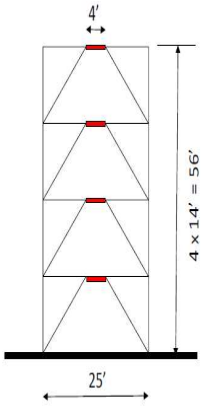


*Figure 3. 1 Elevation view Grid 1-1 4 story EBFs [30]*

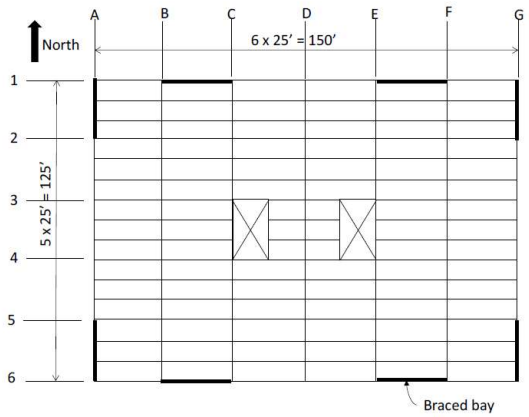


*Figure 3. 2 General Building Plan [30]*

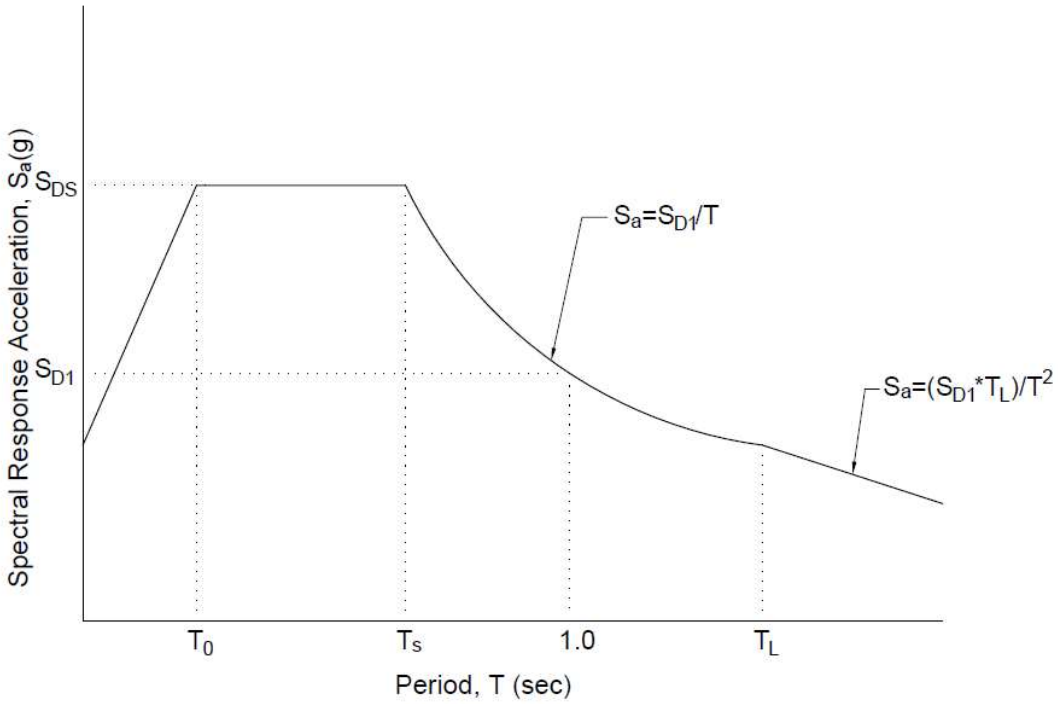


*Figure 3. 3 Design Response Spectrum Adapted from ASCE 7-10 [15]*

| Seismic Calculation | | | | | | | | | |
|---|---|---|---|---|---|---|---|---|---|
| location | California | | Design Response Spectrum | | | | | | |
| Height(h) | 56 | ft | Soil type (firm Soil) | D | | | | | |
| E-W dimension | 150 | ft | Ss | 1.520 | g | | | | |
| N-S dimension | 125 | ft | S1 | 0.616 | g | | | | |
| Soil type | firm | | Fa | 1.000 | | | | | |
| R(Eccentrically Braced Frame) | 8 | | Fv | 1.500 | | | | | |
| Risk Category(densley occupied office building) | II | | | | | | | | |
| | | | Sms | 1.520 | g | | | | |
| Seismic Importance Factor(I) | 1 | | Sm1 | 0.924 | g | | | | |
| | | | Sds | 1.013 | g | | | | |
| | | | Sd1 | 0.616 | g | | | | |
| | | | To | 0.122 | | | | | |
| Approximate Fundamental Time Period | | | Short Period(Ts) | 0.608 | | | | | |
| For Eccentricall Braced Frame | | | | | | | | | |
| Ct | 0.030 | | | | | | | | |
| x | 0.750 | | | | | | | | |
| Ta | 0.614 | s | | | | | | | |
| | | | | | | | | | |
| Since Ta>Ts, it lies in the constant velocity phase. | | | | | | | | | |
| Spectrul Acceleration at Ta(Sa) | 1.003 | | | | | | | | |
| Seismic Coefficient(Cs) | 0.125 | | | | | | | | |
| Effective Seismic Weight(W) | 5923.750 | | | | | | | | |
| Vb | 742.720 | Kips | | | | | | | |
| | | | | | | | | | |
| | | | | | | | | | |
| Vertical Distribution of Base Shear | | | | | | | | | |
| | Seismic Weight(Kips) | Floor Ht(ft) | Elevation(h) | $h^k$ | $Wh^k$ | Ratio | $F_x$(kips) | Storey Shear(Kips) | |
| Roof | 1127.500 | 14.000 | 56.000 | 70.461 | 79445.14 | 0.327 | 243.103 | 243.103 | |
| 3F | 1598.750 | 14.000 | 42.000 | 51.986 | 83111.83 | 0.342 | 254.323 | 497.427 | |
| 2F | 1598.750 | 14.000 | 28.000 | 33.864 | 54140.55 | 0.223 | 165.671 | 663.097 | |
| 1F | 1598.750 | 14.000 | 14.000 | 16.275 | 26020.40 | 0.107 | 79.623 | 742.720 | |
| | | | | $\Sigma Wh^k$= | 242717.92 | | 742.720 | | |
| | | | | | | | | | |
| Value for K is interpolated | | | | Interpolation | | | | | |
| | k | 1.05706639 | | 0.5 | 1 | | 0.114132774 | x-1 | |
| | | | | 0.614 | x | | 2 | 1 | |
| | | | | 2.5 | 2 | | | | |
| Horizontal Distribution of Lateral Force | | | | | | | | | |
| Since, the center of Mass and Center of Rigidity are at the same point, X direction EQ is resisted by Frames along E-W direction only. | | | | | | | | | |
| Also, since the rigidity for all the frames are equal the vertical force is distributed equally on all 4 frames. | | | | | | | | | |
| Lateral Load in Each Frame | | | | | | | | | |
| | Storey Shear(1/4 of Total) | $F_x$(kips) | | | | | | | |
| Roof | 60.78 | 60.78 | Therefore, these Lateral Forces were applied to a single Frame. | | | | | | |
| 3F | 124.36 | 63.58 | | | | | | | |
| 2F | 165.77 | 41.42 | | | | | | | |
| 1F | 185.68 | 19.91 | | | | | | | |

*Figure 3. 4 Equivalent Lateral Force Method for 4 Story EBF (California)*

Modal Response Spectrum

| | | | | | | | | | | | | | | | | | | | | | |
|---|---|---|---|---|---|---|---|---|---|---|---|---|---|---|---|---|---|---|---|---|---|
| Mode 1 | | | Mode 2 | | | | | | | | | | | | | | | | | | |
| Tm1 | 0.797 | | Tm2 | 0.29 | | | 71.547 | 143.09 | | | | | | | | | | | | | |
| Spectrul Acceleration at Ta(Sa) | 0.773 | | | 1.013 | | | | | | | | | | | | | | | | | |
| Seismic Coefficient(Cs) | 0.097 | | | 0.127 | | | | | | | | | | | | | | | | | |
| | W | $\Phi_1$ | $\Phi_1^2$ | $W\Phi_1$ | $W\Phi_1^2$ | | Participating Mass | Mass ratio | Cumm Mass Ratio | Participation Function | | $C_{s1}$ | $W_i$ | $F_x$ | V | | SRSS Method(V) | Fx RSM | Scaled Fx | Shear | SCM |
| Roof | 281.875 | 1 | 1.0000 | 281.8750 | 281.8750 | $W_m$ | 1265.09992 | 0.85 | 0.85 | 1.311607893 | 1.311608 | 0.097 | 281.88 | 35.72 | 35.72 | ROOF | 39.06 | 39.06 | 49.71 | 49.71 | 60.78 |
| 3F | 399.6875 | 0.846 | 0.7157 | 338.1356 | 286.0627 | | | | | | 1.10962 | | 399.69 | 42.85 | 78.57 | 3F | 80.30 | 41.24 | 52.49 | 102.20 | 63.58 |
| 2F | 399.6875 | 0.585 | 0.3422 | 233.8172 | 136.7831 | | | | | | 0.767291 | | 399.69 | 29.63 | 108.19 | 2F | 108.24 | 27.94 | 35.56 | 137.76 | 41.42 |
| 1F | 399.6875 | 0.277 | 0.0767 | 110.7134 | 30.6676 | | | | | | 0.363315 | | 399.69 | 14.03 | 122.22 | 1F | 124.01 | 15.77 | 20.07 | 157.83 | 19.91 |
| | 1480.9375 | | | 964.5413 | 735.3884 | | | | | | | | | | | | | | | | |
| | | | | | | | | | | | | | | | | Vrsm | 124.01 | 0.85Vb | 157.83 | Vb | 185.68 |
| | | | | | | | | | | | | | | | | Scale Factor | 1.27 | | | | |
| | W | $\Phi_2$ | $\Phi_2^2$ | $W\Phi_2$ | $W\Phi_2^2$ | | | | | | | $C_{s2}$ | $W_i$ | $F_x$ | | | | | | | |
| Roof | 281.875 | 1 | 1 | 281.8750 | 281.8750 | Wm | 165.54453 | 0.11 | 0.97 | -0.442618018 | -0.44262 | 0.127 | 281.88 | -15.80 | -15.80 | | | | | | |
| 3F | 399.6875 | 0.035 | 0.001225 | 13.9891 | 0.4896 | | | | (greater than 90%) | | -0.01549 | | 399.69 | -0.78 | -16.59 | | | | | | |
| 2F | 399.6875 | -0.878 | 0.770884 | -350.9256 | 308.1127 | | | | | | 0.388619 | | 399.69 | 19.67 | 3.09 | | | | | | |
| 1F | 399.6875 | -0.798 | 0.636804 | -318.9506 | 254.5226 | | | | | | 0.353209 | | 399.69 | 17.88 | 20.97 | | | | | | |
| | 1480.9375 | | | -374.0122 | 844.9999 | | | | | | | | | | | | | | | | |
| | W | $\Phi_3$ | $\Phi_3^2$ | $W\Phi_3$ | $W\Phi_3^2$ | | | | | | | | | | | | | | | | |
| Roof | 281.875 | 0.942 | 0.887364 | 265.5263 | 250.1257 | Wm | 37.09008 | 0.03 | 0.99 | 0.188102949 | 0.177193 | | | | | | | | | | |
| 3F | 399.6875 | -0.98 | 0.9604 | -391.6938 | 383.8599 | | | | | | -0.18434 | | | | | | | | | | |
| 2F | 399.6875 | -0.191 | 0.036481 | -76.3403 | 14.5810 | | | | | | -0.03593 | | | | | | | | | | |
| 1F | 399.6875 | 1 | 1 | 399.6875 | 399.6875 | | | | | | 0.188103 | | | | | | | | | | |
| | 1480.9375 | | | 197.1797 | 1048.2541 | | | | | | | | | | | | | | | | |
| | W | $\Phi_4$ | $\Phi_4^2$ | $W\Phi_4$ | $W\Phi_4^2$ | | | | | | | | | | | | | | | | |
| Roof | 281.875 | 0.381 | 0.145161 | 107.3944 | 40.9173 | Wm | 13.28423 | 0.01 | 1.00 | -0.120289653 | -0.04583 | | | | | | | | | | |
| 3F | 399.6875 | -0.749 | 0.561001 | -299.3659 | 224.2251 | | 1481.02 | | Total Mass Participation | | 0.090097 | | | | | | | | | | |
| 2F | 399.6875 | 1 | 1 | 399.6875 | 399.6875 | | | | | | -0.12029 | | | | | | | | | | |
| 1F | 399.6875 | -0.796 | 0.633616 | -318.1513 | 253.2484 | | | | | | 0.095751 | | | | | | | | | | |
| | 1480.9375 | | | -110.4353 | 918.0782 | | | | | | | | | | | | | | | | |

$$\bar{W}_m = \frac{\left(\sum_{i=1}^{n} W_i \phi_{im}\right)^2}{\sum_{i=1}^{n} W_i \phi_{im}^2} \qquad (18.4\text{-}2b)$$

*Figure 3. 5 Sample Modal Response Spectrum Calculation for 4 story EBF(California)*

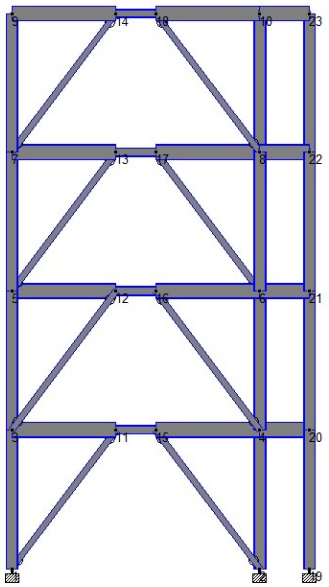


*Figure 3. 6 STAAD.pro Model Extruded View*

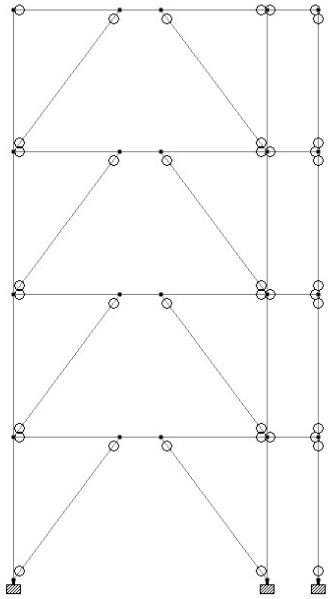

*Figure 3. 7 Typical End Releases*

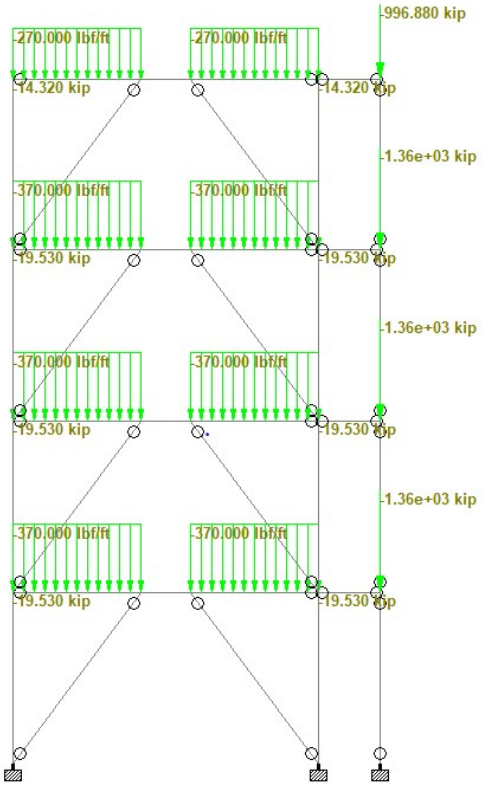


*Figure 3. 8 Typical Dead Load*

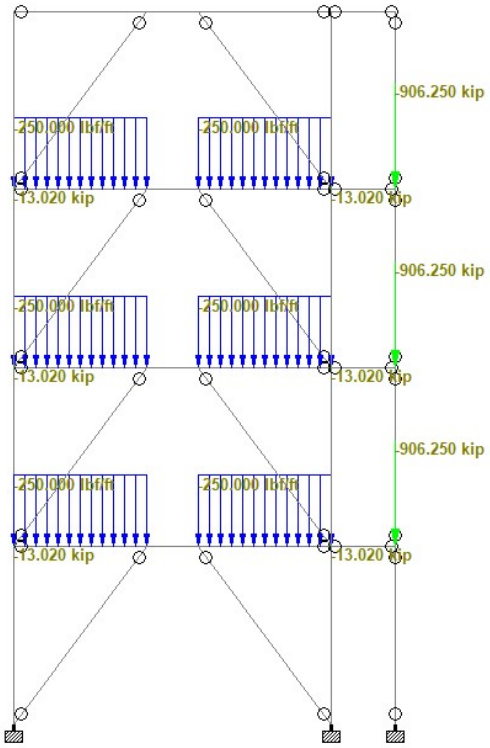


*Figure 3. 9 Typical Live Load*

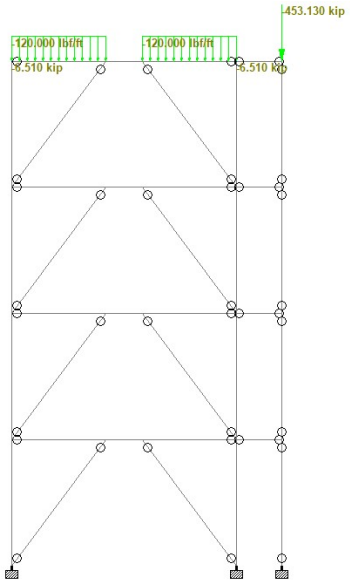


*Figure 3. 10 Typical Roof Live Load*

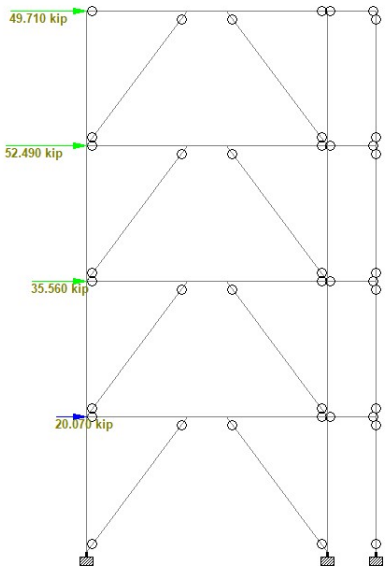


*Figure 3. 11 RSM generated Lateral Forces for 4 Story EBFs (California)*

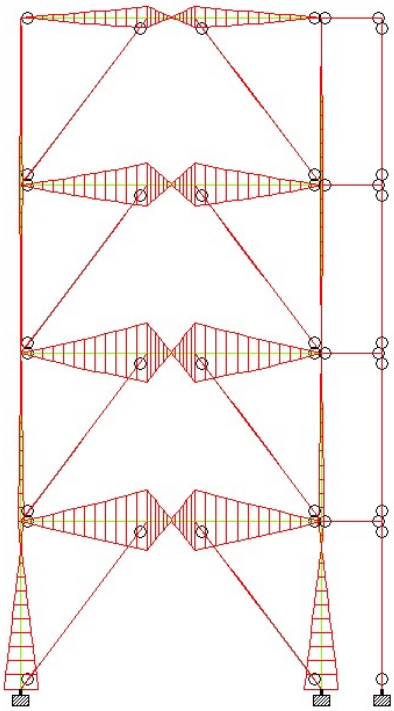

*Figure 3. 12 BMD- Envelope*

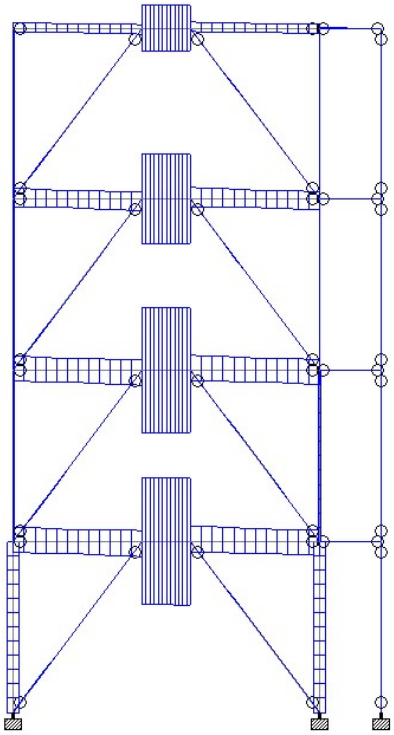

*Figure 3. 13 SFD- Envelope*

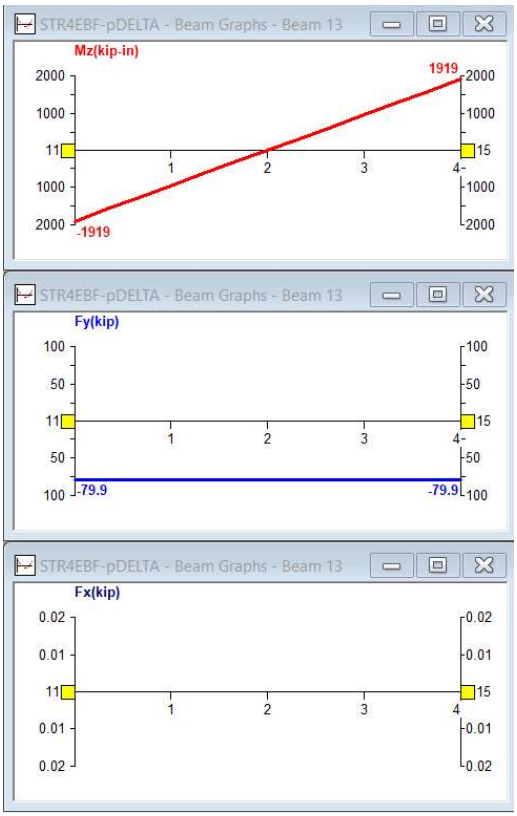


*Figure 3. 14 STAAD.pro Output- 1F Link Beam- 4 Story EBF(California)- Earthquake Load case*

| LINK BEAM DESIGN | | | | | | | | |
|---|---|---|---|---|---|---|---|---|
| | | | | | | | | |
| Compactness Check | | | | | | | | |
| W10*88 | | | | A992 | | | | |
| h | 10.8 | in | Fy | 50 | ksi | Ry | 1.1 | |
| $b_f$ | 10.3 | in | Fu | 65 | ksi | Rt | 1.1 | |
| $t_f$ | 0.99 | in | Fye | 55 | ksi | E | 29000 | ksi |
| $t_w$ | 0.605 | in | Fue | 71.5 | ksi | ry | 2.63 | in |
| Zx | 113 | in3 | Ag | 25.9 | in2 | | | |
| $\frac{b_f}{2t_f}$ | 5.20202 | < | $\lambda_{pf}$ | 9.149962 | OK | | | |
| | | | | | | | | |
| $\frac{h}{t_w}$ | 17.85124 | < | $\lambda_{pw}$ | 90.55209 | OK | | | |
| | | | | | | | | |
| Hence, Section is Compact. | | | | | | | | |
| | | | | | | | | |
| Width to thickness Limitations | | | | | | | | |
| | | | | | | | | |
| Mp | 5650 | in-K | | | | | | |
| Vp | 160.083 | K | | | | | | |
| e | 48 | | | | | | | |
| 1.6Mp/Vp | 56.47071 | <e | OK | PREDOMINANTLY SHEAR YIELDING WILL OCCUR | | | | |
| | | | | | | | | |
| Hence, Moderately ductile flanges allowed. | | | | | | | | |
| $\frac{b_f}{2t_f}$ | 5.20202 | < | $\lambda_{md}$ | 9.184968 | OK | Moderately ductile flanges allowed for shear yielding | | |
| | | | | | | | | |
| $\frac{h}{t_w}$ | 17.85124 | < | $\lambda_{hw}$ | 36.051 | OK | | | |
| | | | | | | | | |
| Hence, Section is Highly ductile | | | | | | | | |
| | | | | | | | | |
| Link Rotation Angle | | | | | | | | |
| | | | | | | | | |
| h | 168 | in | e | 48 | in | Δ | 1.468 | |
| L | 300 | | θ | 0.008738 | | | | |
| ϒ | 0.054613 | rad | OK | | | | | |
| | | | | | | | | |
| Stiffner size and spacing | | | | | | | | |
| b | 8.82 | | 0.75*tw | | | | | |
| t | 0.45375 | | 0.45375 | 0.375 | | | | |
| We know | | | | | Interpolating | | | |
| gamma | 0.08 | s | 15.99 | | if gamma | 0.054613 | s | 21.62166 |
| gamma | 0.02 | s | 29.3 | | | | | |
| s | 20 | in | | | | | | |
| | | | | | | | | |
| Hence, Provide 15.05" by 0.4" web stiffners @ 12"c/c(4 nos) | | | | | | | | |
| | | | | | | | | |
| Shear Strength of Link | | | | | | | | |
| For shear yielding | | | | | | | | |
| Vp | 160.083 | N | | | | | | |
| Py | 1295 | N | | 24 | 7.058824 | | | |
| Pr | 0 | N | From Etabs Envelope | | | | | |
| $\alpha_s$ | 1 | (LRFD) | | | | | | |
| | | | | | | | | |
| $\alpha_s$*Pr/Py | 0 | | | | | | | |
| | | | | | | | | |
| Vn | 160.083 | | | | | | | |
| $\Phi_v$ | 0.9 | | | | | | | |
| $\Phi_v$Vn | 144.0747 | Kips | From Etabs, <Vn Hence OK | | | | | |
| Vu | 106 | Kips | SHEAR,OK | | | | | |
| Mr | 2693 | in-K | From Etabs Envelope | | | | | |
| Mc | 5085 | in-K | | | | | | |
| Pc | 1147.503 | 1295 | | | | | | |
| Pr/Pc | 0 | | | | | | | |
| Mr/Mc | 0.529597 | | | | | | | |
| | | | | | | | | |
| P-M Ratio | 0.529597 | <1 | OK | | | | | |
| | | | | | | | | |
| Hence, the Link is adequate | | | | | | | | |

*Figure 3. 15 Sample Link Beam Design*

| BRACE DESIGN | | | | | | | | |
|---|---|---|---|---|---|---|---|---|
| | | | | | | | | |
| Sectional Properties | | | | | | | | |
| HSS 7*7*5/8 | | | | A500 GRADE B | | | | |
| d | 7 | in | Fy | 46 | ksi | Ry | 1.1 | |
| b | 7 | in | Fu | 58 | ksi | Rt | 1.1 | |
| t | 0.581 | in | Fye | 50.6 | ksi | E | 29000 | ksi |
| | | | Fue | 63.8 | ksi | rx | 2.58 | in |
| Zx | 33.1 | in3 | Ag | 14 | in2 | | | |
| | | | | | | | | |
| Loading and amplification | | | | | | | | |
| | | | | | | | | |
| Loads | Dead Load | Live Load | Eq | | Load combination | | | |
| Axial | -4.58 | 1.99 | -119 | | 0.72D+1.3E | -158.00 | | |
| Shear | -0.25 | 0 | 0 | | 0.72D-1.3E | 151.40 | | |
| Moment | -13.1 | 0 | 0 | | 1.38D+1.3E+1L | -159.03 | | |
| | | | | | 1.38D-1.3E+1L | 150.37 | | |
| Nominal shear strength of link(Vn) | | | 160.083 | kips | | | | |
| 1.25*Ry*Vn | | | 220.114125 | kips | | | | |
| Shear force in link(Vqe) | | | 106 | kips | | | | |
| Overstrength Factor | | | 2.076548349 | | | | | |
| Amplified with overstrength factor | | | | | | | | |
| Loads | Dead Load | Live Load | Eq | | Load combination | Axial Load | | |
| Axial | -4.58 | 1.99 | -247.109254 | | 0.72D+1.3E | -324.54 | | |
| Shear | -0.25 | 0 | 0 | | 0.72D-1.3E | 317.94 | | |
| Moment | -13.1 | 0 | 0 | | 1.38D+1.3E+1L | -325.57 | | |
| | | | | | 1.38D-1.3E+1L | 316.91 | | |
| | | | | | | | | |
| Pu | 325.5724 | kips | | | | | | |
| Mu | 0 | | | | | | | |
| Moment | 0 | | | | | | | |
| | | | | | | | | |
| Determine Unbraced Length | | | | | | | | |
| L | 210 | in | | | | | | |
| KL/r | 81.39535 | | 4.71*(E/fy) | 118.2608 | | | | |
| Fe | 43.20147 | | | | | | | |
| Fcr | 30.74714 | | | | | | | |
| Pc | 387.4139 | | | | | | | |
| Pr | 325.5724 | | | | | | | |
| Pr/Pc | 0.840374 | | | | | | | |
| Mr/Mc | 0 | | | | | | | |
| | | | | | | | | |
| P-M Ratio | 0.840374 | <1 | OK | | | | | |
| | | | | | | | | |
| Hence, the brace is adequate | | | | | | | | |

*Figure 3. 16 Sample Brace Design*

| Beams Outside the Link | | | | | | | | |
|---|---|---|---|---|---|---|---|---|
| | | | | | | | | |
| Compactness Check | | | | | | | | |
| W18*97 | | | | A992 | | | | |
| h | 18.6 | in | Fy | 50 | ksi | Ry | 1.1 | |
| $b_f$ | 11.1 | in | Fu | 65 | ksi | Rt | 1.1 | |
| $t_f$ | 0.87 | in | Fye | 55 | ksi | E | 29000 | ksi |
| $t_w$ | 0.535 | in | Fue | 71.5 | ksi | ry | 2.65 | in |
| Zx | 211 | in3 | Ag | 28.5 | in2 | | | |
| $\frac{b_f}{2t_f}$ | 6.379310345 | < | $\lambda_{pf}$ | 9.149962 | OK | | | |
| $\frac{h}{t_w}$ | 34.76635514 | < | $\lambda_{pw}$ | 90.55209 | OK | | | |
| Hence, Section is Compact. | | | | | | | | |
| | | | | | | | | |
| Hence, Moderately ductile flanges and web allowed. | | | | | | | | |
| $\frac{b_f}{2t_f}$ | 6.379310345 | < | $\lambda_{md}$ | 9.184968 | OK | | | |
| $\frac{h}{t_w}$ | 34.76635514 | < | $\lambda_{hw}$ | 36.051 | OK | | | |
| Hence, Section is Highly ductile | | | | | | | | |
| | | | | | | | | |
| Loading and amplification | | | | | | | | |
| | | | | | | | | |
| Loads | Dead Load | Live Load | Eq | | Load combination | Axial Load | Shear Force | Moment |
| Axial | 0 | 0 | 0 | | 0.72D+1.3E | 0.00 | 21.80 | -2446.75 |
| Shear | 2.83 | 1.59 | 15.2 | | 0.72D-1.3E | 0.00 | -17.72 | 2542.65 |
| Moment | 66.6 | 34.9 | -1919 | | 1.38D+1.3E+1L | 0.00 | 25.26 | -2367.89 |
| | | | | | 1.38D-1.3E+1L | 0.00 | -14.26 | 2621.51 |
| Nominal shear strength of link(Vn) | | | 160.083 | kips | | | | |
| 0.88*1.25*Ry*Vn | | | 193.7004 | kips | | | | |
| Shear force in link(Vqe) | | | 106 | kips | | | | |
| Overstrength Factor | | | 1.827363 | | | | | |
| Amplified with overstrength factor | | | | | | | | |
| Loads | Dead Load | Live Load | Eq | | Load combination | Axial Load | Shear | Moment |
| Axial | 0 | 0 | 0 | | 0.72D+1.3E | 0.00 | 38.15 | -4510.77 |
| Shear | 2.83 | 1.59 | 27.77591 | | 0.72D-1.3E | 0.00 | -34.07 | 4606.67 |
| Moment | 66.6 | 34.9 | -3506.71 | | 1.38D+1.3E+1L | 0.00 | 41.60 | -4431.91 |
| | | | | | 1.38D-1.3E+1L | 0.00 | -30.61 | 4685.53 |
| | | | | | | | | |
| Pu | 0 | | | L | 126 | in | | |
| Vu | 41.60408393 | | | KL/r | 47.54716981 | | 4.71*(E/fy) | 113.43182 |
| Mu | 4685.529346 | | | Fe | 126.6042838 | | | |
| | | | | Fcr | 43.06049926 | | | |
| Pc | 994.0516254 | kips | | Pc | 1104.501806 | | | |
| Mc | 9495 | in-K | | | | | | |
| Vc | 243.5427 | kips | | | | | | |
| Pr/Pc | 0 | | | | | | | |
| Mr/Mc | 0.493473338 | | | | | | | |
| | | | | | | | | |
| P-M Ratio | 0.493473338 | <1 | OK | | | | | |
| | | | | | | | | |
| Hence, the beam is Adequate | | | | | | | | |

*Figure 3. 17 Sample Outside Beam Design*

| | | | | | | | | |
|---|---|---|---|---|---|---|---|---|
| Column Design | | | | | | | | |
| | | | | | | | | |
| Compactness Check | | | | | | | | |
| W14*132 | | | | A992 | | | | |
| h | 14.7 | in | Fy | 50 | ksi | Ry | 1.1 | |
| $b_f$ | 14.7 | in | Fu | 65 | ksi | Rt | 1.1 | |
| $t_f$ | 1.03 | in | Fye | 55 | ksi | E | 29000 | ksi |
| $t_w$ | 0.645 | in | Fue | 71.5 | ksi | ry | 3.76 | in |
| Zx | 234 | in3 | Ag | 38.8 | in2 | | | |
| $\frac{b_f}{2t_f}$ | 7.13592233 | < | $\lambda_{pf}$ | 9.149962 | OK | | | |
| | | | | | | | | |
| $\frac{h}{t_w}$ | 22.79069767 | < | $\lambda_{pw}$ | 90.55209 | OK | | | |
| | | | | | | | | |
| Hence, Section is Compact. | | | | | | | | |
| | | | | | | | | |
| | | | | | | | | |
| Hence, Moderately ductile flanges and web allowed. | | | | | | | | |
| $\frac{b_f}{2t_f}$ | 7.13592233 | < | $\lambda_{hd}$ | 7.347974 | OK | | | |
| | | | | | | | | |
| $\frac{h}{t_w}$ | 22.79069767 | < | $\lambda_{hw}$ | 36.051 | OK | | | |
| | | | | | | | | |
| Hence, Section is Highly ductile | | | | | | | | |
| | | | | | | | | |
| Loading and amplification | | | | | | | | |
| | | | | | | | | |
| Loads | Dead Load | Live Load | Eq | | Load combination | Axial Load | Shear Force | Moment |
| Axial | 96.4 | 45.3 | -148 | | 0.72D+1.3E | -122.99 | 9.74 | 1402.61 |
| Shear | -0.052 | -0.03 | 7.52 | | 0.72D-1.3E | 261.81 | -9.81 | -1394.99 |
| Moment | 5.2848 | 3.0648 | 1076 | | 1.38D+1.3E+1L | -14.07 | 9.67 | 1409.16 |
| | | | | | 1.38D-1.3E+1L | 370.73 | -9.88 | -1388.44 |
| Nominal shear strength of link(Vn) | | | 160.083 | kips | | | | |
| 1.25*Ry*Vn | | | 220.1141 | kips | | | | |
| Shear force in link(Vqe) | | | 106 | kips | | | | |
| Overstrength Factor | | | 2.076548 | | | | | |
| Amplified with overstrength factor | | | | | | | | |
| Loads | Dead Load | Live Load | Eq | | Load combination | Axial Load | Shear | Moment |
| Axial | 96.4 | 45.3 | -307.329 | | 0.72D+1.3E | -330.12 | 20.26 | 2908.48 |
| Shear | -0.052 | -0.03 | 15.61564 | | 0.72D-1.3E | 468.94 | -20.34 | -2900.87 |
| Moment | 5.2848 | 3.0648 | 2234.366 | | 1.38D+1.3E+1L | -221.20 | 20.20 | 2915.03 |
| | | | | | 1.38D-1.3E+1L | 577.86 | -20.40 | -2894.32 |
| | | | | | | | | |
| | | | | | | | | |
| Pu | 577.8599024 | | | L | 168 | in | | |
| Vu | 20.40209666 | | | KL/r | 29.04255319 | | 4.71*(E/fy) | 113.432 |
| Mu | 2915.033655 | | | Fe | 339.3346094 | | | |
| | | | | Fcr | 47.28892836 | | | |
| Pc | 1486.19644 | kips | | Pc | 1651.329378 | | | |
| Mc | 10530 | in-K | | | | | | |
| Vc | 220.1256 | kips | | | | | | |
| Pr/Pc | 0.388817983 | | | | | | | |
| Mr/Mc | 0.276831306 | | | | | | | |
| | | | | | | | | |
| P-M Ratio | 0.634890255 | <1 | OK | | | | | |
| | | | | | | | | |
| Hence, the Column is Adequate | | | | | | | | |

*Figure 3. 18 Sample Column Design*

# Chapter 4: Nonlinear Time History Analysis of EBF Seismic Response

This chapter discusses non-linear analysis of EBF prototype buildings and predicts EBFs responses at design earthquake loading level. Although the seismic design in Chapter 3 is acceptable for design, non-linear analysis technique is more advanced in representing the EBF structural features and its predictions are more accurate in nonlinear response range. However, this enhanced accuracy comes with a price; non-linear analysis is more complex and requires expertise on all the structural components behaviors. Overall, there are two main types of nonlinearity, material, and geometric nonlinearity.

First, Material nonlinearity occurs when the material has a non-linear stress-strain response. In contrast, the seismic design in Chapter 3 assumed a linear stress-strain material relationship to simplify structural analysis. Nevertheless, no material is perfectly elastic and assuming elastic behavior impacts the analysis's accuracy to predict responses. Further, the material's stress-strain variation is directly related to the force-displacement relationship for the structure. Consequently, the force-displacement relationship becomes non-linear. The nonlinearity of the force-displacement curve indicates a change in the stiffness of the structure. Incorporating this stiffness variation in analysis results in better prediction. For steel, the stress-strain curve remains elastic for small displacements and is non-linear for large displacements. Figure 4.1 shows the stress-strain curve for mild steel. In general, the curve is linear until point A as shown in the figure, the proportional limit, and is non-linear beyond this point. Likewise, the slope is steep in the linear part and is relatively flat later in the non-linear part. The

slope of this stress-strain curve is called material rigidity. This sudden change of the slope from steep to flat indicates a significant reduction of material rigidity. Additionally, lateral stiffness of SLRFs is directly proportional to this material rigidity. Hence, the significant reduction in material rigidity decreases the lateral stiffness of SLRFs. Subsequently, reduction in lateral stiffness results in large displacement and impacts the structure's dynamic properties. Hence, this study incorporates material nonlinearity to improve the accuracy of structural analysis. This study uses a combination of linear lines to approximate the general non-linear diagrams, which is quite common. This study uses a bi-linear curve to represent the material stress-strain curve, Figure 4.2. In this study, all loads are applied in steps, and OpenSees revises the structure stiffness matrix after each load step. Second, geometric nonlinearity occurs when the equations of motion are applied to a deformed geometry rather than an undeformed geometry. It is essential to consider geometric nonlinearity when the applied load causes large displacement and/or rotation, large strain, or a combo of both. Here, Lean-on columns are introduced to account for geometric nonlinearity.

Similar to Linear analysis, there are two types of non-linear analysis, non-linear static and non-linear dynamic. The non-linear dynamic analysis gives the best prediction among all the analysis. Hence, this study uses a nonlinear response history analysis to predict the structure's response. Nonlinear response history analysis generates story drift ratios, floor accelerations, and floor velocities, which are used to predict the structure's performance. This study uses OpenSees [30] to perform nonlinear response history analysis. Opensees stands for the open system for earthquake engineering

simulation. It is an opensource software which allows its users to create finite element applications for simulating structural systems subjected to earthquakes.

## *4.1 Nonlinear Modelling*

A numerical model to accurately represent the nonlinear behavior of EBFs was modelled in OpenSees [30]. In OpenSees, the steel material was modelled using the predefined uniaxial Giuffre-Menegotto-Pinto steel material object with isotropic strain hardening [31], Steel02. This material object requires at least three parameters: Yield strength $F_y$, Young's modulus E, and strain hardening ratio b. Table 4.1 shows the Steel02 parameters used in this study. Next, a two-dimensional model having three kinematic degrees of freedom for each node was modelled in OpenSees. Each of these nodes are connected with different elements. Figure 4.3 describes the different types of elements used to model EBFs in OpenSees. In this study, short links behavior is represented numerically using a force-based fiber element to model axial and flexural behavior, along with an uncoupled shear behavior. Assuming no M-V interaction is quite reasonable as discussed in Chapter 1. An approach to model links is derived from O'Reilly et al. [32]. O'Reilly et al. proposes to adopt the Giuffre Menegotto-Pinto hysteresis rule for the shear hinge replacing the yield force input with the link yield force ($V_y$), the initial elastic tangent with $GA_v$, where G is the steel shear modulus and $A_v$ the shear area of the link, along with a strain hardening ratio of 0.01. Additionally, the elastic-plastic transition parameters (R0, cR1 and cR2) are taken as 20, 0.925, and 0.01, respectively. Further, the isotropic hardening parameters (a1, a2, a3, and a4) are taken as 0.02, 1, 0.02, and 1, respectively. Finally, this material is assigned to the fiber-element using the section aggregator tool in OpenSees. Further, O'Reilly et al. validated

the link modelling parameters with existing experimental data. Figure 4.4 shows the comparison between digitized experimental results from Mansour [33] and Okazaki et al. [34] and the proposed link model results. From figure it is evident that the proposed model replicates the experimental results very well. Hence, this model was used throughout this study. Next, a force-based fiber element was used to model the columns and the outside beams, whereas a fiber-based truss element was used to model the braces. This study assumes a pinned connection between the outer beam and column. This is achieved in OpenSees using a zero-length member element having high stiffness in translation and low stiffness for rotation. The braces are also assumed to be pinned, which is automatically achieved as a truss element is used to model braces. Lean-on columns were also modelled using truss element having a considerable cross-sectional area. Overall, this completes the EBFs modelling in OpenSees and the next step is to determine the loading for the EBFs. Loading and load combination for nonlinear analysis is different from the elastic analysis. Gravity loads based on expected dead and live loading are considered in the analysis, along with a quarter of seismic mass of the structure. The gravity combination for analysis is based on FEMA P695 recommendation [17], and is given by:

$$1.05D + 0.25L \qquad \text{Eq 30}$$

where D is the nominal dead load of the structure and the superimposed dead load, and L is the nominal live load. Expected live loads typically include about 25% of the unreduced design live load. In OpenSees, these loads are applied in steps and with each step the stiffness matrix of the structure is revised. Further, time history analysis is performed using the stiffness matrix resulting after the application of gravity loads.

Rayleigh damping is used to model the damping for the structure. Generally, Rayleigh damping method requires two coefficients which are applied to the mass and stiffness matrix, respectively. The first two modes and a common damping ratio of 5% were used to determine the damping coefficients. All the nine EBFs in this study were modelled using the above recommendations. After modelling, modal analysis was performed in OpenSees. Using modal analysis results, Table 4.2 shows the time periods of the first three modes for each EBFs. Additionally, Figure 4.5 to 4.13 display the modal shapes of the first three modes for each EBFs.

## *4.2 Ground Motion Selection and Scaling*

Now that the model is ready, earthquake hazard needs to be determined. Generally, Earthquake hazards are defined in terms of earthquake shaking. Primarily, earthquake shaking occurs in three dimensions. The three dimensions comprise of the two orthogonal horizontal components and one vertical component. Even though there is a vertical component of earthquake shaking, it does not contribute to earthquake damage as compared to the contribution from the other two horizontal dimensions for the considered EBF structural configurations. Consequently, the vertical component has minimal impact on the building's seismic performance. Therefore, only horizontal earthquakes are considered in this study.

After modelling the EBFs, this study requires ground motions to perform response history analysis. This section discusses the selection and scaling of ground motions for this study. Overall, the primary intent of ground motion selection and scaling is to obtain a set of ground motions that can produce unbiased estimates of structural

response after performing a nonlinear response history analysis. According to FEMA P-58, the fundamental steps for ground motion selection and scaling include:

1. Development of a target response spectrum.
2. Selection of a suite of ground motions.
3. Scaling of motions for consistency with the target spectrum.

This study uses an intensity-based approach for performance assessment. This approach evaluates the structure's probable performance assuming the structure is subjected to a specific earthquake shaking intensity. According to FEMA P-58, this type of assessment can be used to assess the performance of a building for design earthquake shaking consistent with a building code response spectrum. Hence, this study uses the design response spectra described in Chapter 3 as the target spectrum.

As per FEMA P-58, ground motions should be selected such that, on average, they reasonably match the target spectrum over a period range. Further, FEMA recommends using at least seven ground motion pairs if the spectral shape of the selected motions matches well with the target spectrum; else, FEMA recommends using eleven or more pairs of motions for a reasonable estimate of median response. Here, the ground motions' spectral shape has not been matched with the target spectrum; hence, eleven or more pairs of motions need to be selected. Therefore, this study uses a set of 22 Far-Field records from FEMA P695 [17] to perform nonlinear time history analysis. Table 4.3 shows a summary of all these records. The twenty-two pairs record set are from sites located at least 10 km from fault rupture. Figure 4.14 shows the 44 individual response spectra (i.e., 22 records, two components each) of the Far-Field record set, the median response spectrum, and spectra representing one standard deviation and two

standard deviations above the median. Further, the sets include records from soft rock and stiff soil sites (predominantly Site Class C and D conditions) and shallow crustal sources (predominantly strike-slip and thrust mechanisms).

Finally, the selected ground motions need to be scaled. According to FEMA P-695, Scaling involves two steps. First, all the records are normalized using their respective peak ground velocity. FEMA P-695 states that normalization of records removes unwarranted variability between records due to inherent differences in event magnitude, distance to source and site conditions without eliminating overall record to record variability. Although FEMA P-695 describes the normalization method briefly, this study uses readily available normalization records for the Far-field set from ATC 63 [35]. Second, these normalized ground motions are collectively scaled to match a design response spectrum at the maximum allowed time period, $T_U$, of the structure being analyzed. In this study, the spectral acceleration corresponding to time periods $T_U$-0.2, $T_U$-0.1, $T_U$, $T_U$+0.1, $T_U$+0.2 were determined for both the normalized ground motion spectra and design response spectrum. After both the spectral accelerations were determined, a factor required to match the ground response spectra to the design response spectrum for each of these points were calculated. Finally, a single scale factor was derived by averaging the five scale factors calculated in the previous step. Ultimately, the scale factors were applied to the normalized ground motions. Table 4.4 shows a sample calculation of ground motion scaling for the four-story EBFs frame in California.

Finally, using these ground motions response time history analysis is performed in OpenSees in compliance with procedure stipulated in ASCE 7-10 [15]. For each ground

motion analyzed, individual response parameters consisting of the maximum value of the individual member forces, member inelastic deformations and story drifts at each story were determined. Since there are more than 7 ground motions, the average of these forces and deformations were used to re-check the structure design. Sections shown in Table 1.14 to 1.17 are the final revised sectional sizes after response time history analysis. Other earthquake demand parameters such as velocity and acceleration were also recorded.

## *4.3 Analyze Building Response*

Although this section is an essential step in FEMA P-58 procedure, it has been described in this chapter. After the ground motions are scaled, they are used to perform structural analysis to generate building response. This structural analysis provides median estimates of key earthquake demand parameters, such as floor accelerations, floor velocity, story drift ratios, and residual drift ratios, that can predict structural and nonstructural damage. For structural analysis, FEMA P-58 describes two alternative procedures, Nonlinear Response History Analysis and Simplified analysis. In general, the former analysis considers nonlinear structural models for analysis, whereas the latter considers linear structural models. Although the linear model is acceptable, the nonlinear model attempts to capture structures' actual behavior and is more precise. Hence, this study uses Nonlinear Response History Analysis for structural analysis. For nonlinear response history analysis, FEMA recommends including nonlinear representation of force-deformation behavior of the components and sufficient number of ground motions to obtain valid estimates of structure’s response. Both the nonlinear modelling parameters and the number of ground motions (22 pairs) were discussed

earlier in section 4.1. Also, the use of OpenSees for structural analysis was discussed earlier. Overall, OpenSees generates typical output from nonlinear response history analysis such as nodal displacement history, nodal acceleration history, nodal velocity history, nonlinear deformation demands and component forces. Only story drift ratio, link rotation angle, and floor acceleration are of concern here as these EDPs are enough to predict the damage states for all the structural and nonstructural components used in this study. Further, all of the aforementioned EDPs can be extracted directly from OpenSees except for the story drift ratio. Instead, Story drift ratio is calculated indirectly using the story lateral displacement and story height. The drift ratio is the difference in displacement at adjacent floor levels divided by the story height. Next, for each of the 22 pairs of ground motions, the peak responses of EDPs are recorded using OpenSees. Table 4.5 to 4.8 show the peak responses of EDPs recorded for the 4 story EBFs in the California location. Also, the maximum inter- story drift ratio and the maximum floor acceleration for each of the EBFs can be seen in Figure 4.17 to 4.34.

Although modern structural analysis has advanced over the years, it is still not precise, and some extent of uncertainty is inevitable. Hence, FEMA P-58 procedure attempts to capture some uncertainties of structural analysis. The methodology takes in account the following uncertainties:

1. Modelling uncertainty
2. Record-to-record variability
3. Ground-motion variability

First, inaccuracies in component modelling, damping and mass assumptions result in modelling uncertainty, $\beta_m$. According to FEMA P-58, $\beta_m$ is associated with the level of building definition and construction quality assurance, $\beta_c$, and the quality and completeness of the nonlinear analysis model, $\beta_q$. Moreover, the total modeling dispersion can be estimated as follows:

$$\beta_m = \sqrt{{\beta_c}^2 + {\beta_q}^2} \qquad \text{Eq 34}$$

Where $\beta_c$ and $\beta_q$ are determined from Table 4.9 and Table 4.10, respectively. For this study, $\beta_c$ is taken as 0.1 as all the EBFs qualify as superior quality, new buildings. Similarly, $\beta_q$ is taken as 0.25 to represent an average quality model as this study uses a bi-linear curve instead of the full backbone curve. Therefore, using $\beta_c$ and $\beta_q$ in the equation above, $\beta_m$ is 0.27. Second, as this study uses 22 pairs of ground motions for analysis, it is safe to assume accuracy against record-to-record variability. Hence, record to record variability was not considered here. Last, according to FEMA P-58, Ground motion variability is only essential for scenario-based assessment. Since this study uses an intensity-based approach it is neglected here.

Another essential demand parameter for performance assessment is Residual drift. Residual drift is the permanent deformation of the building after an earthquake. This permanent drift plays a vital role in determining the post-earthquake safety of a building and the economic feasibility of repair. In the case of large residual drifts, the cost of repair may end up being equal to the replacement cost or a significant percentage of the replacement cost. Hence, the building is deemed uneconomical to repair. Whereas modest residual drifts are also expensive and may require adjustments to nonstructural components like re-alignment of elevator rails and building facades and lead to

concerns that a building is unsafe for post-earthquake inspection or repair. Therefore, it is essential to predict residual drifts accurately. Accurate residual drift prediction requires advanced component models, accurate hysteretic response, and a large number of ground motions pairs. All of these requirements for accurate prediction of residual drifts are computationally complex and not practical. Hence, the following equations were developed from different analytical studies to estimate the median residual drift ratio, $\Delta_r$, as a function of the peak transient response of the structure:

$$\Delta_r = 0 \; for \; \Delta \leq \Delta_y \quad \text{Eq 35}$$

$$\Delta_r = 0.3(\Delta - \Delta_y) \; for \; \Delta_y < \Delta < 4\Delta_y \quad \text{Eq 36}$$

$$\Delta_r = (\Delta - 3\Delta_y) \; for \; \Delta \geq \Delta_y \quad \text{Eq 37}$$

where $\Delta$ is the median story drift ratio calculated by analysis, and $\Delta_y$ is the median story drift ratio calculated at yield. The yield drift ratio, $\Delta_y$, is associated with significant yielding in the structure. For this study, $\Delta_y$ is assumed to be equal to the drift corresponding to 0.08 rotation in the shear links. Table 29 shows the residual drift calculation for the 4 story EBFs in California. Although PACT assessment is discussed later in Chapter 5, this section also describes the structural analysis input in PACT. Overall, the structural analysis and residual drift data are fed into PACT. Figure 4.15 and 4.16 show the structural analysis and Residual drift tabs in PACT, filled with inputs for the 4 story EBFs in California.

*Table 4.1 Steel02 Material Parameters*

| Element | Fy(ksi) | E(ksi) | b |
|---|---|---|---|
| Columns Link and outside Beams | 50 | 29,000 | 0.02 |
| Braces | 46 | 29,000 | 0.02 |

*Table 4. 2 Summary of Earthquake Event and Recording Station Data for the Far- Field Record Set Adapted from FEMA P-695 [17]*

| | Earthquake | | | Recording Station | |
|---|---|---|---|---|---|
| ID No. | M | Year | Name | Name | Owner |
| 1 | 6.7 | 1994 | Northridge | Beverly Hills- Mulhol | USC |
| 2 | 6.7 | 1994 | Northridge | Canyon Country- WLC | USC |
| 3 | 7.1 | 1999 | Duzce, Turkey | Bolu | ERD |
| 4 | 7.1 | 1999 | Hector Mine | Hector | SCSN |
| 5 | 6.5 | 1979 | Imperial Valley | Delta | UNAMUCSD |
| 6 | 6.5 | 1979 | Imperial Valley | El Centro Array #11 | USGS |
| 7 | 6.9 | 1995 | Kobe, Japan | Nishi-Akashi | CUE |
| 8 | 6.9 | 1995 | Kobe, Japan | Shin-Osaka | CUE |
| 9 | 7.5 | 1999 | Kocaeli, Turkey | Duzce | ERD |
| 10 | 7.5 | 1999 | Kocaeli, Turkey | Arcelik | KOERI |
| 11 | 7.3 | 1992 | Landers | Yermo Fire Station | CDMG |
| 12 | 7.3 | 1992 | Landers | Coolwater | SCE |
| 13 | 6.9 | 1989 | Loma Prieta | Capitola | CDMG |
| 14 | 6.9 | 1989 | Loma Prieta | Gilroy Array #3 | CDMG |
| 15 | 7.4 | 1990 | Manjil, Iran | Abbar | BHRC |
| 16 | 6.5 | 1987 | Supersition Hills | El Centro Imp. Co. | CDMG |
| 17 | 6.5 | 1987 | Supersition Hills | Poe Road (temp) | USGS |
| 18 | 7 | 1992 | Cape Mendocino | Rio Dll Overpass | CDMG |
| 19 | 7.6 | 1999 | Chi-Chi, Taiwan | CHY101 | CWB |
| 20 | 7.6 | 1999 | Chi-Chi, Taiwan | TCU045 | CWB |
| 21 | 6.6 | 1971 | San Fernando | LA- Holywoord Stor | CDMG |
| 22 | 6.5 | 1976 | Friuli, Italy | Tolmezzo | -- |

*Table 4. 3 Sample ground motion scaling using Excel for 4-story EBF (California Location)*

| | | | | | | | | | | | | | | | | | | | | | |
|---|---|---|---|---|---|---|---|---|---|---|---|---|---|---|---|---|---|---|---|---|---|
| | | | 1.52 | | | | | | | | | | | | | | | | | | |
| Given | | | 0.924 | | | | Scaled Spectra | | | | | | | | | | | | | | |
| Sms | 1.013 | g | | | | | | | | | | | | | | | | | | | |
| Sm1 | 0.616 | g | Generate Scale Factor | | | | | | | | | | | | | | | | | | |
| | | | | | | | | | | | | | | | | | | | | | |
| To | 0.122 | s | | | | | | | | | | | | | | | | | | | |
| Ts | 0.608 | s | | | | | | | | | | | | | | | | | | | |
| | | | | | | | | | | | | | | | | | | | | | |
| Tn | 0.860 | s | | | | | | | | | | | | | | | | | | | |
| | | PEER-NGA Number: | | 953 | 953 | 960 | 960 | 1602 | 1602 | 1787 | 1787 | 169 | 169 | 174 | 174 | 1111 | 1111 | 1116 | 1116 | 1158 | 1158 |
| | Period | Sa | EQ ID: | 120111 | 120112 | 120121 | 120122 | 120411 | 120412 | 120521 | 120522 | 120611 | 120612 | 120621 | 120622 | 120711 | 120712 | 120721 | 120722 | 120811 | 120812 |
| Tn-0.2 | 0.66 | 0.933 | | 0.5521 | 0.688115 | 0.854478 | 0.982617 | 0.576207 | 0.750015 | 0.355864 | 0.484011 | 0.720793 | 0.982902 | 0.421175 | 0.512209 | 0.951255 | 1.038945 | 0.985727 | 0.747524 | 0.458184 | 0.450289 |
| Tn-0.1 | 0.76 | 0.811 | | 0.570264 | 0.563352 | 0.513327 | 0.759127 | 0.569929 | 0.827269 | 0.348605 | 0.361092 | 0.698249 | 0.687888 | 0.366052 | 0.495014 | 0.661639 | 0.809585 | 0.571537 | 0.654425 | 0.334336 | 0.378904 |
| Tn | 0.86 | 0.716 | | 0.885444 | 0.79088 | 0.359827 | 0.457207 | 0.505358 | 0.864701 | 0.321819 | 0.37239 | 0.587024 | 0.648086 | 0.290135 | 0.267931 | 0.591786 | 0.459527 | 0.616663 | 0.430103 | 0.310899 | 0.386069 |
| Tn+0.1 | 0.96 | 0.642 | | 0.733607 | 0.658503 | 0.350672 | 0.532294 | 0.499488 | 0.783484 | 0.32696 | 0.384997 | 0.484822 | 0.625253 | 0.236765 | 0.194224 | 0.401473 | 0.328374 | 0.43029 | 0.269943 | 0.310004 | 0.416273 |
| Tn+0.2 | 1.06 | 0.581 | | 0.606977 | 0.590505 | 0.257366 | 0.478436 | 0.404198 | 0.636588 | 0.456122 | 0.476272 | 0.26725 | 0.510802 | 0.245677 | 0.273903 | 0.293101 | 0.260445 | 0.371459 | 0.270547 | 0.270295 | 0.421236 |
| | | | | | | | | | | | | | | | | | | | | | |
| | | | | Scale | | | | | | | | | | | | | | | | | |
| | Period | Sa | | | | | | | | | | | | | | | | | | | |
| Tn-0.2 | 0.66 | 0.933 | | 1.690517 | 1.356363 | 1.092284 | 0.949845 | 1.619788 | 1.244419 | 2.622726 | 1.928332 | 1.29487 | 0.949569 | 2.216022 | 1.822172 | 0.98116 | 0.898347 | 0.946848 | 1.248567 | 2.037026 | 2.072741 |
| Tn-0.1 | 0.76 | 0.811 | | 1.421318 | 1.438756 | 1.578966 | 1.067708 | 1.422154 | 0.979761 | 2.325056 | 2.244651 | 1.160798 | 1.178282 | 2.214238 | 1.63738 | 1.225029 | 1.001162 | 1.418152 | 1.238531 | 2.424289 | 2.139133 |
| Tn | 0.86 | 0.716 | | 0.808949 | 0.905674 | 1.99062 | 1.566639 | 1.417371 | 0.828355 | 2.225722 | 1.923466 | 1.220187 | 1.105223 | 2.468782 | 2.67337 | 1.210368 | 1.558732 | 1.161541 | 1.665365 | 2.3039 | 1.855311 |
| Tn+0.1 | 0.96 | 0.642 | | 0.874673 | 0.974433 | 1.82982 | 1.205473 | 1.284649 | 0.818992 | 1.962524 | 1.66668 | 1.323511 | 1.026251 | 2.710138 | 3.303745 | 1.59828 | 1.954074 | 1.491241 | 2.377049 | 2.069868 | 1.541457 |
| Tn+0.2 | 1.06 | 0.581 | | 0.95742 | 0.984128 | 2.257996 | 1.214649 | 1.437741 | 0.912885 | 1.274072 | 1.22017 | 2.17449 | 1.137686 | 2.36543 | 2.121673 | 1.982702 | 2.231307 | 1.564456 | 2.147989 | 2.149994 | 1.379589 |
| | | | Avg | 1.150575 | 1.131871 | 1.749937 | 1.200863 | 1.43634 | 0.956882 | 2.08202 | 1.79666 | 1.434771 | 1.079402 | 2.394922 | 2.311668 | 1.399508 | 1.528725 | 1.316448 | 1.7355 | 2.197015 | 1.797646 |

*Table 4. 4 OpenSees Peak Acceleration record (in g) for 4 story EBF (California)*

Acceleration in terms of g

| California | 1 | 2 | 3 | 4 | 5 | 6 | 7 | 8 | 9 | 10 | 11 | 12 | 13 | 14 | 15 | 16 | 17 | 18 | 19 | 20 | 21 | 22 | 23 | 24 | 25 | 26 | 27 | 28 | 29 | 30 | 31 | 32 | 33 | 34 | 35 | 36 | 37 | 38 | 39 | 40 | 41 | 42 | 43 | 44 |
|---|---|---|---|---|---|---|---|---|---|---|---|---|---|---|---|---|---|---|---|---|---|---|---|---|---|---|---|---|---|---|---|---|---|---|---|---|---|---|---|---|---|---|---|---|
| 10F | 0 | 0 | 0 | 0 | 0 | 0 | 0 | 0 | 0 | 0 | 0 | 0 | 0 | 0 | 0 | 0 | 0 | 0 | 0 | 0 | 0 | 0 | 0 | 0 | 0 | 0 | 0 | 0 | 0 | 0 | 0 | 0 | 0 | 0 | 0 | 0 | 0 | 0 | 0 | 0 | 0 | 0 | 0 | 0 |
| 9F | 0 | 0 | 0 | 0 | 0 | 0 | 0 | 0 | 0 | 0 | 0 | 0 | 0 | 0 | 0 | 0 | 0 | 0 | 0 | 0 | 0 | 0 | 0 | 0 | 0 | 0 | 0 | 0 | 0 | 0 | 0 | 0 | 0 | 0 | 0 | 0 | 0 | 0 | 0 | 0 | 0 | 0 | 0 | 0 |
| 8F | 0 | 0 | 0 | 0 | 0 | 0 | 0 | 0 | 0 | 0 | 0 | 0 | 0 | 0 | 0 | 0 | 0 | 0 | 0 | 0 | 0 | 0 | 0 | 0 | 0 | 0 | 0 | 0 | 0 | 0 | 0 | 0 | 0 | 0 | 0 | 0 | 0 | 0 | 0 | 0 | 0 | 0 | 0 | 0 |
| 7F | 0 | 0 | 0 | 0 | 0 | 0 | 0 | 0 | 0 | 0 | 0 | 0 | 0 | 0 | 0 | 0 | 0 | 0 | 0 | 0 | 0 | 0 | 0 | 0 | 0 | 0 | 0 | 0 | 0 | 0 | 0 | 0 | 0 | 0 | 0 | 0 | 0 | 0 | 0 | 0 | 0 | 0 | 0 | 0 |
| 6F | 0 | 0 | 0 | 0 | 0 | 0 | 0 | 0 | 0 | 0 | 0 | 0 | 0 | 0 | 0 | 0 | 0 | 0 | 0 | 0 | 0 | 0 | 0 | 0 | 0 | 0 | 0 | 0 | 0 | 0 | 0 | 0 | 0 | 0 | 0 | 0 | 0 | 0 | 0 | 0 | 0 | 0 | 0 | 0 |
| 5F | 0 | 0 | 0 | 0 | 0 | 0 | 0 | 0 | 0 | 0 | 0 | 0 | 0 | 0 | 0 | 0 | 0 | 0 | 0 | 0 | 0 | 0 | 0 | 0 | 0 | 0 | 0 | 0 | 0 | 0 | 0 | 0 | 0 | 0 | 0 | 0 | 0 | 0 | 0 | 0 | 0 | 0 | 0 | 0 |
| 4F | 0.38132 | 0.435125 | 0.520075 | 0.546298 | 0.536871 | 0.424144 | 0.503727 | 0.512756 | 0.489476 | 0.433857 | 0.54517 | 0.599024 | 0.510148 | 0.537356 | 0.385992 | 0.526164 | 0.489143 | 0.450246 | 0.587586 | 0.507758 | 0.371595 | 0.483745 | 0.538578 | 0.472832 | 0.594772 | 0.515634 | 0.554622 | 0.546046 | 0.595614 | 0.541161 | 0.493321 | 0.446438 | 0.577193 | 0.494632 | 0.458115 | 0.556807 | 0.390433 | 0.368325 | 0.625906 | 0.517101 | 0.528458 | 0.559442 | 0.541244 | 0.521272 |
| 3F | 0.333916 | 0.355654 | 0.450696 | 0.485522 | 0.353142 | 0.365823 | 0.431846 | 0.423357 | 0.449248 | 0.362799 | 0.495276 | 0.444004 | 0.389178 | 0.447141 | 0.326363 | 0.41863 | 0.456962 | 0.313402 | 0.491627 | 0.387387 | 0.316038 | 0.416597 | 0.417694 | 0.409427 | 0.369273 | 0.46913 | 0.375813 | 0.455887 | 0.408159 | 0.48385 | 0.283316 | 0.421648 | 0.379984 | 0.372997 | 0.363756 | 0.415317 | 0.318534 | 0.304418 | 0.51927 | 0.447902 | 0.496286 | 0.404752 | 0.386035 | 0.441829 |
| 2F | 0.280593 | 0.387195 | 0.518248 | 0.427016 | 0.617797 | 0.29988 | 0.447507 | 0.592242 | 0.371816 | 0.354124 | 0.733797 | 0.74857 | 0.685153 | 0.519043 | 0.29342 | 0.290633 | 0.329645 | 0.501918 | 0.533707 | 0.540968 | 0.343576 | 0.448437 | 0.781081 | 0.474383 | 0.721965 | 0.551299 | 0.863483 | 0.469326 | 0.618325 | 0.640707 | 0.569752 | 0.411941 | 0.626829 | 0.614975 | 0.350929 | 0.999111 | 0.306288 | 0.284808 | 0.841596 | 0.351594 | 0.550016 | 0.552859 | 0.68101 | 0.48795 |
| 1F | 0.283613 | 0.421483 | 0.564434 | 0.664095 | 0.58216 | 0.339718 | 0.536983 | 0.596134 | 0.410826 | 0.418919 | 0.680145 | 0.785905 | 0.78238 | 0.716563 | 0.303175 | 0.396078 | 0.487614 | 0.448294 | 0.875294 | 0.482299 | 0.379089 | 0.453537 | 0.657758 | 0.61661 | 0.569861 | 0.614266 | 1.095105 | 0.512504 | 0.656713 | 0.517262 | 0.394716 | 0.669214 | 0.638951 | 0.555529 | 0.466535 | 1.160508 | 0.288661 | 0.276917 | 0.917362 | 0.577053 | 0.510316 | 0.817048 | 0.732759 | 0.600218 |
| GF | 0.311348 | 0.380447 | 0.596659 | 0.481305 | 0.657447 | 0.495083 | 0.603559 | 0.660446 | 0.44738 | 0.497041 | 0.883776 | 0.884568 | 0.73712 | 0.794763 | 0.351911 | 0.404199 | 0.472012 | 0.442817 | 1.167915 | 0.717971 | 0.377988 | 0.396413 | 0.720799 | 0.533592 | 0.637835 | 0.661606 | 1.084721 | 0.670998 | 0.774072 | 0.733512 | 0.564717 | 0.839016 | 0.841565 | 0.61145 | 0.477914 | 0.931973 | 0.44996 | 0.354898 | 0.834556 | 0.650591 | 0.6288 | 0.831128 | 0.910543 | 0.505203 |

*Table 4. 5 OpenSees Peak link rotation angle for 4 story EBF (California)*

| California | 1 | 2 | 3 | 4 | 5 | 6 | 7 | 8 | 9 | 10 | 11 | 12 | 13 | 14 | 15 | 16 | 17 | 18 | 19 | 20 | 21 | 22 | 23 | 24 | 25 | 26 | 27 | 28 | 29 | 30 | 31 | 32 | 33 | 34 | 35 | 36 | 37 | 38 | 39 | 40 | 41 | 42 | 43 | 44 |
|---|---|---|---|---|---|---|---|---|---|---|---|---|---|---|---|---|---|---|---|---|---|---|---|---|---|---|---|---|---|---|---|---|---|---|---|---|---|---|---|---|---|---|---|---|
| 10F | 0 | 0 | 0 | 0 | 0 | 0 | 0 | 0 | 0 | 0 | 0 | 0 | 0 | 0 | 0 | 0 | 0 | 0 | 0 | 0 | 0 | 0 | 0 | 0 | 0 | 0 | 0 | 0 | 0 | 0 | 0 | 0 | 0 | 0 | 0 | 0 | 0 | 0 | 0 | 0 | 0 | 0 | 0 | 0 |
| 9F | 0 | 0 | 0 | 0 | 0 | 0 | 0 | 0 | 0 | 0 | 0 | 0 | 0 | 0 | 0 | 0 | 0 | 0 | 0 | 0 | 0 | 0 | 0 | 0 | 0 | 0 | 0 | 0 | 0 | 0 | 0 | 0 | 0 | 0 | 0 | 0 | 0 | 0 | 0 | 0 | 0 | 0 | 0 | 0 |
| 8F | 0 | 0 | 0 | 0 | 0 | 0 | 0 | 0 | 0 | 0 | 0 | 0 | 0 | 0 | 0 | 0 | 0 | 0 | 0 | 0 | 0 | 0 | 0 | 0 | 0 | 0 | 0 | 0 | 0 | 0 | 0 | 0 | 0 | 0 | 0 | 0 | 0 | 0 | 0 | 0 | 0 | 0 | 0 | 0 |
| 7F | 0 | 0 | 0 | 0 | 0 | 0 | 0 | 0 | 0 | 0 | 0 | 0 | 0 | 0 | 0 | 0 | 0 | 0 | 0 | 0 | 0 | 0 | 0 | 0 | 0 | 0 | 0 | 0 | 0 | 0 | 0 | 0 | 0 | 0 | 0 | 0 | 0 | 0 | 0 | 0 | 0 | 0 | 0 | 0 |
| 6F | 0 | 0 | 0 | 0 | 0 | 0 | 0 | 0 | 0 | 0 | 0 | 0 | 0 | 0 | 0 | 0 | 0 | 0 | 0 | 0 | 0 | 0 | 0 | 0 | 0 | 0 | 0 | 0 | 0 | 0 | 0 | 0 | 0 | 0 | 0 | 0 | 0 | 0 | 0 | 0 | 0 | 0 | 0 | 0 |
| 5F | 0 | 0 | 0 | 0 | 0 | 0 | 0 | 0 | 0 | 0 | 0 | 0 | 0 | 0 | 0 | 0 | 0 | 0 | 0 | 0 | 0 | 0 | 0 | 0 | 0 | 0 | 0 | 0 | 0 | 0 | 0 | 0 | 0 | 0 | 0 | 0 | 0 | 0 | 0 | 0 | 0 | 0 | 0 | 0 |
| 4F | 0.000361 | 0.000441 | 0.001845 | 0.000441 | 0.001746 | 0.000381 | 0.000424 | 0.004591 | 0.000899 | 0.000568 | 0.003445 | 0.005836 | 0.002596 | 0.002043 | 0.00038 | 0.000362 | 0.000435 | 0.000547 | 0.000746 | 0.00059 | 0.000357 | 0.000748 | 0.00257 | 0.000582 | 0.003696 | 0.001053 | 0.002302 | 0.000689 | 0.002015 | 0.00165 | 0.000563 | 0.001087 | 0.002315 | 0.000571 | 0.000525 | 0.003475 | 0.001189 | 0.000497 | 0.000847 | 0.00054 | 0.0007 | 0.00231 | 0.001981 | 0.000905 |
| 3F | 0.006462 | 0.008543 | 0.015103 | 0.006434 | 0.009228 | 0.010962 | 0.00968 | 0.019023 | 0.00914 | 0.008438 | 0.0092 | 0.01566 | 0.008699 | 0.012785 | 0.009327 | 0.010612 | 0.007089 | 0.015378 | 0.008265 | 0.015694 | 0.008919 | 0.010164 | 0.0086 | 0.014845 | 0.010545 | 0.009271 | 0.012816 | 0.015872 | 0.006106 | 0.00813 | 0.01661 | 0.01823 | 0.01201 | 0.01002 | 0.016009 | 0.012948 | 0.012263 | 0.011653 | 0.013569 | 0.010047 | 0.008387 | 0.011455 | 0.00767 | 0.010629 |
| 2F | 0.009738 | 0.016306 | 0.019893 | 0.010167 | 0.014761 | 0.016517 | 0.013918 | 0.023296 | 0.012872 | 0.011709 | 0.015377 | 0.020568 | 0.009992 | 0.015118 | 0.010788 | 0.011159 | 0.015971 | 0.023219 | 0.008856 | 0.021355 | 0.012822 | 0.016017 | 0.007988 | 0.018398 | 0.013705 | 0.008125 | 0.018106 | 0.027704 | 0.01048 | 0.015517 | 0.022211 | 0.030601 | 0.014574 | 0.011052 | 0.01699 | 0.013358 | 0.016633 | 0.018719 | 0.013625 | 0.011637 | 0.011431 | 0.011807 | 0.011422 | 0.012106 |
| 1F | 0.006218 | 0.011036 | 0.009429 | 0.005461 | 0.010605 | 0.009413 | 0.010607 | 0.018098 | 0.006183 | 0.006968 | 0.009292 | 0.015723 | 0.005143 | 0.006952 | 0.0057 | 0.005822 | 0.011312 | 0.011562 | 0.005498 | 0.014503 | 0.007698 | 0.010076 | 0.004986 | 0.009565 | 0.007201 | 0.005516 | 0.01052 | 0.022473 | 0.005775 | 0.007711 | 0.014758 | 0.021599 | 0.006597 | 0.007392 | 0.009 | 0.008418 | 0.010044 | 0.013146 | 0.006206 | 0.00426 | 0.007131 | 0.006605 | 0.012281 | 0.006525 |

*Table 4. 6 OpenSees Peak Story Drift Ratio for 4 story EBF (California)*

| Seattle | 1 | 2 | 3 | 4 | 5 | 6 | 7 | 8 | 9 | 10 | 11 | 12 | 13 | 14 | 15 | 16 | 17 | 18 | 19 | 20 | 21 | 22 | 23 | 24 | 25 | 26 | 27 | 28 | 29 | 30 | 31 | 32 | 33 | 34 | 35 | 36 | 37 | 38 | 39 | 40 | 41 | 42 | 43 | 44 |
|---|---|---|---|---|---|---|---|---|---|---|---|---|---|---|---|---|---|---|---|---|---|---|---|---|---|---|---|---|---|---|---|---|---|---|---|---|---|---|---|---|---|---|---|---|
| 10F | 0 | 0 | 0 | 0 | 0 | 0 | 0 | 0 | 0 | 0 | 0 | 0 | 0 | 0 | 0 | 0 | 0 | 0 | 0 | 0 | 0 | 0 | 0 | 0 | 0 | 0 | 0 | 0 | 0 | 0 | 0 | 0 | 0 | 0 | 0 | 0 | 0 | 0 | 0 | 0 | 0 | 0 | 0 | 0 |
| 9F | 0 | 0 | 0 | 0 | 0 | 0 | 0 | 0 | 0 | 0 | 0 | 0 | 0 | 0 | 0 | 0 | 0 | 0 | 0 | 0 | 0 | 0 | 0 | 0 | 0 | 0 | 0 | 0 | 0 | 0 | 0 | 0 | 0 | 0 | 0 | 0 | 0 | 0 | 0 | 0 | 0 | 0 | 0 | 0 |
| 8F | 0 | 0 | 0 | 0 | 0 | 0 | 0 | 0 | 0 | 0 | 0 | 0 | 0 | 0 | 0 | 0 | 0 | 0 | 0 | 0 | 0 | 0 | 0 | 0 | 0 | 0 | 0 | 0 | 0 | 0 | 0 | 0 | 0 | 0 | 0 | 0 | 0 | 0 | 0 | 0 | 0 | 0 | 0 | 0 |
| 7F | 0 | 0 | 0 | 0 | 0 | 0 | 0 | 0 | 0 | 0 | 0 | 0 | 0 | 0 | 0 | 0 | 0 | 0 | 0 | 0 | 0 | 0 | 0 | 0 | 0 | 0 | 0 | 0 | 0 | 0 | 0 | 0 | 0 | 0 | 0 | 0 | 0 | 0 | 0 | 0 | 0 | 0 | 0 | 0 |
| 6F | 0 | 0 | 0 | 0 | 0 | 0 | 0 | 0 | 0 | 0 | 0 | 0 | 0 | 0 | 0 | 0 | 0 | 0 | 0 | 0 | 0 | 0 | 0 | 0 | 0 | 0 | 0 | 0 | 0 | 0 | 0 | 0 | 0 | 0 | 0 | 0 | 0 | 0 | 0 | 0 | 0 | 0 | 0 | 0 |
| 5F | 0 | 0 | 0 | 0 | 0 | 0 | 0 | 0 | 0 | 0 | 0 | 0 | 0 | 0 | 0 | 0 | 0 | 0 | 0 | 0 | 0 | 0 | 0 | 0 | 0 | 0 | 0 | 0 | 0 | 0 | 0 | 0 | 0 | 0 | 0 | 0 | 0 | 0 | 0 | 0 | 0 | 0 | 0 | 0 |
| 4F | 0.001846 | 0.001587 | 0.00352 | 0.001827 | 0.001833 | 0.001707 | 0.001845 | 0.005749 | 0.002078 | 0.002117 | 0.002838 | 0.007017 | 0.002473 | 0.003526 | 0.002216 | 0.00188 | 0.001525 | 0.002199 | 0.000359 | 0.00215 | 0.001886 | 0.001909 | 0.002888 | 0.002182 | 0.004057 | 0.002184 | 0.003479 | 0.002689 | 0.001966 | 0.001196 | 0.002256 | 0.00274 | 0.00346 | 0.002264 | 0.003145 | 0.000352 | 0.002452 | 0.001974 | 0.003071 | 0.002969 | 0.002755 | 0.00333 | 0.002688 | 0.001424 |
| 3F | 0.008245 | 0.010067 | 0.016327 | 0.008279 | 0.007456 | 0.012972 | 0.008415 | 0.02186 | 0.011259 | 0.010862 | 0.01209 | 0.017739 | 0.010321 | 0.014406 | 0.011245 | 0.012176 | 0.00951 | 0.01842 | 0.004167 | 0.017007 | 0.011743 | 0.012548 | 0.009715 | 0.015034 | 0.011678 | 0.008001 | 0.01501 | 0.017579 | 0.00799 | 0.011107 | 0.015173 | 0.021228 | 0.014355 | 0.010515 | 0.019161 | 0.006624 | 0.014569 | 0.013208 | 0.014873 | 0.01261 | 0.010861 | 0.013918 | 0.005225 | 0.009459 |
| 2F | 0.012876 | 0.019783 | 0.022898 | 0.013426 | 0.017848 | 0.019974 | 0.017342 | 0.02472 | 0.016156 | 0.013641 | 0.018073 | 0.023793 | 0.012901 | 0.018153 | 0.013369 | 0.013635 | 0.01855 | 0.0263 | 0.009983 | 0.024208 | 0.016487 | 0.019949 | 0.009858 | 0.021271 | 0.017041 | 0.01127 | 0.019986 | 0.032037 | 0.013686 | 0.019485 | 0.025817 | 0.034769 | 0.017355 | 0.013525 | 0.02038 | 0.015828 | 0.020545 | 0.022558 | 0.016287 | 0.015247 | 0.014806 | 0.013071 | 0.013068 | 0.014376 |
| 1F | 0.009348 | 0.014427 | 0.012613 | 0.008371 | 0.013765 | 0.012489 | 0.014024 | 0.021284 | 0.009165 | 0.010111 | 0.012726 | 0.018734 | 0.007803 | 0.010149 | 0.008402 | 0.00871 | 0.014418 | 0.015181 | 0.00869 | 0.017372 | 0.010938 | 0.013281 | 0.007805 | 0.012583 | 0.010308 | 0.008135 | 0.013714 | 0.025939 | 0.008613 | 0.011364 | 0.018153 | 0.025108 | 0.009501 | 0.010287 | 0.012117 | 0.011918 | 0.013482 | 0.016438 | 0.008772 | 0.007661 | 0.010739 | 0.010111 | 0.015397 | 0.009868 |

*Table 4. 7 Residual Drift calculation for 4 story EBF (California)*

| Residual Drift | 1 | 2 | 3 | 4 | 5 | 6 | 7 | 8 | 9 | 10 | 11 | 12 | 13 | 14 | 15 | 16 | 17 | 18 | 19 | 20 | 21 | 22 | 23 | 24 | 25 | 26 | 27 | 28 | 29 | 30 | 31 | 32 | 33 | 34 | 35 | 36 | 37 | 38 | 39 | 40 | 41 | 42 | 43 | 44 |
|---|---|---|---|---|---|---|---|---|---|---|---|---|---|---|---|---|---|---|---|---|---|---|---|---|---|---|---|---|---|---|---|---|---|---|---|---|---|---|---|---|---|---|---|---|
| 10F | 0 | 0 | 0 | 0 | 0 | 0 | 0 | 0 | 0 | 0 | 0 | 0 | 0 | 0 | 0 | 0 | 0 | 0 | 0 | 0 | 0 | 0 | 0 | 0 | 0 | 0 | 0 | 0 | 0 | 0 | 0 | 0 | 0 | 0 | 0 | 0 | 0 | 0 | 0 | 0 | 0 | 0 | 0 | 0 |
| 9F | 0 | 0 | 0 | 0 | 0 | 0 | 0 | 0 | 0 | 0 | 0 | 0 | 0 | 0 | 0 | 0 | 0 | 0 | 0 | 0 | 0 | 0 | 0 | 0 | 0 | 0 | 0 | 0 | 0 | 0 | 0 | 0 | 0 | 0 | 0 | 0 | 0 | 0 | 0 | 0 | 0 | 0 | 0 | 0 |
| 8F | 0 | 0 | 0 | 0 | 0 | 0 | 0 | 0 | 0 | 0 | 0 | 0 | 0 | 0 | 0 | 0 | 0 | 0 | 0 | 0 | 0 | 0 | 0 | 0 | 0 | 0 | 0 | 0 | 0 | 0 | 0 | 0 | 0 | 0 | 0 | 0 | 0 | 0 | 0 | 0 | 0 | 0 | 0 | 0 |
| 7F | 0 | 0 | 0 | 0 | 0 | 0 | 0 | 0 | 0 | 0 | 0 | 0 | 0 | 0 | 0 | 0 | 0 | 0 | 0 | 0 | 0 | 0 | 0 | 0 | 0 | 0 | 0 | 0 | 0 | 0 | 0 | 0 | 0 | 0 | 0 | 0 | 0 | 0 | 0 | 0 | 0 | 0 | 0 | 0 |
| 6F | 0 | 0 | 0 | 0 | 0 | 0 | 0 | 0 | 0 | 0 | 0 | 0 | 0 | 0 | 0 | 0 | 0 | 0 | 0 | 0 | 0 | 0 | 0 | 0 | 0 | 0 | 0 | 0 | 0 | 0 | 0 | 0 | 0 | 0 | 0 | 0 | 0 | 0 | 0 | 0 | 0 | 0 | 0 | 0 |
| 5F | 0 | 0 | 0 | 0 | 0 | 0 | 0 | 0 | 0 | 0 | 0 | 0 | 0 | 0 | 0 | 0 | 0 | 0 | 0 | 0 | 0 | 0 | 0 | 0 | 0 | 0 | 0 | 0 | 0 | 0 | 0 | 0 | 0 | 0 | 0 | 0 | 0 | 0 | 0 | 0 | 0 | 0 | 0 | 0 |
| 4F | 8.91E-05 | 0.000265 | 0.001349 | 0.000218 | 0.001139 | 0.00028 | -1.8E-05 | 0.004461 | 0.000265 | -0.00021 | 0.001669 | 0.00515 | 0.000417 | 0.001226 | 0.000284 | 0.00029 | 0.000267 | 0.00025 | 0.000327 | 0.00055 | 0.000376 | -0.00011 | -0.00012 | 0.000695 | 0.002523 | 0.000386 | 0.001989 | 0.001069 | 0.00078 | -0.00024 | 0.000973 | 9.65E-05 | 0.002084 | 0.000414 | 0.000555 | -0.00019 | 0.001584 | 0.00057 | 0.000691 | 0.000492 | 0.000177 | 0.000801 | 0.000694 | 0.000353 |
| 3F | 0.001626 | 0.003517 | 0.008473 | 0.001622 | 0.006765 | 0.006482 | 0.00176 | 0.016785 | 0.001852 | 0.0003 | 0.007548 | 0.012208 | 0.00362 | 0.006391 | 0.005465 | 0.002497 | 0.004547 | 0.005886 | 0.002352 | 0.00725 | 0.0071 | 0.000474 | -0.0003 | 0.010209 | 0.008231 | 0.001356 | 0.01095 | 0.014743 | 0.002812 | 0.001849 | 0.014356 | 0.000994 | 0.010435 | 0.005644 | 0.009705 | 0.005915 | 0.00967 | 0.007654 | 0.008689 | 0.004684 | 0.001688 | -0.00049 | 0.004215 | 0.004504 |
| 2F | 0.002059 | 0.004937 | 0.010781 | 0.003786 | 0.009835 | 0.009974 | 0.002666 | 0.022824 | 0.002416 | 0.000883 | 0.011828 | 0.015917 | 0.004503 | 0.006941 | 0.007948 | 0.003459 | 0.007592 | 0.00854 | 0.003924 | 0.008741 | 0.010719 | 0.001252 | 0.00028 | 0.014462 | 0.010941 | 0.001369 | 0.015712 | 0.024341 | 0.003831 | 0.002862 | 0.021455 | 0.00075 | 0.012255 | 0.008591 | 0.014378 | 0.008886 | 0.0131 | 0.01137 | 0.009886 | 0.006323 | 0.002295 | 0.000241 | 0.007602 | 0.007508 |
| 1F | 0.001013 | 0.003265 | 0.005403 | 0.002609 | 0.005626 | 0.005463 | 0.001022 | 0.015633 | 0.001417 | 0.000702 | 0.007142 | 0.010682 | 0.002137 | 0.003139 | 0.004056 | 0.002011 | 0.005064 | 0.005268 | 0.001782 | 0.00477 | 0.005788 | 0.001361 | 0.000152 | 0.007605 | 0.005635 | 0.00067 | 0.008612 | 0.018965 | 0.001872 | 0.001451 | 0.013806 | 0.000267 | 0.005838 | 0.004716 | 0.007628 | 0.005222 | 0.00711 | 0.007255 | 0.004653 | 0.002803 | 0.001062 | 0.000355 | 0.00652 | 0.004474 |
| | | | | | | | | | | | | | | | | | | | | | | | | | | | | | | | | | | | | | | | | | | | | | |
| Maximum | 0.002059 | 0.004937 | 0.010781 | 0.003786 | 0.009835 | 0.009974 | 0.002666 | 0.022824 | 0.002416 | 0.000883 | 0.011828 | 0.015917 | 0.004503 | 0.006941 | 0.007948 | 0.003459 | 0.007592 | 0.00854 | 0.003924 | 0.008741 | 0.010719 | 0.001361 | 0.00028 | 0.014462 | 0.010941 | 0.001369 | 0.015712 | 0.024341 | 0.003831 | 0.002862 | 0.021455 | 0.000994 | 0.012255 | 0.008591 | 0.014378 | 0.008886 | 0.0131 | 0.01137 | 0.009886 | 0.006323 | 0.002295 | 0.000801 | 0.007602 | 0.007508 |
| | | | | | | | | | | | | | | | | | | | | | | | | | | | | | | | | | | | | | | | | | | | | |
| delta y | 0.013393 | -0.00846 | | | | | | | | | | | | | | | | | | | | | | | | | | | | | | | | | | | | | | | | | | |
| 4*delta y | 0.053571 | -0.00254 | | | | | | | | | | | | | | | | | | | | | | | | | | | | | | | | | | | | | | | | | | |
| | | | | | | | | | | | | | | | | | | | | | | | | | | | | | | | | | | | | | | | | | | | | |
| delta r | 0 | 0 | 0 | 0 | 0 | 0 | 0 | 0.002829 | 0 | 0 | 0 | 0.000757 | 0 | 0 | 0 | 0 | 0 | 0 | 0 | 0 | 0 | 0 | 0 | 0.000321 | 0 | 0 | 0.000696 | 0.003284 | 0 | 0 | 0.002419 | 0 | 0 | 0 | 0.000295 | 0 | 0 | 0 | 0 | 0 | 0 | 0 | 0 | 0 |

*Table 4. 8 Values of Dispersion for Construction Quality Assurance Adapted from FEMA P-58 [16]*

| Building Definition and Construction Quality Assurance | $\beta_c$ |
|---|---|
| Superior Quality, New Buildings: The building is completely designed and will be constructed with rigorous construction quality assurance, including special inspection, material testing, and structural observation. | 0.1 |
| Superior Quality, Exisiting Buildings: Drawings and specifications are available and field investigation confirms they are representative of the actual construction, or if not, the acutal construction is understood. Material properties are confirmed by extensive materials testing | |
| Average Quality, New Buildings: The building design is completed to a level typical of design development; construction quality assurance and inspection are anticipated to be of limited quality. | 0.25 |
| Average Quality, Exisiting buildings: Documents defining the building design are available and are confirmed by visual observation. Material properties are confirmed by limited materials testing. | |
| Limited Quality, New Buildings: The building design is completed to a level typical of schematic design or other similar level of detail. | 0.4 |
| Limited Quality, Exisiting Buildings: Construction documents are not available and knowledge of the structure is based on default values typical for buildings of the type, location, and age of construction. | |

*Table 4. 9 Values of Dispersion for Quality of the Analytical Model Adapted from FEMA P-58 [16]*

| Quality and Completeness of the Analytical Model | $\beta_q$ |
|---|---|
| Superior Quality: The numerical model is robust over the anticipated range of response. Strength and stiffness deterioration and all likely failure modes are explicitly odeled. Model accuracy is established with data from large-scale component tests through failure. | 0.1 |
| Completeness: The mathematical model includes all structural components and nonstructural components in the building that contribute to strength or stiffness | |
| Average Quality: The numerical model for each component is robust over the anticipated range of displacement or defromation response. Strength and stiffness deterioration is fairly well represented, though some failure modes are simulated indirectly. Accuracy is established through a combination of judgement and large-scale component tests. | 0.25 |
| Completeness: The mathematical model includes most structural components and nonstructural components in the building that contribute significant strength or stiffness | |
| Limited Quality: The numerical model for each component is based on idealized cyclic envelope curves from ASCE/SEI 41-13 or comparable guidelines, where strength and stiffness deterioration and failure modes are not directly incorporated in the model. | 0.4 |
| Completeness: The mathematical model includes structural components in the seismic-force-resisting system. | |

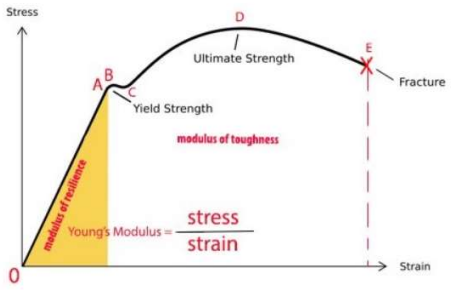


*Figure 4. 1 Stress-Strain Curve- Mild Steel [36]*

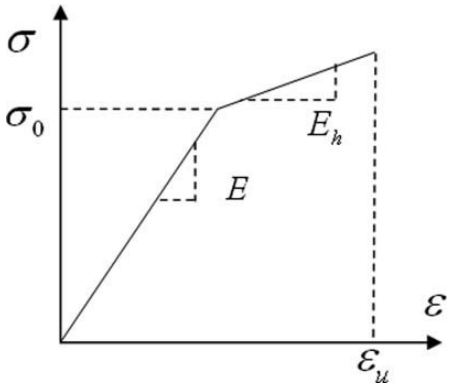


*Figure 4. 2 Bi-linear curve [37]*

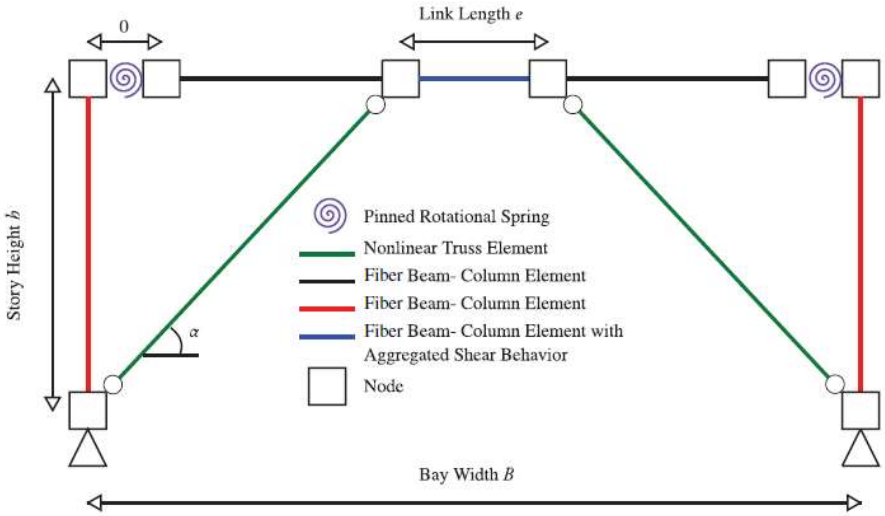


*Figure 4. 3 Modelling Parameters of a single story EBF [32]*

| Reference | Specimen ID | Section Size | Link Length [mm] | Loading Protocol |
|---|---|---|---|---|
| Mansour [2010] | UT3A | W360 × 101 | 900 | AISC 341-05 [2005] |
| Mansour [2010] | UT3B | W360 × 101 | 900 | AISC 341-05 [2005] |
| Okazaki *et al.* [2009] | AISC-2 | W18 × 40 | 980 | AISC 341-05 [2005] |
| Okazaki *et al.* [2009] | AISC-6 | W10 × 68 | 980 | AISC 341-05 [2005] |

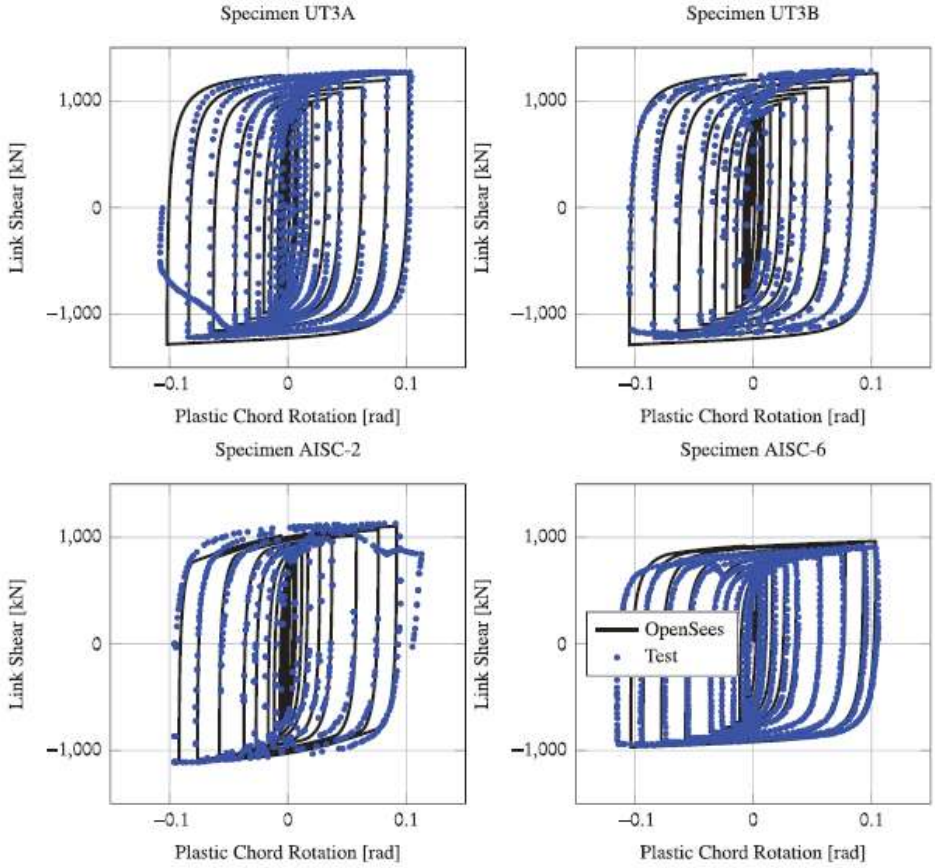


*Figure 4. 4 Validation of Link Parameters by O'Reilly et al. with experimental data [32]*

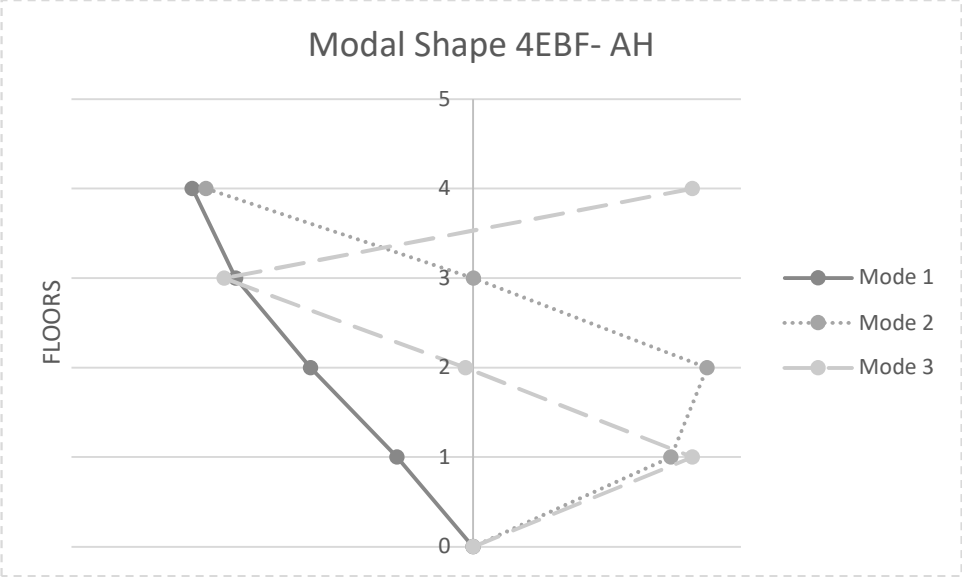


*Figure 4. 5 Modal Shape 4EBF- AH*

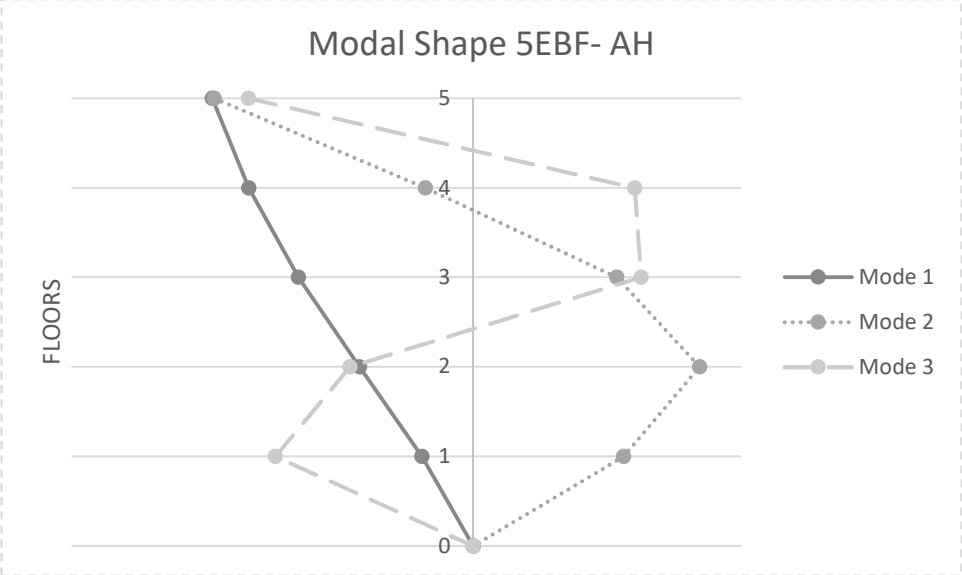


*Figure 4. 6 Modal Shape 5EBF- AH*

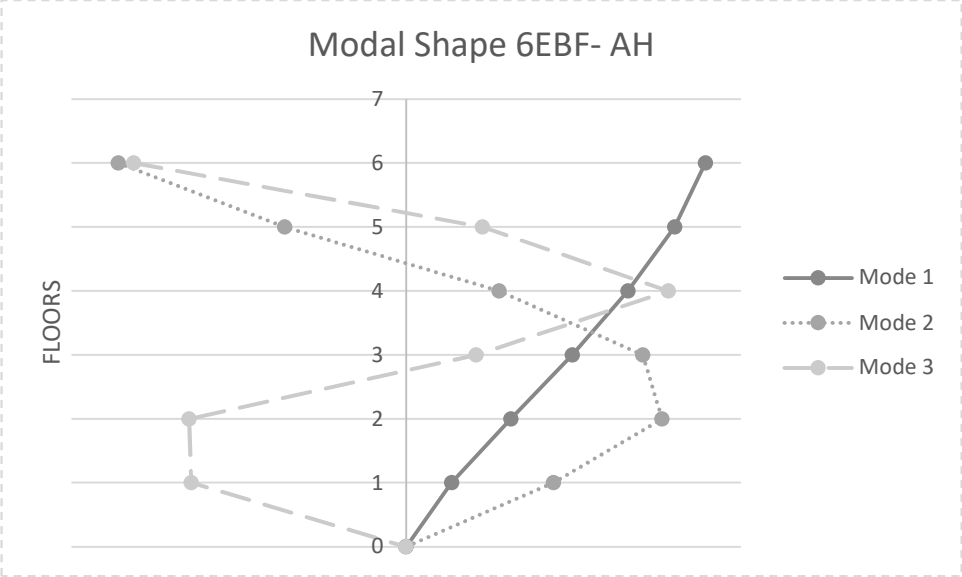


*Figure 4. 7 Modal Shape 6EBF- AH*

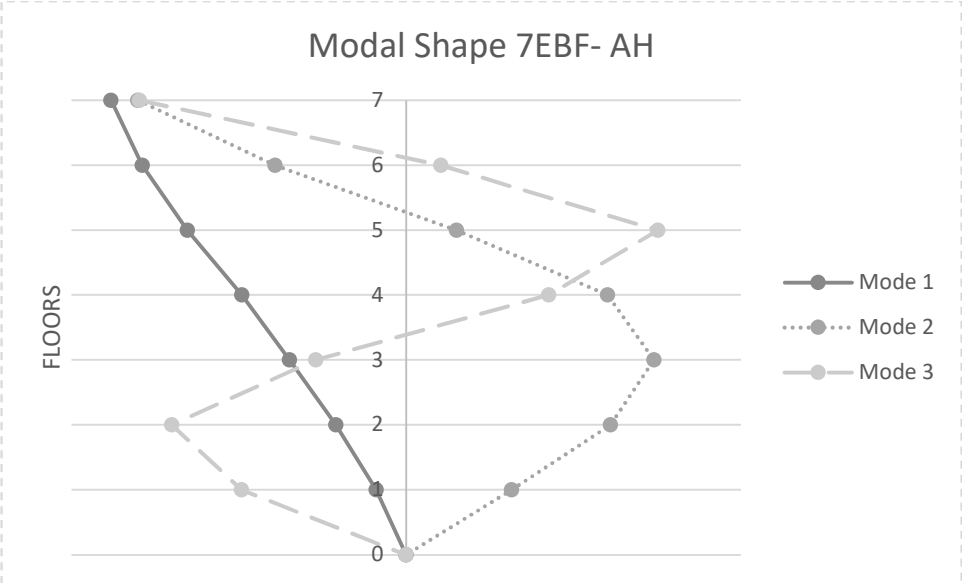


*Figure 4. 8 Modal Shape 7EBF- AH*

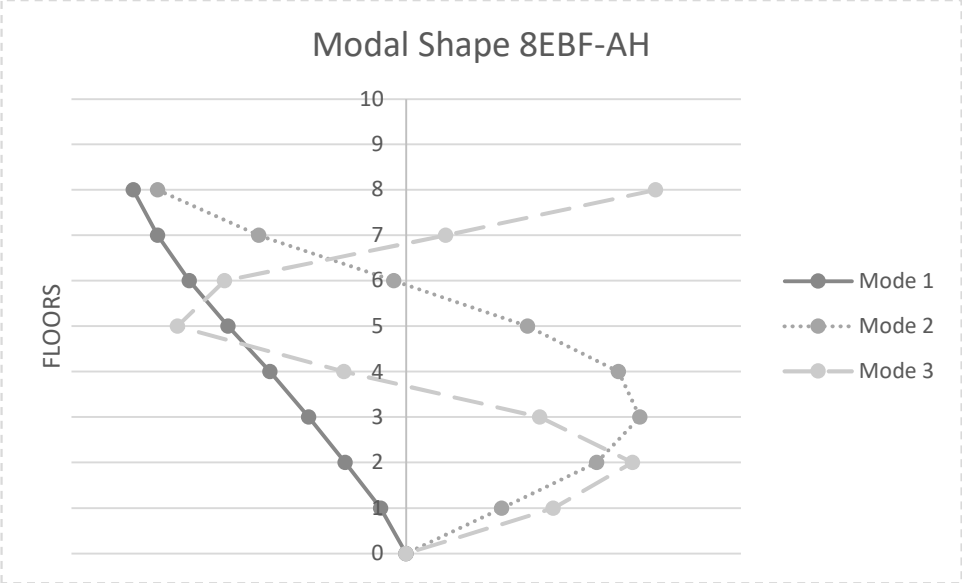


*Figure 4. 9 Modal Shape 8EBF- AH*

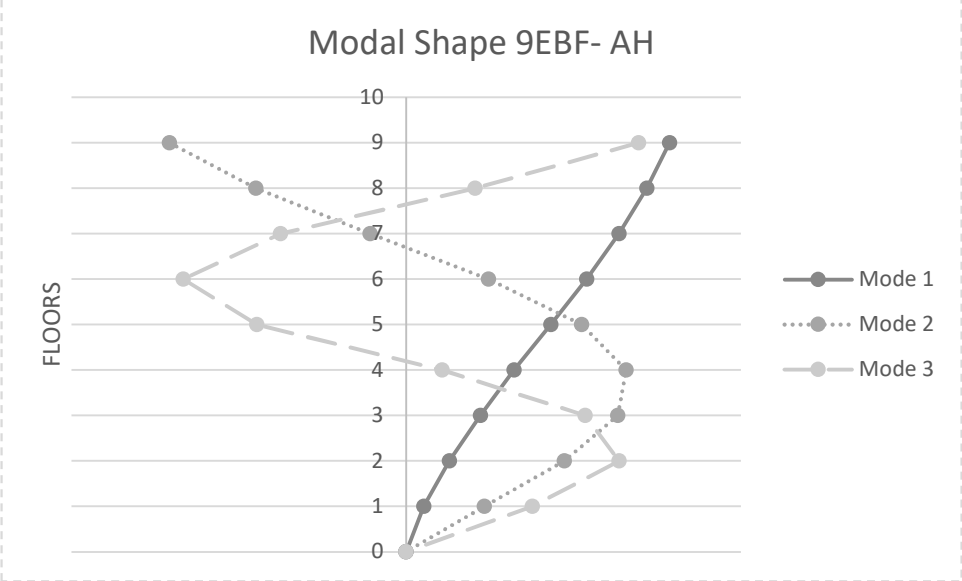


*Figure 4. 10 Modal Shape 9EBF- AH*

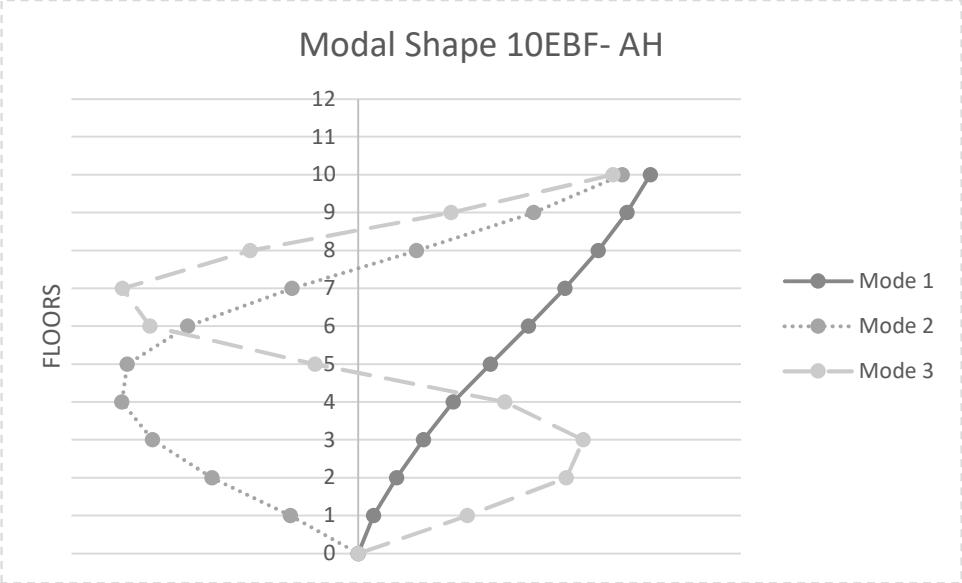


*Figure 4. 11 Modal Shape 10EBF- AH*

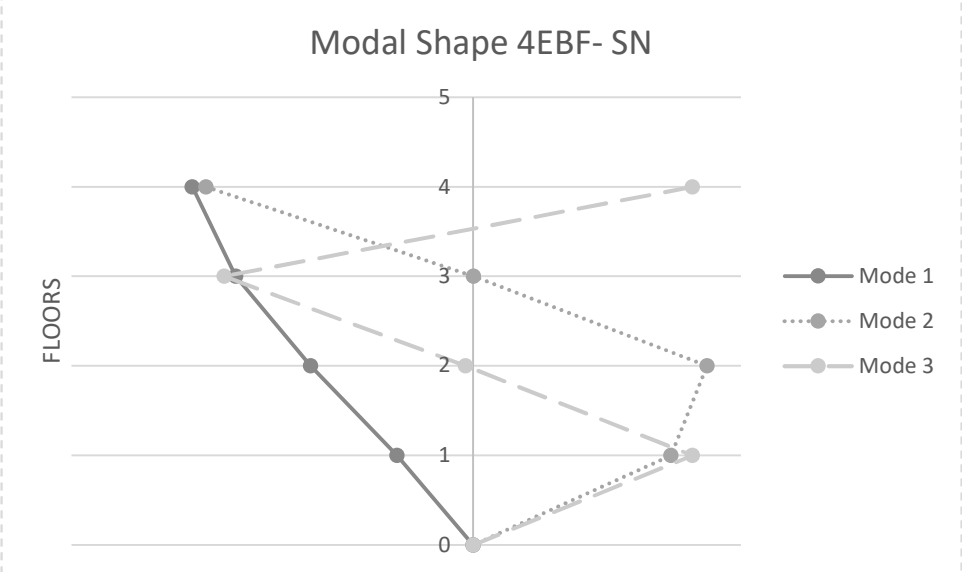


*Figure 4. 12 Modal Shape 4EBF- SN*

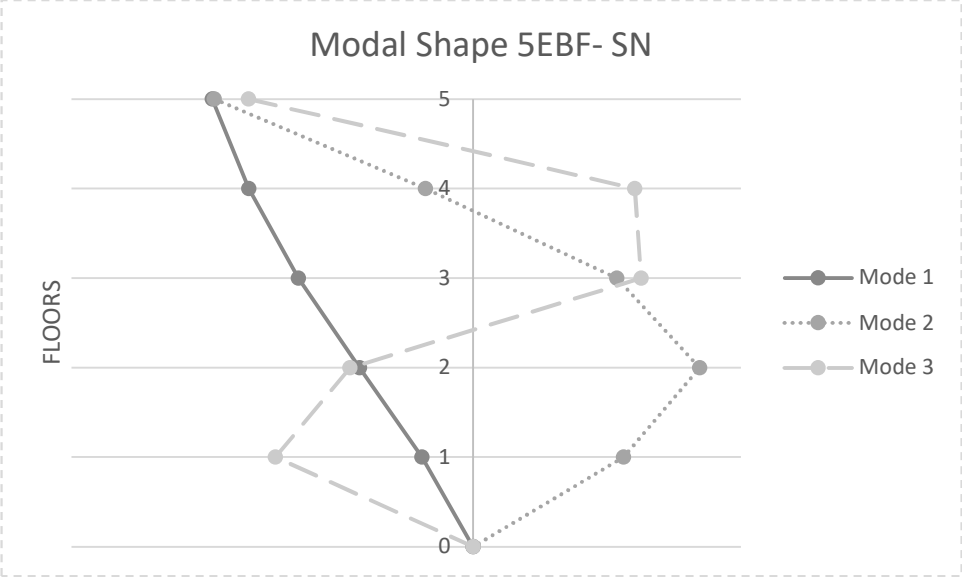


*Figure 4. 13 Modal Shape 5EBF- SN*

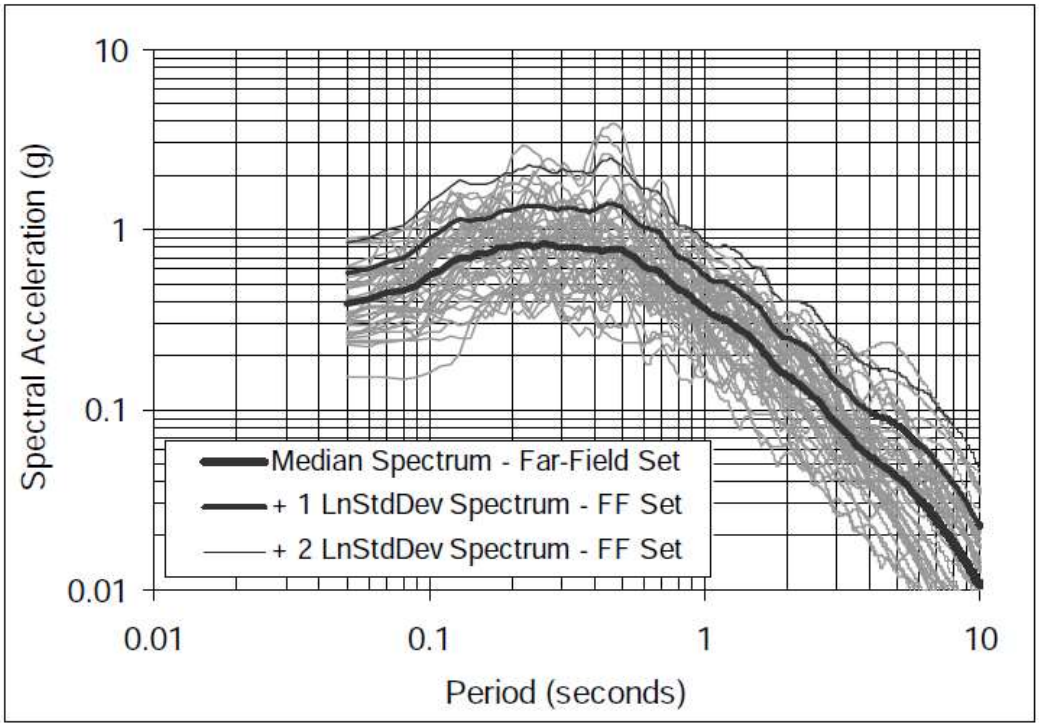


*Figure 4. 14 Schematic FEMA P-695 Far-field record set response spectra [17]*

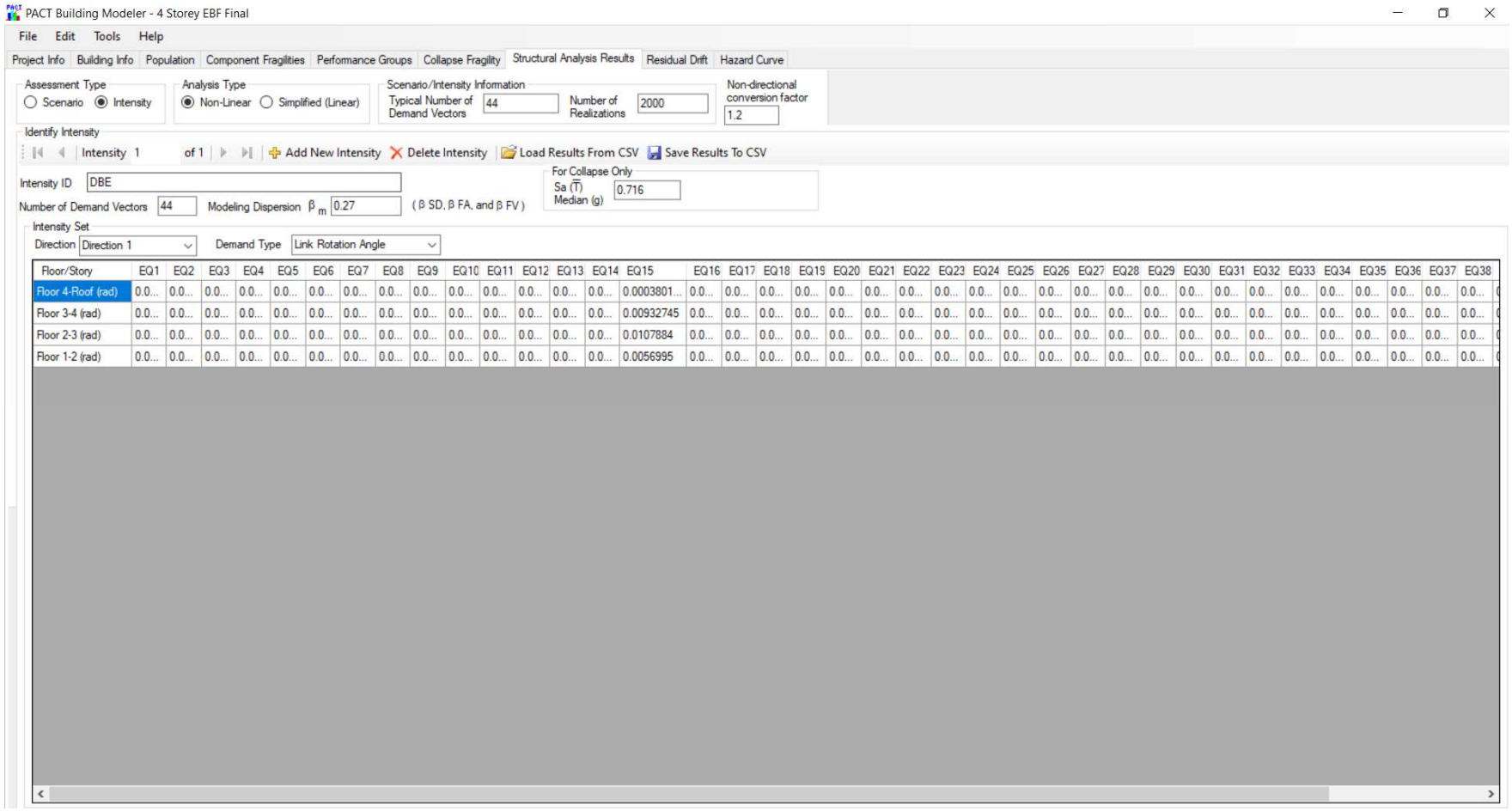


*Figure 4. 15 PACT Structural Analysis Tab*

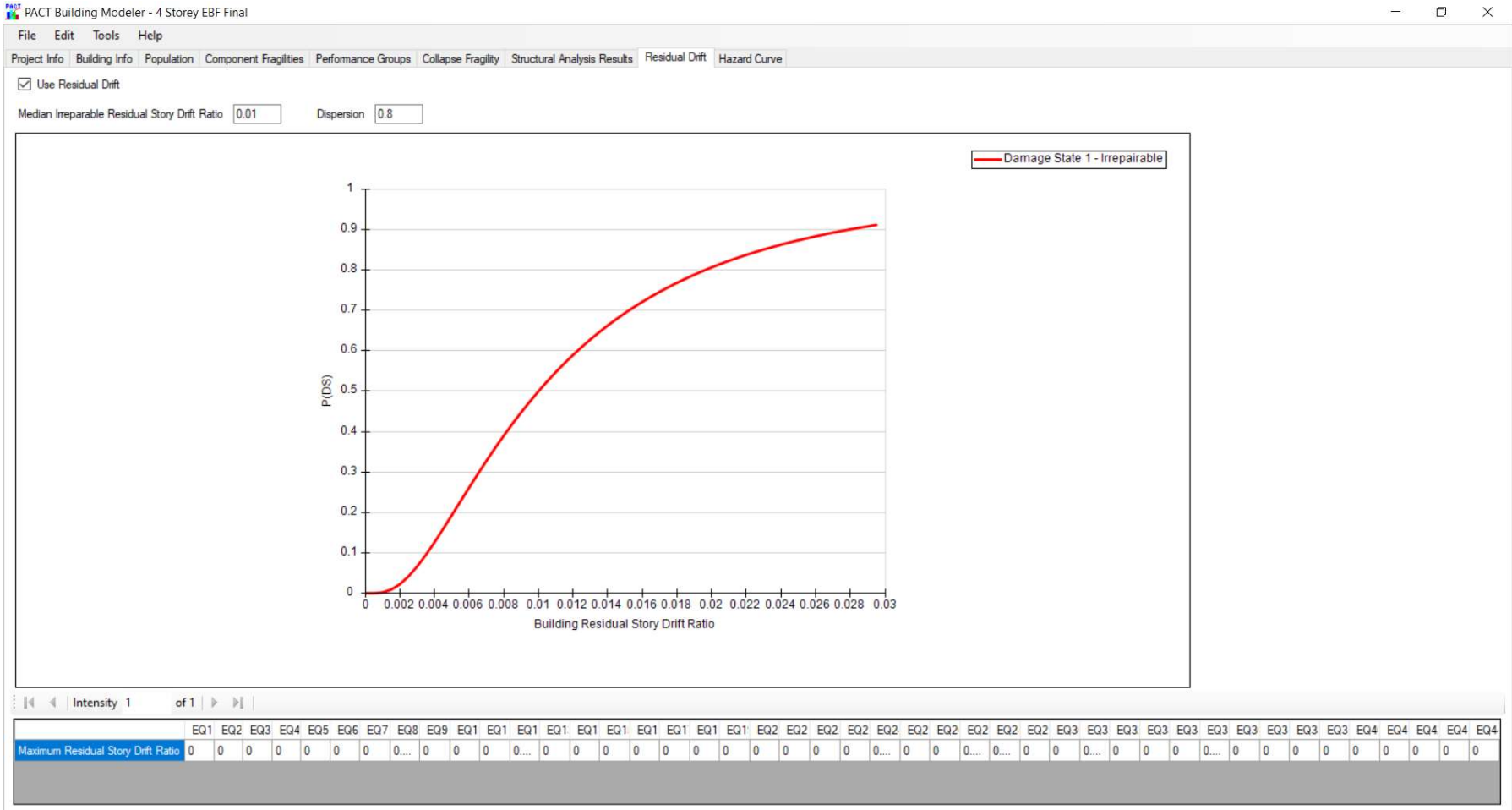


*Figure 4. 16 PACT Residual Drift Tab*

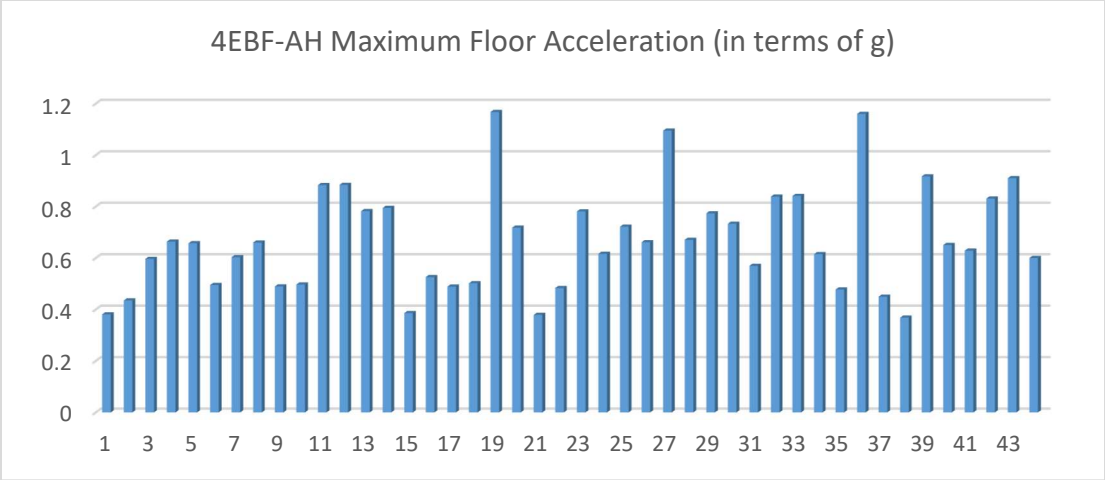


*Figure 4. 17 4EBF-AH Maximum floor acceleration response over 44 far-field earthquake ground motion records scaled to design basis earthquake (unit: g)*

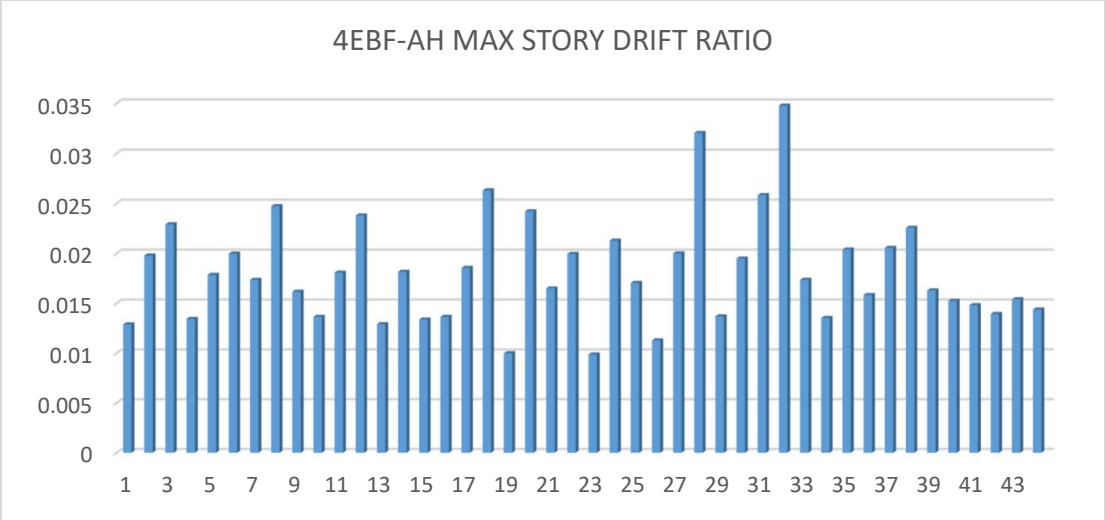


*Figure 4. 18 4EBF-AH Maximum Inter-story Drift Ratio over 44 far-field earthquake ground motion records scaled to design basis earthquake*

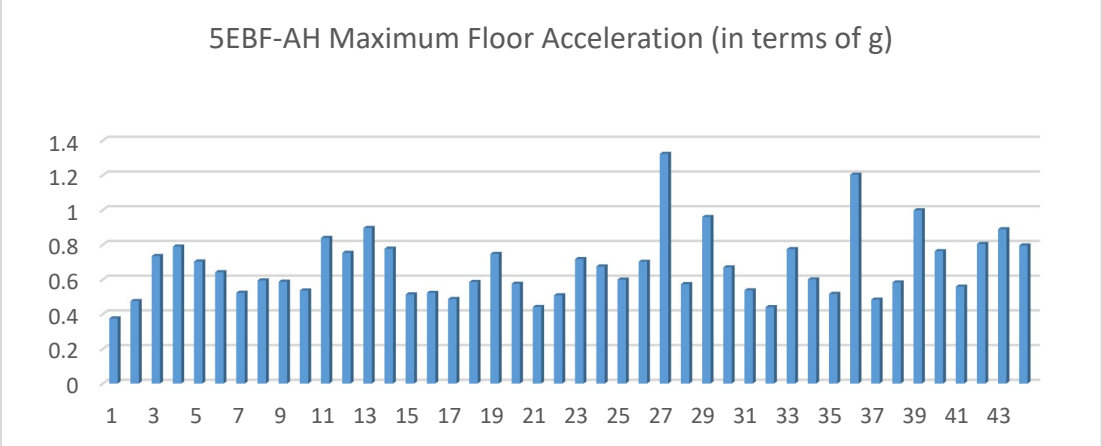


*Figure 4. 19 5EBF- Maximum floor acceleration response over 44 far-field earthquake ground motion records scaled to design basis earthquake (unit: g)*

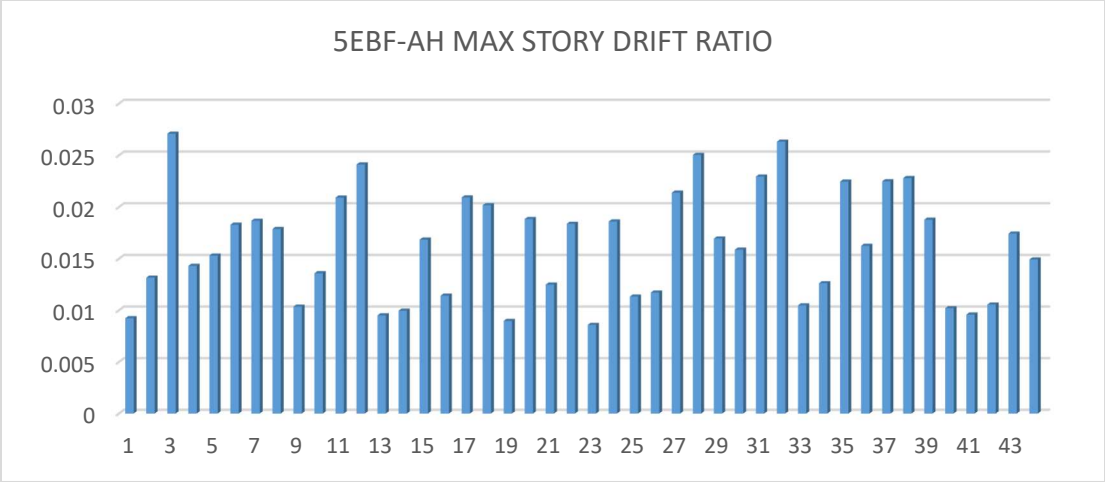


*Figure 4. 20 5EBF-AH Maximum Inter-story Drift Ratio over 44 far-field earthquake ground motion records scaled to design basis earthquake*

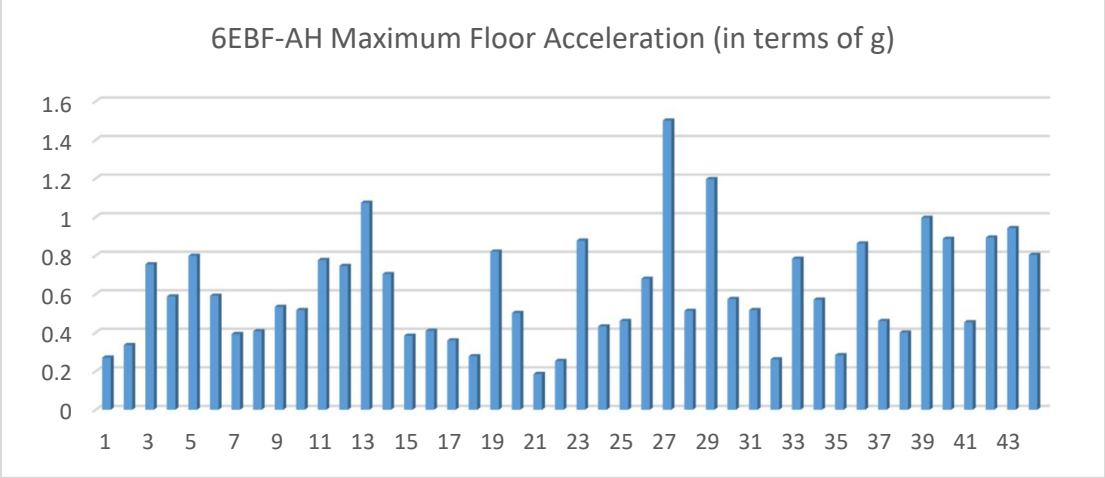


*Figure 4. 21 6EBF-AH floor acceleration response over 44 far-field earthquake ground motion records scaled to design basis earthquake (unit: g)*

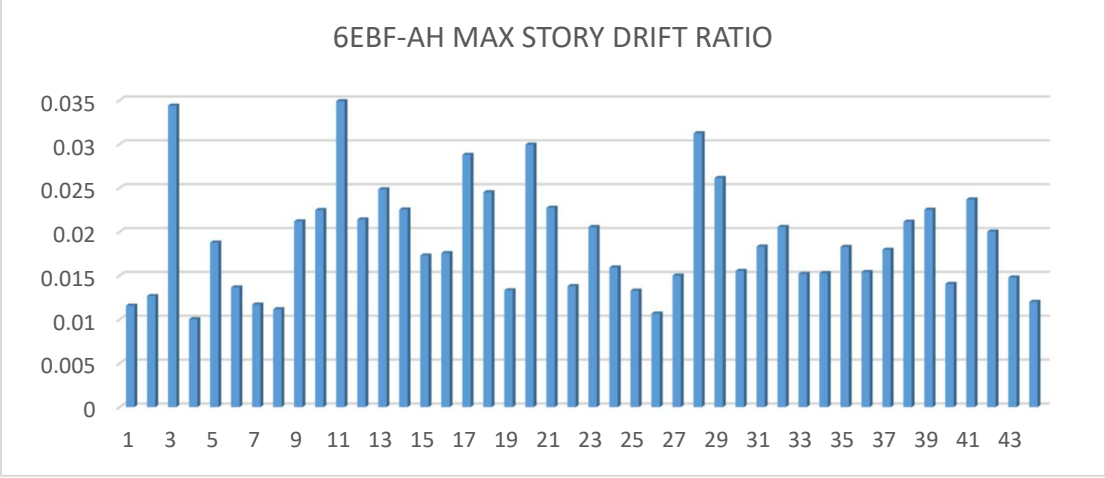


*Figure 4. 22 6EBF-AH Maximum Inter-story Drift Ratio over 44 far-field earthquake ground motion records scaled to design basis earthquake*

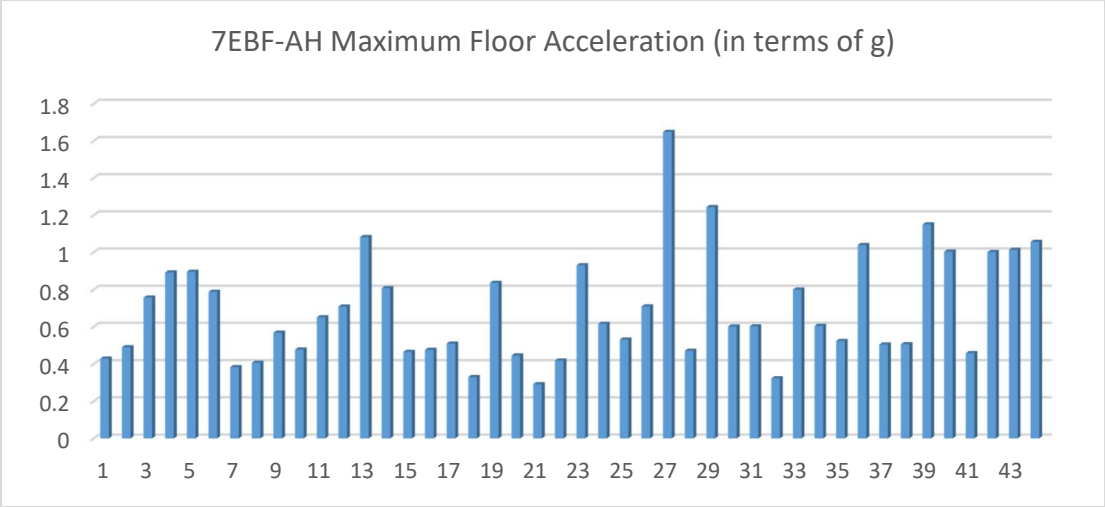


*Figure 4. 23 7EBF-AH floor acceleration response over 44 far-field earthquake ground motion records scaled to design basis earthquake (unit: g)*

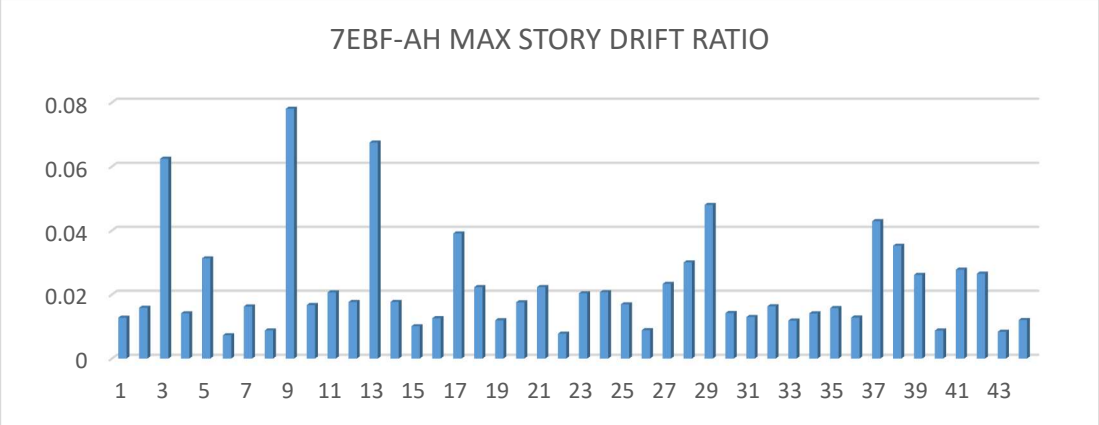


*Figure 4. 24 7EBF-AH Maximum Inter-story Drift Ratio over 44 far-field earthquake ground motion records scaled to design basis earthquake*

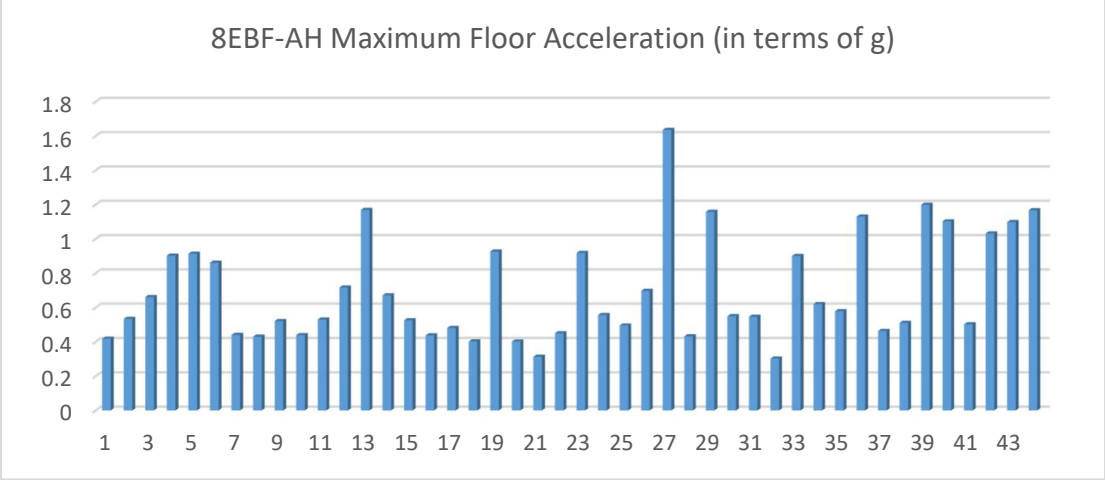


*Figure 4. 25 8EBF-AH floor acceleration response over 44 far-field earthquake ground motion records scaled to design basis earthquake (unit: g)*

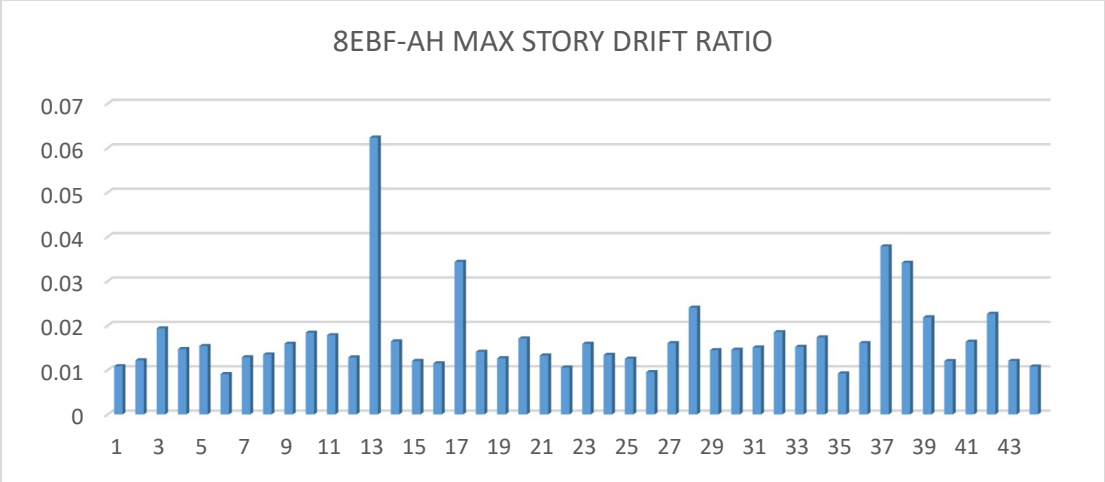


*Figure 4. 26 8EBF-AH Maximum Inter-story Drift Ratio over 44 far-field earthquake ground motion records scaled to design basis earthquake*

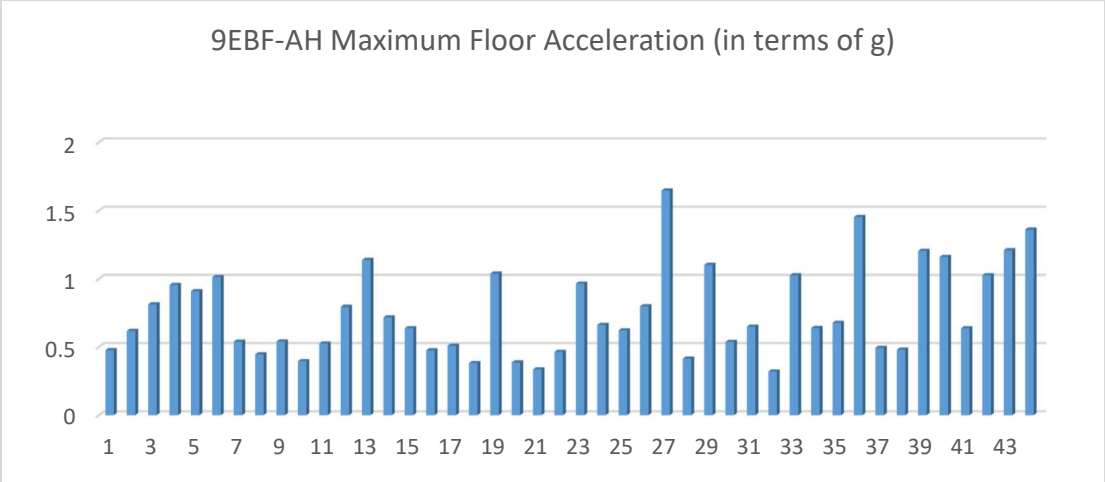


*Figure 4. 27 9EBF-AH floor acceleration response over 44 far-field earthquake ground motion records scaled to design basis earthquake (unit: g)*

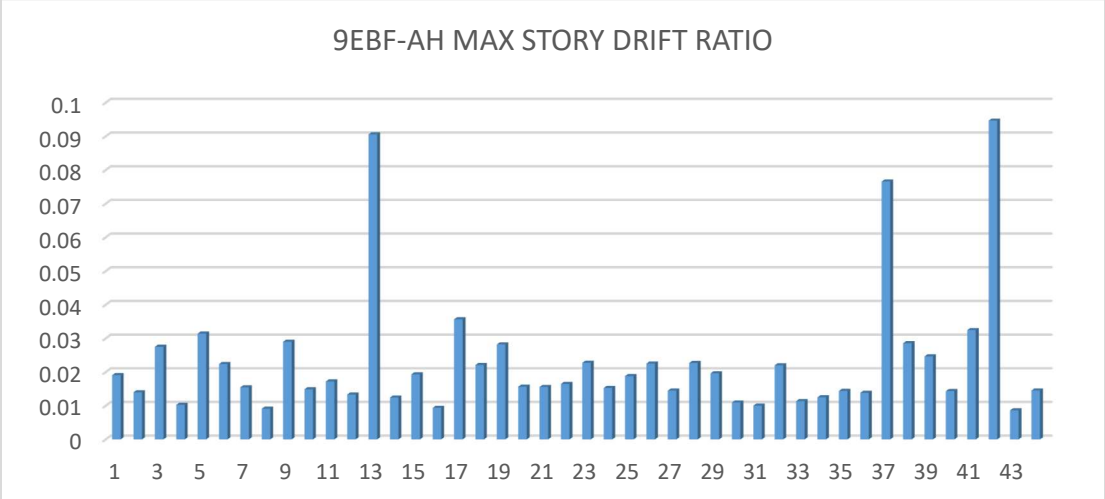


*Figure 4. 28 9EBF-AH Maximum Inter-story Drift Ratio over 44 far-field earthquake ground motion records scaled to design basis earthquake*

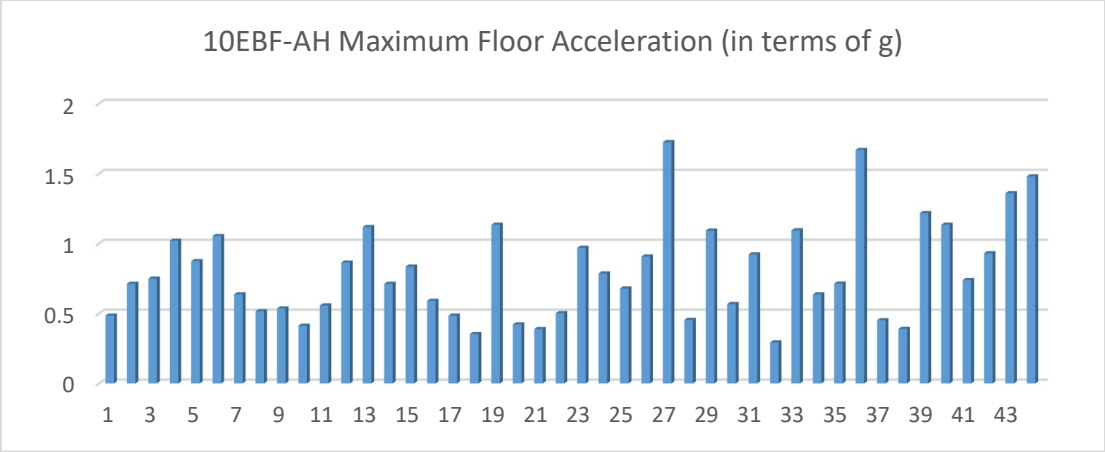


*Figure 4. 29 10EBF-AH floor acceleration response over 44 far-field earthquake ground motion records scaled to design basis earthquake (unit: g)*

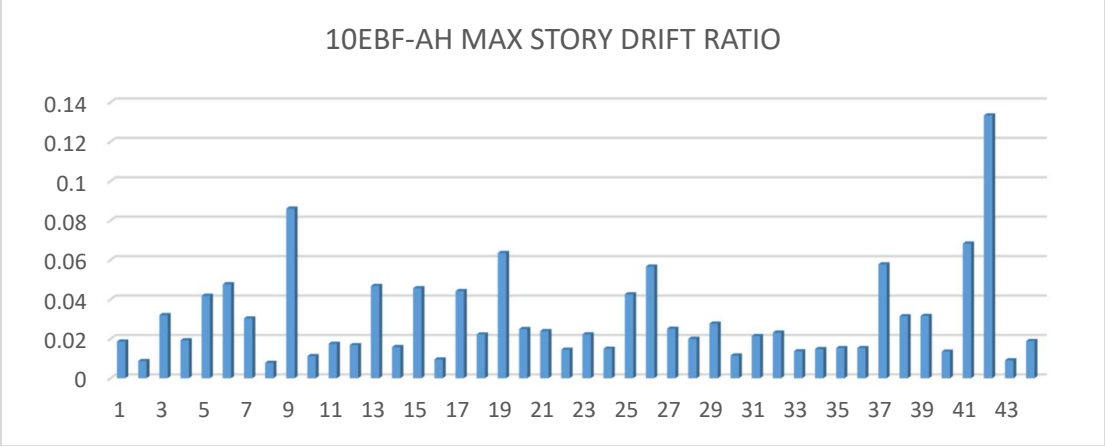


*Figure 4. 30 10EBF-AH Maximum Inter-story Drift Ratio over 44 far-field earthquake ground motion records scaled to design basis earthquake*

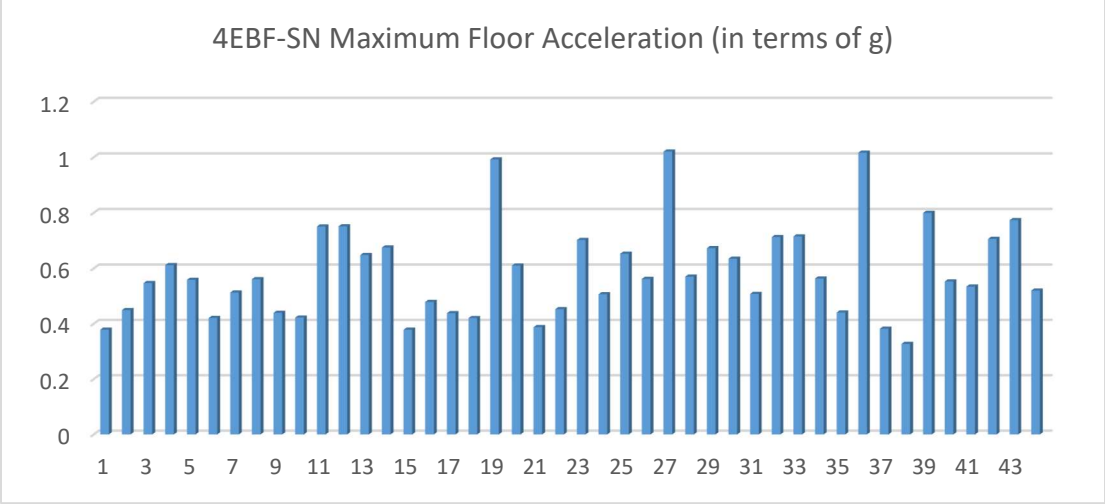


*Figure 4. 31 4EBF-SN floor acceleration response over 44 far-field earthquake ground motion records scaled to design basis earthquake (unit: g)*

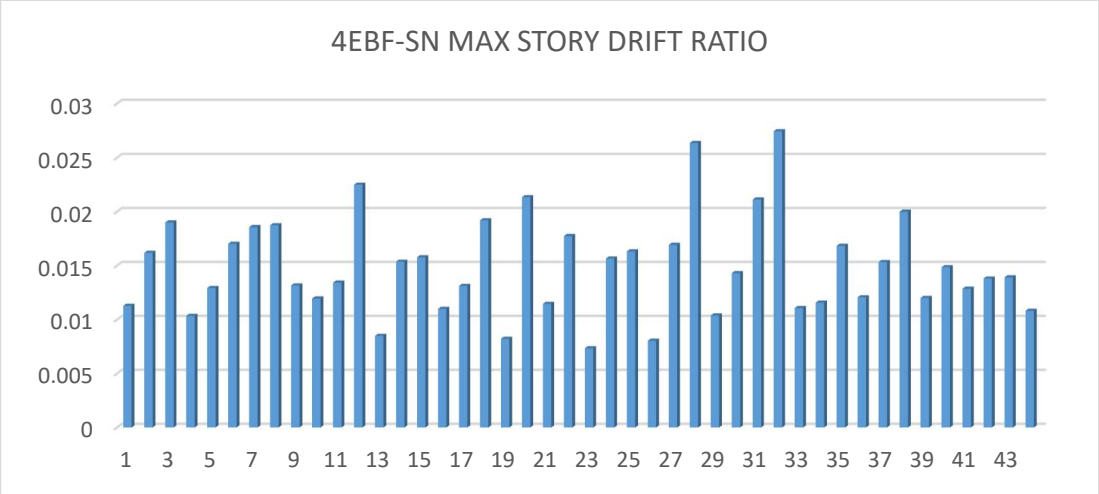


*Figure 4. 32 4EBF-SN Maximum Inter-story Drift Ratio over 44 far-field earthquake ground motion records scaled to design basis earthquake*

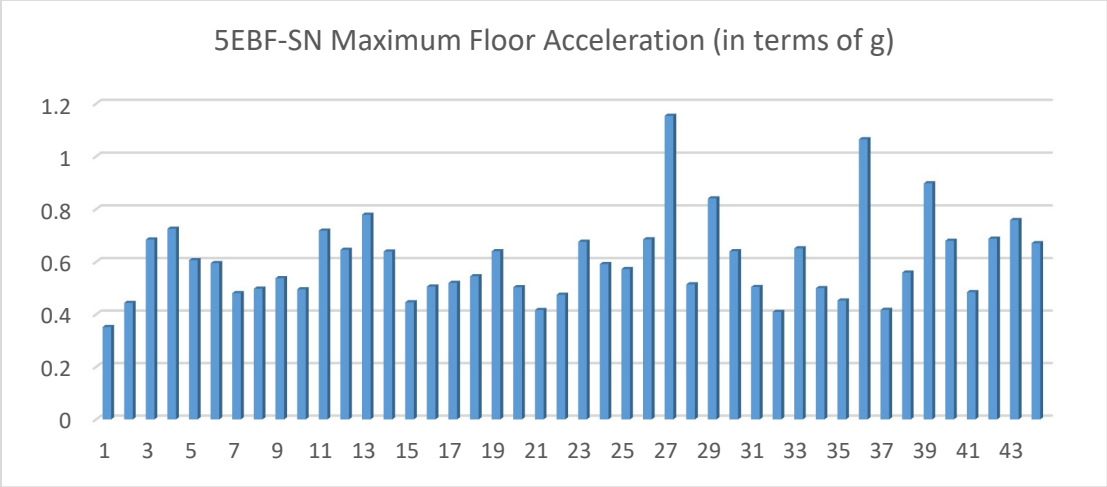


*Figure 4. 33 5EBF-SN acceleration response over 44 far-field earthquake ground motion records scaled to design basis earthquake (unit: g)*

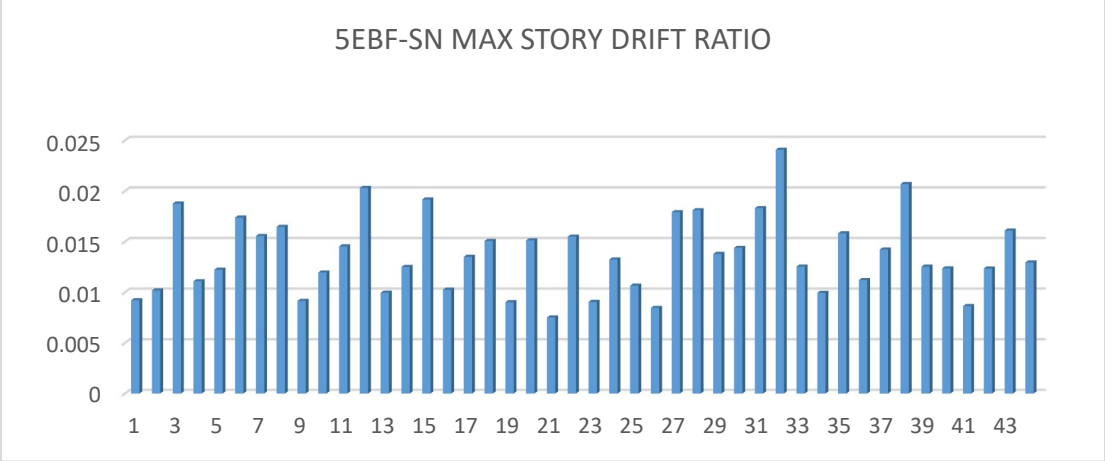


*Figure 4. 34 5EBF-SN Maximum Inter-story Drift Ratio over 44 far-field earthquake ground motion records scaled to design basis earthquake*

# Chapter 5: Resilience Evaluation using FEMA P-58 Procedure

This chapter deals with the seismic assessment of EBFs designed previously. Here, the seismic evaluation is performed using FEMA P-58 procedure. This methodology assesses individual buildings' seismic performance based on their unique site, structural, nonstructural, and occupancy characteristics. Ultimately, this procedure expresses the building's performance in terms of the probability of incurring casualties, repair and replacement costs, repair time, environmental impacts, and unsafe placarding. Also, this procedure considers the unpredictability of earthquake shaking, subsequent damage and resulting consequences by expressing performance in the form of probable impacts. Casualties, Repair Cost, Repair Time, Environmental impacts, and Unsafe placarding are the performance measures in FEMA P-58 methodology. Although numerous factors affect the level of damage buildings experience during an earthquake and the consequences associated with this damage, FEMA P-58 methodology considers the following factors only:

1. ground shaking intensity and other earthquake effects experienced by the structure.
2. the building's response to ground shaking and the induced demands on both the structural and nonstructural components.
3. The damage vulnerability of the building components, systems, and contents.
4. The number of people and the type, location, and the number of contents present within the building envelope when the earthquake occurs.

5. Inspectors' interpretation of visible evidence of damage while performing post-earthquake investigations.
6. Choice of repair methods and specific details.

Besides, each of these factors considered has significant uncertainty associated with them. For instance, it is impossible to predict which fault will produce the next earthquake, where the rupture will initiate along the fault line or the magnitude of shaking. Further, the latest analytical modelling techniques of structures are also not precise due to assumed material strength, cross-section geometry, damping, and construction details. Moreover, most damage vulnerability of components is based on laboratory experiments. The lab tested component behavior may differ significantly from the same component's behavior in the actual structure. Likewise, when an earthquake occurs, the building's population during this exact time and the type or number of nonstructural components present are also difficult to predict. Finally, even though the damage is predicted, the repair technique the designer will choose cannot be known for sure. As a result, it is very challenging to assess the seismic performance precisely. Therefore, it is preferred approach at present to express performance measures in the form of probabilistic performance functions. Performance functions are statistical distributions that indicate the probability that losses of a specified or smaller magnitude will be incurred as a result of future earthquakes [16]. Overall, the methodology and procedures presented in FEMA P-58 describe a means to determine performance functions. Although other factors such as the speed and care given to the injured people, the approval speed of repair designs, post-disaster availability of materials and labor, and the decision to repair an occupied structure or repair a vacant

structure account for uncertainty, they are not considered in this methodology as they are incredibly unpredictable.

Figure 5.1 illustrates the FEMA P-58 performance assessment process. The first step of the assessment process is to select an assessment type and performance measures from the figure. For this study, an Intensity-based assessment was selected as discussed earlier, and the building's performance is expressed in terms of repair costs as a percentage of total replacement cost and repair time as a percentage of total replacement time. Subsequent sections in this chapter will describe the remaining performance assessment steps.

Further, FEMA P-58 also developed a tool to implement this methodology for user convenience, known as the Performance Assessment Calculation Tool, PACT. PACT is an electronic calculation tool and a repository of fragility and consequence data used for performance assessment. Overall, PACT uses the Monte Carlo procedure to assess a range of possible outcomes given a limited set of inputs. In general, PACT provides three primary functions:

1. Collecting and arranging building information, fragility functions and demand parameters.
2. Performing loss calculations which include repair cost, downtime, and casualty estimates
3. Providing overall and performance group-specific loss information obtained from the above calculation.

This study uses PACT to evaluate performance for all the nine EBFs. Figure 5.2 displays the PACT control panel, which opens first when PACT is started. As can be

seen in the figure, the control panel is divided into two sub-sections PACT operations and PACT utilities. Further, the PACT operations section is subdivided into Model the building and import analyses results, evaluate performance, and examine results. All the inputs and calculations for performance assessment are performed in this subsection. Similarly, the PACT utilities section is subdivided into Fragility Specification Manager and Building Population Modeler. These sub-sections allow the user to create new or view pre-existing fragility specifications and building population model. Since this study uses pre-defined fragility and population model, only the PACT operations section was utilized. Figure 5.3 shows the flowchart for the FEMA P-58 performance assessment methodology. Each of the steps in the flowchart is described in detail with examples for the 4-story EBFs (California) in the subsequent sections.

## *5.1 Assemble Building Performance Model*

The first step for performance assessment methodology, from Figure 5.3, is to assemble the building performance model. According to FEMA P-58, the buildings performance model is an organized collection of data necessary to define building assets at risk and vulnerable to earthquake shaking. This model should include:

1. General building data including the size, replacement cost, replacement time, and replacement quantities for embodied energy and carbon.
2. Occupancy, including population distribution in the building over time and the number of nonstructural components present in the building.
3. Vulnerable structural and nonstructural components and assemblies in sufficient detail; their vulnerability to damage during the earthquake; and the consequences of this damage.

Overall, the building performance model includes population models, fragility groups, and performance groups. Fragility specifications are assigned to components that are vulnerable to damage. These specifications comprise the component damage states, fragility functions, and consequence functions. This study uses PACT to assemble the building performance model. Further, PACT assessment for the 4-story EBFs (California) is broken down into sub-sections and described in detail.

### 5.1.1 Project Information

After starting PACT and selecting Model the building and import analyses results under the PACT operations panel, a new window pops out. This window has different tabs that require user input. First, data are input on the Project Information tab, as shown in Figure 5.4. Here, Project ID, building description, Client and Engineer text boxes allow the user to describe the project so each project can be discrete. Next, the Project Information tab requires cost multipliers values. As can be seen from Figure 5.4, both the regional and date cost multipliers are set to 1, which is the default value. These multipliers are based on the building's location and the time value of escalation or devaluation effects. PACT default consequence function reflects 2011 costs for the Northern California Region. Since, both the locations in this study are very close to the Northern California Region assuming default value is quite reasonable. Next, the Solver Random Seed Value is set to 5; this ensures the assessment model produces the same answer for multiple executions even though the same data is input.

### 5.1.2 Building Information

The next input tab is the Building Information tab, Figure 5.5. Major inputs in this Tab are the shell replacement cost, total replacement cost, replacement time and replacement quantities for embodied energy and carbon. Shell replacement cost includes replacing the structure, exterior enclosure and MEP infrastructure that are present before tenant improvements are made. In contrast, the total replacement cost includes all tenant improvements as well as the shell replacement cost. Here, the total replacement cost and the shell replacement cost are assumed based on the floor area. This study assumes a unit price of $250/ sq. ft and $150/sq. ft for the total replacement and the shell replacement costs, respectively. Similarly, the replacement time is assumed based on the number of stories, 180 days per story. Next, Carbon emissions and embodied energy replacement costs consider the amount of energy and carbon released during repair or demolition of the building. Here, Carbon emissions and embodied energy replacement were calculated based on the building's total replacement cost. The total replacement cost was multiplied with an environmental impact factor (0.414 kg CO2e/$) and divided by an inflation factor (0.88) to convert it into the 2011 prices for the carbon emissions replacement cost. Similarly, embodied energy replacement cost was calculated by multiplying the total replacement cost with an environmental impact factor (5.729 MJ/$) and divided by the same inflation factor used for carbon emissions cost. All the per unit area prices and factors used in this study are taken directly from an example in FEMA P-58 [16]. Further, the input for maximum workers per square foot was assigned with its default value, i.e., 0.001. This default value implies a single worker for every 1000 square foot area. Finally, the input for

Total Loss Threshold value remains. This threshold sets a pre-determined cap on the level of the repair effort. The total loss threshold value was set to the default value of 1. This value is the ratio of repair cost to total replacement cost beyond which repair is no longer feasible.

Detailed Calculation of all the parameters, mentioned above, can be seen in Figure 5.6. Additionally, this tab requires the height and area input, along with different floor definitions. The story height and the floor area input were already discussed in Chapter 3. Note, it is important to understand how PACT defines floor and story numbers. Figure 5.7 illustrates these definitions visually. Also, from Figure 5.5, each floor level has additional factors to account for the repair difficulty, presence of lead-based paints and the possibility of vacancy for repairs called Height factor, Hazmat factor and Occupancy factor, respectively. This study assumes the cost of repair work on each floor to be fairly similar; hence a Height factor of 1 is selected. Further, no lead-based paints and full vacancy of the building for repair was also assumed. Therefore, both the Hazmat and Occupancy factor were set equal to 1.

### 5.1.3 Population Distribution

The next tab following the building information tab is the population tab, Figure 5.8. In this tab, the user defines the building's population model. This model should include the peak population, the likelihood of people present at times of peak occupancy, and the population likely to be present at other times. In general, population patterns differ with time of the day, day of week and month of the year. For instance, the building's population may change during lunch breaks or weekdays and weekends or holidays. Additionally, the type of occupancy also affects population distribution. Hence, taking

both occupancy and time variation, FEMA provides population models which are shown in Table 5.1. These models are used to generate estimates of casualties. This study uses the predefined population model for commercial office occupancy, having a peak population of four per 1000 square feet of area. Figure 5.9 and 5.10 shows the population distribution for the commercial office occupancy for weekdays and weekends, respectively. Further, each population model is assigned an equivalent continuous occupancy (ECO), a time-weighted average population continually occupying a building, which enables rapid estimation of mean casualties by reducing the apparent dispersion in casualty estimates.

### 5.1.4 Component Fragility and Performance groups

After the population tab, PACT requires input for the component fragilities tab (Figure 5.11). Here, all vulnerable structural components, nonstructural components and contents need to be identified and categorized into fragility groups and further sub-divided into performance groups. The components or assemblies are categorized into the same fragility group when they have similar construction characteristics, potential modes of damage, probability of incurring these damage modes during an earthquake and potential consequences resulting from damage. Further, these fragility groups are sub-divided into performance groups, the sub-categorization of the fragility group components affected by the same earthquake demands.

PACT is a repository of fragility and performance specifications. In PACT, the fragility groups are identified by a unique classification number based on NISTIR 6389, UNIFORMAT II Elemental Classification for Building Specifications, Cost Estimating and Cost Analysis [38]. For example, B1035.062a represents an EBF Shear Link with

floor beams. For this study, the shear link is the only vulnerable structural component expected to be damaged. Hence, B1035.062a component fragility was selected. Further, adding this component fragility as most typical specification in PACT automatically adds it to all the floors. Also, since there are EBFs in both directions, both the direction boxes are checked.

Each of the pre-defined fragility group has its own fragility specification. Figure 5.12 shows the fragility specification for EBF Shear Link with floor beams (B1035.062a). From figure as expected, the demand parameter this component is vulnerable to is the link rotation angle. Additionally, this specification includes different damage states associated with the demand parameter and the consequences of each of these damage states. For example, B1035.062a has three damage states which are defined:

1. Damage State DS1- Damage to the concrete slab above the link beam
2. Damage State DS2- Web Local buckling, flange local buckling
3. Damage State DS3- Initiation of fracture in the link beam and link flange.

These damage states occur sequentially for this fragility group. In other words, damages progress to higher levels as demand increases. Further, a unique fragility function is assigned to each damage states. Figure 5.13 shows the fragility functions for the three damage states of B1035.062a. This fragility function combined with the calculated demands determines the component's damage state for each realization. Ultimately, all the component damage states define the building damage state.

After identifying the structural components, it is now essential to include the nonstructural components. Usually, the nonstructural components can be estimated using design drawings such as architectural, mechanical, electrical, and plumbing;

however, this level of detail is rarely available during the design process. Hence, FEMA P-58 has developed a tool to estimate the nonstructural components found typically in buildings with similar occupancy and size, known as the Normative quantity estimation tool. FEMA developed this tool based on a detailed analysis of approximately 3000 buildings across typical occupancies. Although the tool allows for the estimation of quantities at the 10th, 50th, and 90th percentile levels, FEMA recommends the use of 50th percentile quantities. Due to the lack of nonstructural data, this study uses the Normative estimation tool to estimate the nonstructural components typically present in a commercial office. Table 5.2 shows the input for the Normative estimation tool typical for this study. The tool then runs a VBA code and generates an estimation for the nonstructural components on each floor. The nonstructural components along with their quantities are generated by this tool. Table 5.3 shows the nonstructural components estimated for 3rd floor of the 4 story EBFs in California. Next in PACT, the user manually finds the estimated structural and nonstructural components using their unique classification number. Also, after both the structural and nonstructural components are added in the fragility tab, they are automatically added to the Performance groups tab. In the performance groups tab, the structural and nonstructural components are reorganized automatically based on directional effects. In other words, PACT determines whether direction matters or not for the component damage assessment. Figure 5.14 and 5.15 show the directional and non-directional performance groups for the 4 story EBFs in California. Further, PACT requires performance group quantities, quantity dispersion, fragility correlation, population model and demand parameters. The performance group quantities and quantity dispersion are taken

directly from the Normative Estimation Tool. In addition, the quantity of components in PACT depends on the fragility group specification i.e., if the fragility specification is for an assembly of four components then the quantity of components input in PACT becomes the actual quantity estimated divided by four. Here, no fragility correlation is assumed, and the population model defined earlier was used.

## *5.2 Define Earthquake Hazards*

This step in the performance assessment process describes how earthquake hazards are defined, selected, and specified. Since Chapter 3 discusses most of this section in detail, this section will only focus on the development of the site-specific hazard curve. In general, a hazard curve is a plot of the annual frequency of exceedance against peak ground acceleration or one of the spectral accelerations. This study uses a USGS tool to obtain a site-specific seismic hazard curve known as the Unified Hazard Tool [39]. Figure 5.16 shows the input for the Unified Hazard Tool. In the figure, the latitude and longitude inputs are for the California Apple headquarters location. Also, according to FEMA P-58, for structures in the period range of 0.7 to 2.0 seconds, it is generally considered sufficiently accurate to obtain Sa(T) from the formula:

$$S_a = \frac{S_a(1.0)}{T} \qquad \text{Eq 31}$$

Since all the structures in this study have their fundamental period within this range, the above equation is used to develop the site-specific hazard curve. Hence, the 1-second spectral acceleration input was selected in the USGS Tool. Further, the site class in the Unified Hazard tool is limited to B/C boundary. As all the sites in this study are classified as Site Class D and all the natural periods are within the constant velocity

zone of the design response spectrum, the $F_v$ factor from Table 3.4 is used to convert the site class. Figure 5.18 shows the hazard curve generated using the previous inputs in Unified Hazard Tool. If the mouse cursor is hovered over each of these points, annual frequency of exceedance and its corresponding 1 second spectral acceleration is displayed. These values for each of the points are shown in Table 5.4. This table is for the 4 story EBFs in California location having a maximum fundamental time period of 0.86 seconds. Overall, the table shows the spectral acceleration values (at 1.0s) and mean annual frequency of exceedance, $\lambda$, values obtained from the Unified Hazard Tool, and values of *Sa* (0.86s) derived using the above formula with T= 0.86s. The table also provides values of $F_v$ obtained from Table 3.4 at each $\lambda$ and the corresponding *Sa* (0.86s) values at Site Class D, using $F_v$.

PACT has a hazard curve tab which requires at least three points; $S_a^{min}$ (T), $S_a$(T) and $S_a^{max}$(T). First, $S_a$(T) can be easily obtained using interpolation as shown in Table 5.5. Second, $S_a^{min}$ (T) and $S_a^{max}$(T) are determined as per FEMA P-58 recommendation using the following equations:

$$S_a^{min}(T) = \frac{0.05}{T} \quad \text{Eq 32}$$

$$S_a^{max}(T)\ is\ Larger\ of\ median\ collapse\ capacity\ or\ 2 * (S_a(T)\ with\ \lambda = 0.004) \quad \text{Eq 33}$$

Both these values are obtained using interpolation, as shown in Table 5.5. Last, the median collapse capacity will be discussed later in section 5.4. These parameters were input to the PACT hazard curve tab as shown in Figure 5.17. Likewise, the hazard curve for the Seattle location was also developed.

## *5.4 Develop Collapse Fragility*

Although the next step in the methodology is to analyze building response, this step has been skipped here since it was discussed in detail in Chapter 4. Hence, this section deals with the next step after analyze building response which is to develop collapse fragility for the system. Generally, building collapse is responsible for most casualties during earthquakes. The assessment of these casualties requires a relationship between the probability of incurring structural collapse and ground motion intensity. This relationship is known as the building collapse fragility. Determining casualties is essential for performance assessment. Overall, the probability of collapse is expressed as a lognormal distribution of spectral acceleration at the fundamental period, defined by a median value, $\hat{S}_a(T)$, and dispersion, β. FEMA P-58 presents three different procedures to develop the building collapse fragility functions for input into the building performance model. However, this section will only focus on Nonlinear Response History analysis as it is the most reliable out of all other procedures. In summary, this analysis involves running numerous analyses with increasing intensity levels ranging from intensities that produce an almost linear response to those that cause collapse. Lastly, the fraction of ground motions at each intensity level that causes collapse is fitted using a smooth lognormal distribution to form the building's collapse fragility.

Foremost, the collapse criteria need to be defined in order to develop collapse fragility. These criteria will help identify if the building collapses or not. Usually, collapse is defined by numerical instability, load capacity deterioration, excessive lateral drifts, or demands exceeding the capacity of gravity-load carrying components. Likewise, in this

study, building collapse is deemed to occur when numerical instability occurs, the roof drifts exceed 4% of the total height, or gravity-load carrying members fail.

Second, nonlinear response history analyses are performed at multiple intensity levels, some of which result in collapse. At each intensity level, I, an estimated conditional probability of collapse, P (C | I), is obtained from the equation:

$$P(C|I) = \frac{n}{N} \qquad \text{Eq 38}$$

where n is the number of analyses at intensity, I, for which collapse is predicted, and N is the total number of analyses performed at intensity. Finally, these probabilities are plotted with their respective intensities and fitted to form the building's collapse fragility. This study uses an excel workbook application designed by FEMA P-58 to help fit lognormal curves to develop the collapse fragility known as the Collapse fragility tool. Figure 5.18 shows the collapse fragility developed for a four-story EBF (California location) using the Collapse Fragility Tool. The curve in the figure is fitted to data near the median collapse point and has a dispersion of 0.6. Detailed calculation for this curve is shown in Table 5.6.

Next, this median collapse intensity and dispersion is input in Collapse Fragility Tab in PACT, Figure 5.19. Additionally, PACT requires collapse mode inputs such as the number of independent collapse modes that can occur and their probability of occurrence. According to FEMA P-58, to determine these data, the user must use judgment based on building type, structural system, experience, and analytical inferences. For this study, collapse modes and their probability were determined judgmentally by comparing maximum story drift from each analysis. Further, PACT input requires the fraction of each floor subject to collapse-associated debris and the

resulting fatality and injury rates. These inputs were also determined judgmentally. Finally, this completes all the inputs required for PACT assessment.

## *5.5 Performance Calculation*

At last, the final step for the performance assessment procedure is to calculate performance. This section describes the building performance calculation procedure, which includes the generation of simulated demands, assessment of collapse, determination of damage, and computation of losses in various performance measures. In general, the model should include a significant number of structural analyses and analytical models with randomly varying properties to account for uncertainties and variability in the building performance model. Currently, this approach is impractical and complex for use. Instead, a Monte Carlo procedure is used to generate a large number of possible outcomes from a limited set of inputs. Overall, limited suites of analyses are performed to generate a series of building response states to a particular ground motion intensity. Next, a statistical relationship between these demands is established from which a large number of statistically consistent possible outcomes are generated. Lastly, these possible demand sets, in combination with fragility and consequence functions of each component, determine the damage state and consequences associated with this damage state. Further, the combination of consequences of all the components in the system determines the performance of the whole system.

Figure 5.20 shows the performance calculation steps for each realization. First, simulated demand sets are generated using the Monte Carlo procedure. Next, each realization initiates by assuming a time of day, and day of the year for an earthquake

occurrence. Next, this assumed time and the population model determine the number of people present in the building for this realization. After the realization initiates, the next step is to determine if the structure collapsed or not. This step uses collapse fragility developed earlier to determine the possibility of collapse. Only two possible cases exist, i.e., building collapses, or it does not. In case the structure collapses, repair cost, repair time, and embodied energy and carbon for the realization are set equal to the building replacement values. Also, casualties are determined using the number of people present in the building, which was assumed earlier. In case the structure does not collapse, the damage sustained by each component needs to be calculated. Therefore, each realization with a single vector of simulated demands and fragility functions are used to determine each performance group's damage state. Finally, after the damage state have been identified, the losses are calculated based on the damage sustained by each component and the consequence functions assigned to each performance group. The overall building loss for the realization is the sum of each performance group's losses. Additionally, the procedure also considers the repairability of the building. The maximum residual drift ratio is used, together with a building repair fragility, to determine if repair is practical. If the repair is impractical, repair cost, repair time, and embodied energy and carbon for the realization are set equal to the building replacement values. These aforementioned calculations are repeated for a large number of realizations, and loss distribution is developed. These values are sorted in ascending order to enable the calculation of the probability that loss will not exceed a specific value for a given intensity of shaking. For instance, if calculations for 1000 realizations are assembled in ascending order, the repair cost with a 90% probability of

exceedance would be the repair cost for the realization with the 100th highest cost, as 90% of the realizations exceeded this computed cost.

This study uses PACT to calculate performance using 2,000 realizations for each of the nine EBFs. Figure 5.21 to 5.27 show all PACT calculation results in terms of repair cost, repair time, environmental impacts, and unsafe placarding for the 4-story EBF in California. From the figures, it is evident that PACT developed performance functions for each of these performance measures. Ultimately, the decision makers can use these performance functions to make informed decisions. Finally, the performance assessment using FEMA P-58 is complete. This study primarily focuses on repair cost and repair time among the performance measures. Therefore, Table 5.7 shows the repair cost and time as a percentage of the total replacement cost and time for all the 9 structures with an exceedance probability of 25%. Similarly, the steps described above were repeated to generate performance results for all the 9 EBFs. Next, it is essential to validate these results. Therefore, an existing structure was assessed using the same procedure which is described in detail in the next section.

## *5.6 Case Study: Pacific Tower (Christchurch)*

Lastly, to verify the PACT results for the nine newly designed EBFs, this study assesses an existing structure's performance in PACT. After the assessment, this study compares the results with the actual performance of the building during an earthquake. Hence, a building with extensive data on seismic performance needs to be selected. For this study, the structure selected is the 22-story Pacific Tower in Christchurch, New Zealand, as it performed well during the 2011 Christchurch earthquake and has sufficient actual performance data available for comparison to the PACT assessment.

Figures 5.28 and 5.29 show the location and a picture of the Pacific Tower, respectively. Overall, this structure is a twenty-two storied steel frame building with precast concrete cladding panels for most of its height. Further, this structure uses a combination of both EBFs (K and D type) and MRFs to resist lateral loads. Figure 5.30 and 5.31 show the plan view of the Pacific Tower for level 6 and level 11, respectively. Here, the markups help identify the different lateral load resisting frames of the structure. Since this study focuses on K-type eccentric braced frames, only the Grid 6 K-type EBF was of interest. Figure 5.32 shows an elevation view of this grid. Additionally, this building has a mixed occupancy of a hotel (1-14 level) and an apartment (14-22 level). Next, the performance assessment steps for this structure are described briefly.

First, the total replacement cost and total replacement time are estimated using the same assumptions in section 5.1 due to the lack of sufficient cost data. Figure 5.33 shows the Building information Tab inputs for Pacific Tower. Next, using the Normative Estimation Tool and the floor occupancy, Non-structural components are estimated as the nonstructural component data is unavailable. Table 5.8 shows the Normative Estimation Tool input while Tables 5.9 and 5.10 show the nonstructural estimates for the hotel and apartment occupancies, respectively. Next, for the structural component, the same link fragility group, B1035.062a, was used as earlier. Hence, the building performance model was assembled. Second, earthquake hazards need to be defined. Here, actual ground records from stations within 10 km of the site were used for response history analysis, Table 5.13. All the recording stations distance were verified using google maps, an example can be seen in Figure 5.36. Additionally, all the ground

motion components considered are along the N-S direction which is the direction of interest. Further, a site-specific hazard curve was also generated using the NZS 2004 [40]. Third, a nonlinear model with parameters as described in section 4.1 was modelled in OpenSees. A seismic weight of 125 psf was assumed to calculate the seismic mass of the structure. As this study focuses on the EBF along N-S direction, the calculated seismic weight is then distributed to each of the lateral resisting frames along this direction based on their relative rigidity. Figure 5.38 shows a structural model in ETABS software of all the lateral resisting frames along N-S direction modelled side by side and connected by rigid beams. Next, an arbitrary point load was applied to the roof node. The shear distribution in each of frames due to this arbitrary load was used to distribute seismic mass in each frame. Using this mass distribution, only the EBF was modelled in OpenSees. Table 5.12 and Figure 5.37 show the modal analysis results in OpenSees. Further, Table 5.11 shows the actual fundamental period in translation for the Pacific Tower [41]. Since the modal results from OpenSees closely match with Table 5.11 values, the OpenSees model is valid. Next, the model was subjected to the actual ground motions records and their responses were recorded.

Next, the structural collapse fragility was developed using the same procedure in section 5.4. The ground motions were scaled at different intensities to determine the intensity at which half the ground motions caused failure. Failure definition remained unchanged for this model too. Using this median collapse intensity and a dispersion factor, the collapse fragility of the system was developed. Finally, all of these inputs are fed in PACT and performance is assessed in terms of repair time. Figure 5.39 shows the PACT results for Pacific Tower in terms of repair time.

This building was out of service from February 2011 (Christchurch earthquake) until 1 May 2013 for repairs [42]. This implies that the building lost its function for almost 26 months. Since this study focuses on the N-S direction, this downtime needs to be adjusted for comparison. This study assumes that the repair time for each orthogonal direction is equal. Hence, the N-S direction is responsible for 13 months of the downtime. Further, the damaged link beams in the Pacific tower were cut off which subsequently increased the downtime. In contrast, this study uses replaceable links, the replacement time for these links is shorter than the time for cutting the beams. Hence, to take this into consideration the downtime was further reduced to 2/3. Applying this reduction, the downtime predicted is 8.67 months or 261 days. From PACT results in Figure 5.39, the probability that the repair time will be less than or equal to 261 days was found to be 77% as can be seen in figure 5.39. Evidently, this result is coherent with the actual performance of the structure. Therefore, this coherence verifies the performance assessment procedure and validates the assessment of all new design EBFs.

*Table 5. 1 Default Peak Population by Occupancy Adapted from FEMA P-58 [16]*

| Occupancy | Peak Population Values (per 1000 sq. ft.) | Peak Population Time of Day |
|---|---|---|
| Commercial Office | 4.0 | Daytime(3 pm) |
| Education (K-12): Elementary Schools | 14.0 | Daytime |
| Education (K-12): Middle Schools | 14.0 | Daytime |
| Education (K-12): High Schools | 12.0 | Daytime |
| Healthcare | 5.0 | Daytime(3 pm) |
| Hospitality | 2.5 | Nighttime(3 pm) |
| Multi-Unit Residential | 3.1 | Nighttime(3 pm) |
| Research Laboratories | 3.0 | Daytime(3 pm) |
| Retail | 6.0 | Daytime(5 pm) |
| Warehouse | 1.0 | Daytime(3 pm) |

*Table 5. 2 Normative Estimation Tool- Building Definition*

**USER NOTES**

**This sheet takes the builidng occupancy input and displays the quantity results computed by this tool.**

**Do not edit not shaded cells. Do not shift cells. See the Usage Notes on the Notes Tab for additional information.**

N floors: 4

**BUILDING DEFINITION TABLE**

| Floor Name | Floor # | Total Floor Area | Occupancy 1 | | Occupancy 2 | | Occupancy 3 | | SUM % AREA |
|---|---|---|---|---|---|---|---|---|---|
| | | ( sf ) | Type | % Area | Type | % Area | Type | % Area | |
| Roof | 4 | 18750 | none | 100% | none | 0% | none | 0% | 100% |
| 3rd | 3 | 18750 | OFFICE | 100% | none | 0% | none | 0% | 100% |
| 2nd | 2 | 18750 | OFFICE | 100% | none | 0% | none | 0% | 100% |
| 1st | 1 | 18750 | OFFICE | 100% | none | 0% | none | 0% | 100% |
| | | | | | | | | | |
| | | | | | | | | | -- |
| | | | | | | | | | -- |
| | | | | | | | | | -- |

*Table 5. 3 Normative Estimation Tool- 3rd floor non-structural estimate*

**COMPONENT SUMMARY MATRIX**

| OCCUPANCY | | | | Fragility Number | Fragility Name | Assumed Quantity per component within PACT | Quantity | | Correlated Fragility? | Acutal Quantity | | PACT Basic Unit | Fragility Quantity Beta (LogNormal Distribution) |
|---|---|---|---|---|---|---|---|---|---|---|---|---|---|
| Type | Occupancy # | Floor Name | Component Area (sq ft ) | | | | Directional | Non Directional | | Value | Unit | | |
| T OF STANDARD INPUT | | | | | | | | | | | | | |
| OFFICE | 1 | 3rd | 18750 | **None Found** | Cladding - Gross Wall Area | -- | -- | -- | ?? | -- | -- | None Found | 0.5 |
| OFFICE | 1 | 3rd | 18750 | **B2022.001** | B2022.001 Curtain Walls - Generic Midrise Stick-Built Curtain | 30 SF | 187.50 | -- | NO | 5625.0 | SF | Each | 0.6 |
| OFFICE | 1 | 3rd | 18750 | **B3011.011** | B3011.011 Concrete tile roof, tiles secured and compliant wit | 100 SF | -- | 50.63 | NO | 5062.5 | SF | Each | 1.3 |
| OFFICE | 1 | 3rd | 18750 | **C1011.001a** | C1011.001a Wall Partition, Type: Gypsum with metal studs, F | 100 LF | 18.75 | -- | NO | 1875.0 | LF | Each | 0.2 |
| OFFICE | 1 | 3rd | 18750 | **C3021.001k** | C3021.001k Generic Floor Covering - Flooding of floor caused | User By | -- | -- | NO | -- | By | Each | 0.7 |
| OFFICE | 1 | 3rd | 18750 | **C3011.001a** | C3011.001a Wall Partition, Type: Gypsum + Wallpaper, Full He | 100 LF | 1.42 | -- | NO | 141.8 | LF | Each | 0.7 |
| OFFICE | 1 | 3rd | 18750 | **C3027.001** | C3027.001 Raised Access Floor, non seismically rated. | 100 SF | -- | 140.63 | NO | 14062.5 | SF | Each | 0.2 |
| OFFICE | 1 | 3rd | 18750 | **C3032.001a** | C3032.001a Suspended Ceiling, SDC A,B,C, Area (A): A < 250, V | 250 SF | -- | 67.50 | NO | 16875.0 | SF | Each | 0.0 |
| OFFICE | 1 | 3rd | 18750 | **C3032.001a** | C3032.001a Suspended Ceiling, SDC A,B,C, Area (A): A < 250, V | 250 SF | -- | 3.75 | NO | 937.5 | SF | Each | 0.0 |
| OFFICE | 1 | 3rd | 18750 | **C3032.001a** | C3032.001a Suspended Ceiling, SDC A,B,C, Area (A): A < 250, V | 250 SF | -- | 2.25 | NO | 562.5 | SF | Each | 0.0 |
| OFFICE | 1 | 3rd | 18750 | **C3032.001a** | C3032.001a Suspended Ceiling, SDC A,B,C, Area (A): A < 250, V | 250 SF | -- | 1.50 | NO | 375.0 | SF | Each | 0.0 |
| OFFICE | 1 | 3rd | 18750 | **None Found** | Fixed Casework | -- | -- | -- | ?? | -- | -- | None Found | 0.0 |
| OFFICE | 1 | 3rd | 18750 | **None Found** | Fume Hoods | -- | -- | -- | ?? | -- | -- | None Found | 0.0 |
| OFFICE | 1 | 3rd | 18750 | **E2022.001** | E2022.001 Modular office work stations. | 1 EA | -- | UNIT MISMATCH | NO | -- | EA | Each | 0.2 |
| OFFICE | 1 | 3rd | 18750 | **E2022.112a** | E2022.112a Vertical Filing Cabinet, 2 drawer, unanchored late | 1 EA | -- | 15.00 | NO | 15.0 | EA | Each | 0.6 |
| OFFICE | 1 | 3rd | 18750 | **E2022.102a** | E2022.102a Bookcase, 2 shelves, unanchored laterally | 1 EA | -- | 37.50 | NO | 37.5 | EA | Each | 0.6 |
| OFFICE | 1 | 3rd | 18750 | **None Found** | Domestic Plumbing Fixtures | -- | -- | -- | ?? | -- | -- | None Found | 0.7 |
| OFFICE | 1 | 3rd | 18750 | **None Found** | Lab Plumbing Fixtures | -- | -- | -- | ?? | -- | -- | None Found | 0.0 |
| OFFICE | 1 | 3rd | 18750 | **D2021.011a** | D2021.011a Cold or Hot Potable - Small Diameter Threaded | 1000 LF | -- | 0.79 | NO | 787.5 | LF | Each | 0.7 |
| OFFICE | 1 | 3rd | 18750 | **None Found** | Piping - Gas supply piping | -- | -- | -- | ?? | -- | -- | None Found | 0.2 |
| OFFICE | 1 | 3rd | 18750 | **None Found** | HVAC - Boiler capacity | -- | -- | -- | ?? | -- | -- | None Found | 0.3 |
| OFFICE | 1 | 3rd | 18750 | **D3041.012a** | D3041.012a HVAC Galvanized Sheet Metal Ducting - 6 sq. ft c | 1000 LF | -- | 0.38 | NO | 375.0 | LF | Each | 0.2 |
| OFFICE | 1 | 3rd | 18750 | **D3041.011a** | D3041.011a HVAC Galvanized Sheet Metal Ducting less than 6 | 1000 LF | -- | 1.41 | NO | 1406.3 | LF | Each | 0.2 |
| OFFICE | 1 | 3rd | 18750 | **D3041.031a** | D3041.031a HVAC Drops / Diffusers in suspended ceilings - No | 10 EA | -- | 16.88 | NO | 168.8 | EA | Each | 0.5 |
| OFFICE | 1 | 3rd | 18750 | **D3041.041a** | D3041.041a Variable Air Volume (VAV) box with in-line coil, S | 10 EA | -- | 9.38 | NO | 93.8 | EA | Each | 0.2 |
| OFFICE | 1 | 3rd | 18750 | **D3041.041a** | D3041.041a Variable Air Volume (VAV) box with in-line coil, S | 10 EA | -- | 3.75 | NO | 37.5 | EA | Each | 0.5 |
| OFFICE | 1 | 3rd | 18750 | **None Found** | HVAC - Pressure Dependent Air Valves (Phoenix type boxes) | -- | -- | -- | ?? | -- | -- | None Found | 0.0 |
| OFFICE | 1 | 3rd | 18750 | **None Found** | Electrical - Electrical Distribution conduits | -- | -- | -- | ?? | -- | -- | None Found | 0.6 |
| OFFICE | 1 | 3rd | 18750 | **None Found** | Electrical - Electrical Distribution – cable trays | -- | -- | -- | ?? | -- | -- | None Found | 0.9 |
| OFFICE | 1 | 3rd | 18750 | **C3034.001** | C3034.001 Independent Pendant Lighting - non seismic | 1 EA | -- | 281.25 | NO | 281.3 | EA | Each | 0.3 |
| OFFICE | 1 | 3rd | 18750 | **C3034.001** | C3034.001 Independent Pendant Lighting - non seismic | 1 EA | -- | 281.25 | NO | 281.3 | EA | Each | 0.3 |
| OFFICE | 1 | 3rd | 18750 | **D4011.021a** | D4011.021a Fire Sprinkler Water Piping - Horizontal Mains an | 1000 LF | -- | 3.75 | NO | 3750.0 | LF | Each | 0.1 |
| OFFICE | 1 | 3rd | 18750 | **D4011.031a** | D4011.031a Fire Sprinkler Drop Standard Threaded Steel - Dro | 100 EA | -- | 1.69 | NO | 168.8 | EA | Each | 0.2 |

*Table 5. 4 Unified Hazard Tool Data, Corrected for Building Period and Site Class*

| Sa(T=1s) site class B/C | MAFE | Sa(T=0.86s) site class B | Fv | Sa(T=0.86s) site class D |
|---|---|---|---|---|
| **0.0025** | 0.62960300 | 0.002906977 | 2.4 | 0.006976744 |
| **0.00375** | 0.47754200 | 0.004360465 | 2.4 | 0.010465116 |
| **0.00563** | 0.34806300 | 0.006546512 | 2.4 | 0.015711628 |
| **0.00844** | 0.24525500 | 0.009813953 | 2.4 | 0.023553488 |
| **0.0127** | 0.16706300 | 0.014767442 | 2.4 | 0.03544186 |
| **0.019** | 0.11149500 | 0.022093023 | 2.4 | 0.053023256 |
| **0.0285** | 0.07263620 | 0.033139535 | 2.4 | 0.079534884 |
| **0.0427** | 0.04654220 | 0.049651163 | 2.4 | 0.119162791 |
| **0.0641** | 0.02914130 | 0.074534884 | 2.4 | 0.178883721 |
| **0.0961** | 0.01765850 | 0.111744186 | 2 | 0.223488372 |
| **0.144** | 0.01014930 | 0.16744186 | 2 | 0.334883721 |
| **0.216** | 0.00541537 | 0.251162791 | 1.8 | 0.452093023 |
| **0.324** | 0.00263058 | 0.376744186 | 1.6 | 0.602790698 |
| **0.487** | 0.00112560 | 0.56627907 | 1.5 | 0.849418605 |
| **0.73** | 0.00041285 | 0.848837209 | 1.5 | 1.273255814 |
| **1.09** | 0.00012610 | 1.26744186 | 1.5 | 1.901162791 |
| **1.64** | 0.00002833 | 1.906976744 | 1.5 | 2.860465116 |

*Table 5. 5 Hazard Curve- Samin and Samax Calculation*

| Sa(T=0.86s) siteclass D | MAFE | | | | | |
|---|---|---|---|---|---|---|
| 0.006976744 | 0.62960300 | | Min | | | |
| 0.010465116 | 0.47754200 | | Sa(min) | MAFE | | |
| 0.015711628 | 0.34806300 | | 0.058139535 | 0.10399593 | | |
| 0.023553488 | 0.24525500 | | Max | | | |
| 0.03544186 | 0.16706300 | | Sa | MAFE | | |
| 0.053023256 | 0.11149500 | | 1.28089586 | 0.004 | 2*Sa with 0.004 | |
| 0.079534884 | 0.07263620 | | Sa(max) | 2.561791727 | | |
| 0.119162791 | 0.04654220 | | or | | Smaller | |
| 0.178883721 | 0.02914130 | | Sa(median) | 1.41 | of two | |
| 0.223488372 | 0.01765850 | | | | | |
| 0.334883721 | 0.01014930 | | Sa(max) | MAFE | | |
| 0.452093023 | 0.00541537 | | 1.41000000 | 0.00035040 | | |
| 0.602790698 | 0.00263058 | | | | | |
| 0.849418605 | 0.00112560 | | At intensity | | | |
| 1.273255814 | 0.00041285 | | Sa | MAFE | | |
| 1.901162791 | 0.00012610 | | 0.71600000 | 0.00193975 | | |
| 2.860465116 | 0.00002833 | | | | | |

*Table 5. 6 Collapse Fragility Tool- Fragility Calculations*

FEMA P-58 Conditional Probability of Collapse Curve Fit tool
developed by Jack Baker
distributed August 2012
last updated July 15, 2011

The user should populate the gray-shaded cells with results from analysis

| Sa | Number of analyses | Number of collapses | Fraction causing collapse | Theoretical fragility function | Likelihood | Log likelihood |
|---|---|---|---|---|---|---|
| 0.1 | 44 | 0 | 0.00 | 0.00 | 1.000 | 0.000 |
| 0.2 | 44 | 0 | 0.00 | 0.00 | 0.975 | -0.025 |
| 0.3 | 44 | 0 | 0.00 | 0.00 | 0.804 | -0.218 |
| 0.4 | 44 | 0 | 0.00 | 0.02 | 0.452 | -0.794 |
| 0.5 | 44 | 0 | 0.00 | 0.04 | 0.151 | -1.888 |
| 0.6 | 44 | 0 | 0.00 | 0.08 | 0.029 | -3.536 |
| 0.65 | 44 | 0 | 0.00 | 0.10 | 0.010 | -4.559 |
| 0.68 | 44 | 0 | 0.00 | 0.11 | 0.005 | -5.232 |
| 0.716 | 44 | 0 | 0.00 | 0.13 | 0.002 | -6.095 |
| 0.9308 | 44 | 0 | 0.00 | 0.24 | 0.000 | -12.332 |
| 1.1456 | 44 | 14 | 0.32 | 0.36 | 0.104 | -2.263 |
| 1.3604 | 44 | 20 | 0.45 | 0.48 | 0.115 | -2.161 |
| 1.5752 | 44 | 29 | 0.66 | 0.57 | 0.064 | -2.749 |
| | | | | | | |
| | median Sa | 1.41 | | | sum = | -41.851 |
| | $\sigma_{lnSa}$ | 0.6 | | | | |

Let Solver change these two values

*Table 5. 7 PACT results Summary*

| SN | Name | Location | Total Replacement Cost | Shell Replacement Cost | 75% probability repair cost <= | | Total Replacement Time | 75% probability Downtime <= Serial Time | |
|---|---|---|---|---|---|---|---|---|---|
| 1 | 4EBF-AH | California | 18750000 | 11250000 | 1349315.068 | 7.20% | 720 | 48.47015 | 6.73% |
| 2 | 5EBF-AH | California | 23437500 | 14062500 | 1655102.041 | 7.06% | 900 | 58.75 | 6.53% |
| 3 | 6EBF-AH | California | 28125000 | 16875000 | 2423076.923 | 8.62% | 1080 | 88 | 8.15% |
| 4 | 7EBF-AH | California | 32812500 | 19687500 | 3466666.667 | 10.57% | 1260 | 120.7692 | 9.58% |
| 5 | 8EBF-AH | California | 37500000 | 22500000 | 2487500 | 6.63% | 1440 | 86.77966 | 6.03% |
| 6 | 9EBF-AH | California | 42187500 | 25312500 | 4666666.667 | 11.06% | 1620 | 175 | 10.80% |
| 7 | 10EBF-AH | California | 46875000 | 28125000 | 5869565.217 | 12.52% | 1800 | 240 | 13.33% |
| 8 | 4EBF-SN | space needle | 18750000 | 11250000 | 1120422.535 | 5.98% | 720 | 38.9698 | 5.41% |
| 9 | 5EBF-SN | space needle | 23437500 | 14062500 | 1334090.909 | 5.69% | 900 | 46.86747 | 5.21% |
| | | | | | Avg | **8.37%** | | | **7.97%** |

*Table 5. 8 Normative Estimation Tool Input*

| N floors | 23 |
|---|---|

**BUILDING DEFINITION TABLE**

| Floor Name | Floor # | Total Floor Area | Occupancy 1 | | Occupancy 2 | | Occupancy 3 | | SUM % AREA |
|---|---|---|---|---|---|---|---|---|---|
| | | ( sf ) | Type | % Area | Type | % Area | Type | % Area | |
| Roof | 23 | 6317 | none | 100% | none | 0% | none | 0% | 100% |
| 22th | 22 | 6317 | APARTMENT | 100% | none | 0% | none | 0% | 100% |
| 21th | 21 | 6317 | APARTMENT | 100% | none | 0% | none | 0% | 100% |
| 20th | 20 | 6317 | APARTMENT | 100% | none | 0% | none | 0% | 100% |
| 19th | 19 | 6317 | APARTMENT | 100% | none | 0% | none | 0% | 100% |
| 18th | 18 | 6317 | APARTMENT | 100% | none | 0% | none | 0% | 100% |
| 17th | 17 | 6317 | APARTMENT | 100% | none | 0% | none | 0% | 100% |
| 16th | 16 | 6317 | APARTMENT | 100% | none | 0% | none | 0% | 100% |
| 15th | 15 | 6317 | APARTMENT | 100% | none | 0% | none | 0% | 100% |
| 14th | 14 | 6317 | HOSPITALITY | 100% | none | 0% | none | 0% | 100% |
| 13th | 13 | 6317 | HOSPITALITY | 100% | none | 0% | none | 0% | 100% |
| 12th | 12 | 6317 | HOSPITALITY | 100% | none | 0% | none | 0% | 100% |
| 11th | 11 | 6317 | HOSPITALITY | 100% | none | 0% | none | 0% | 100% |
| 10th | 10 | 6317 | HOSPITALITY | 100% | none | 0% | none | 0% | 100% |
| 9th | 9 | 6317 | HOSPITALITY | 100% | none | 0% | none | 0% | 100% |
| 8th | 8 | 6317 | HOSPITALITY | 100% | none | 0% | none | 0% | 100% |
| 7th | 7 | 6317 | HOSPITALITY | 100% | none | 0% | none | 0% | 100% |
| 6th | 6 | 6317 | HOSPITALITY | 100% | none | 0% | none | 0% | 100% |
| 5th | 5 | 6317 | HOSPITALITY | 100% | none | 0% | none | 0% | 100% |
| 4th | 4 | 6317 | HOSPITALITY | 100% | none | 0% | none | 0% | 100% |
| 3rd | 3 | 6317 | HOSPITALITY | 100% | none | 0% | none | 0% | 100% |
| 2nd | 2 | 6317 | HOSPITALITY | 100% | none | 0% | none | 0% | 100% |
| 1st | 1 | 6317 | HOSPITALITY | 100% | none | 0% | none | 0% | 100% |

*Table 5. 9 Normative Estimation Output- Typical Apartment*

**COMPONENT SUMMARY MATRIX**

| OCCUPANCY | | | | Fragility Number | Fragility Name | Assumed Quantity per component within PACT | Quantity | | Correlated Fragility? | Acutal Quantity | | PACT Basic Unit | Fragility Quantity Beta (LogNormal Distribution) |
|---|---|---|---|---|---|---|---|---|---|---|---|---|---|
| Type | Occupancy # | Floor Name | Component Area (sq ft ) | | | | Directional | Non Directional | | Value | Unit | | |
| APARTMENT | 1 | 22th | 6317 | **None Found** | Cladding - Gross Wall Area | -- | -- | -- | ?? | -- | -- | None Found | 0.5 |
| APARTMENT | 1 | 22th | 6317 | **B2022.001** | B2022.001 Curtain Walls - Generic Midrise Stick-Built Curtain | 30 SF | 31.59 | -- | NO | 947.6 | SF | Each | 0.6 |
| APARTMENT | 1 | 22th | 6317 | **B3011.011** | B3011.011 Concrete tile roof, tiles secured and compliant wit | 100 SF | -- | 20.21 | NO | 2021.4 | SF | Each | 0.9 |
| APARTMENT | 1 | 22th | 6317 | **C1011.001a** | C1011.001a Wall Partition, Type: Gypsum with metal studs, F | 100 LF | 7.58 | -- | NO | 758.0 | LF | Each | 0.3 |
| APARTMENT | 1 | 22th | 6317 | **C3021.001k** | C3021.001k Generic Floor Covering - Flooding of floor caused | User By | -- | -- | NO | -- | By | Each | 0.4 |
| APARTMENT | 1 | 22th | 6317 | **C3011.001a** | C3011.001a Wall Partition, Type: Gypsum + Wallpaper, Full He | 100 LF | 2.41 | -- | NO | 241.1 | LF | Each | 0.4 |
| APARTMENT | 1 | 22th | 6317 | **C3032.001a** | C3032.001a Suspended Ceiling, SDC A,B,C, Area (A): A < 250, V | 250 SF | -- | 24.00 | NO | 6001.2 | SF | Each | 0.0 |
| APARTMENT | 1 | 22th | 6317 | **C3032.001a** | C3032.001a Suspended Ceiling, SDC A,B,C, Area (A): A < 250, V | 250 SF | -- | 1.26 | NO | 315.9 | SF | Each | 0.0 |
| APARTMENT | 1 | 22th | 6317 | **None Found** | Fixed Casework | -- | -- | -- | ?? | -- | -- | None Found | 0.0 |
| APARTMENT | 1 | 22th | 6317 | **None Found** | Fume Hoods | -- | -- | -- | ?? | -- | -- | None Found | 0.0 |
| APARTMENT | 1 | 22th | 6317 | **E2022.001** | E2022.001 Modular office work stations. | 1 EA | -- | UNIT MISMATCH | NO | -- | EA | Each | 0.0 |
| APARTMENT | 1 | 22th | 6317 | **None Found** | Domestic Plumbing Fixtures | -- | -- | -- | ?? | -- | -- | None Found | 0.4 |
| APARTMENT | 1 | 22th | 6317 | **None Found** | Lab Plumbing Fixtures | -- | -- | -- | ?? | -- | -- | None Found | 0.0 |
| APARTMENT | 1 | 22th | 6317 | **D2021.011a** | D2021.011a Cold or Hot Potable - Small Diameter Threaded | 1000 LF | -- | 0.67 | NO | 669.6 | LF | Each | 0.4 |
| APARTMENT | 1 | 22th | 6317 | **None Found** | Piping - Gas supply piping | -- | -- | -- | ?? | -- | -- | None Found | 0.2 |
| APARTMENT | 1 | 22th | 6317 | **None Found** | HVAC - Boiler capacity | -- | -- | -- | ?? | -- | -- | None Found | 0.3 |
| APARTMENT | 1 | 22th | 6317 | **D3041.011a** | D3041.011a HVAC Galvanized Sheet Metal Ducting less than 6 | 1000 LF | -- | 0.32 | NO | 315.9 | LF | Each | 0.6 |
| APARTMENT | 1 | 22th | 6317 | **D3041.031a** | D3041.031a HVAC Drops / Diffusers in suspended ceilings - No | 10 EA | -- | 5.05 | NO | 50.5 | EA | Each | 0.4 |
| APARTMENT | 1 | 22th | 6317 | **None Found** | HVAC - Pressure Dependent Air Valves (Phoenix type boxes) | -- | -- | -- | ?? | -- | -- | None Found | 0.0 |
| APARTMENT | 1 | 22th | 6317 | **D3041.041a** | D3041.041a Variable Air Volume (VAV) box with in-line coil, S | 10 EA | -- | 2.53 | NO | 25.3 | EA | Each | p90 low |
| APARTMENT | 1 | 22th | 6317 | **None Found** | Electrical - Electrical Distribution conduits | -- | -- | -- | ?? | -- | -- | None Found | 0.6 |
| APARTMENT | 1 | 22th | 6317 | **None Found** | Electrical - Electrical Distribution – cable trays | -- | -- | -- | ?? | -- | -- | None Found | 0.0 |
| APARTMENT | 1 | 22th | 6317 | **D4011.021a** | D4011.021a Fire Sprinkler Water Piping - Horizontal Mains an | 1000 LF | -- | 1.39 | NO | 1389.7 | LF | Each | 0.1 |
| APARTMENT | 1 | 22th | 6317 | **D4011.031a** | D4011.031a Fire Sprinkler Drop Standard Threaded Steel - Dro | 100 EA | -- | 0.76 | NO | 75.8 | EA | Each | 0.1 |

*Table 5. 10 Normative Estimation Output- Typical Hotel*

**COMPONENT SUMMARY MATRIX**

| OCCUPANCY | | | | Fragility Number | Fragility Name | Assumed Quantity per component within PACT | Quantity | | Correlated Fragility? | Acutal Quantity | | PACT Basic Unit | Fragility Quantity Beta (LogNormal Distribution) |
|---|---|---|---|---|---|---|---|---|---|---|---|---|---|
| Type | Occupancy # | Floor Name | Component Area (sq ft ) | | | | Directional | Non Directional | | Value | Unit | | |
| HOSPITALITY | 1 | 14th | 6317 | **None Found** | Cladding - Gross Wall Area | -- | -- | -- | ?? | -- | -- | None Found | 0.2 |
| HOSPITALITY | 1 | 14th | 6317 | **B2022.001** | B2022.001 Curtain Walls - Generic Midrise Stick-Built Curtain | 30 SF | 25.27 | -- | NO | 758.0 | SF | Each | 0.3 |
| HOSPITALITY | 1 | 14th | 6317 | **B3011.011** | B3011.011 Concrete tile roof, tiles secured and compliant wit | 100 SF | -- | 12.63 | NO | 1263.4 | SF | Each | p90 low |
| HOSPITALITY | 1 | 14th | 6317 | **C1011.001a** | C1011.001a Wall Partition, Type: Gypsum with metal studs, F | 100 LF | 3.79 | -- | NO | 379.0 | LF | Each | 0.2 |
| HOSPITALITY | 1 | 14th | 6317 | **C3021.001k** | C3021.001k Generic Floor Covering - Flooding of floor caused | User By | -- | -- | NO | -- | By | Each | 0.3 |
| HOSPITALITY | 1 | 14th | 6317 | **C3011.001a** | C3011.001a Wall Partition, Type: Gypsum + Wallpaper, Full He | 100 LF | 1.82 | -- | NO | 181.9 | LF | Each | 0.3 |
| HOSPITALITY | 1 | 14th | 6317 | **C3032.001a** | C3032.001a Suspended Ceiling, SDC A,B,C, Area (A): A < 250, V | 250 SF | -- | 3.79 | NO | 947.6 | SF | Each | 0.0 |
| HOSPITALITY | 1 | 14th | 6317 | **C3032.001a** | C3032.001a Suspended Ceiling, SDC A,B,C, Area (A): A < 250, V | 250 SF | -- | 17.69 | NO | 4421.9 | SF | Each | 0.0 |
| HOSPITALITY | 1 | 14th | 6317 | **C3032.001a** | C3032.001a Suspended Ceiling, SDC A,B,C, Area (A): A < 250, V | 250 SF | -- | 2.02 | NO | 505.4 | SF | Each | 0.0 |
| HOSPITALITY | 1 | 14th | 6317 | **C3032.001a** | C3032.001a Suspended Ceiling, SDC A,B,C, Area (A): A < 250, V | 250 SF | -- | 1.77 | NO | 442.2 | SF | Each | 0.0 |
| HOSPITALITY | 1 | 14th | 6317 | **None Found** | Fixed Casework | -- | -- | -- | ?? | -- | -- | None Found | 0.0 |
| HOSPITALITY | 1 | 14th | 6317 | **None Found** | Fume Hoods | -- | -- | -- | ?? | -- | -- | None Found | 0.0 |
| HOSPITALITY | 1 | 14th | 6317 | **E2022.001** | E2022.001 Modular office work stations. | 1 EA | -- | UNIT MISMATCH | NO | -- | EA | Each | 0.0 |
| HOSPITALITY | 1 | 14th | 6317 | **None Found** | Domestic Plumbing Fixtures | -- | -- | -- | ?? | -- | -- | None Found | 0.3 |
| HOSPITALITY | 1 | 14th | 6317 | **None Found** | Lab Plumbing Fixtures | -- | -- | -- | ?? | -- | -- | None Found | 0.0 |
| HOSPITALITY | 1 | 14th | 6317 | **D2021.011a** | D2021.011a Cold or Hot Potable - Small Diameter Threaded | 1000 LF | -- | 0.51 | NO | 505.4 | LF | Each | 0.3 |
| HOSPITALITY | 1 | 14th | 6317 | **None Found** | Piping - Gas supply piping | -- | -- | -- | ?? | -- | -- | None Found | 0.2 |
| HOSPITALITY | 1 | 14th | 6317 | **None Found** | HVAC - Boiler capacity | -- | -- | -- | ?? | -- | -- | None Found | 0.2 |
| HOSPITALITY | 1 | 14th | 6317 | **D3041.011a** | D3041.011a HVAC Galvanized Sheet Metal Ducting less than 6 | 1000 LF | -- | 0.32 | NO | 315.9 | LF | Each | 0.6 |
| HOSPITALITY | 1 | 14th | 6317 | **D3041.031a** | D3041.031a HVAC Drops / Diffusers in suspended ceilings - No | 10 EA | -- | 5.05 | NO | 50.5 | EA | Each | 0.4 |
| HOSPITALITY | 1 | 14th | 6317 | **None Found** | HVAC - Pressure Dependent Air Valves (Phoenix type boxes) | -- | -- | -- | ?? | -- | -- | None Found | 0.0 |
| HOSPITALITY | 1 | 14th | 6317 | **D3041.041a** | D3041.041a Variable Air Volume (VAV) box with in-line coil, S | 10 EA | -- | 3.79 | NO | 37.9 | EA | Each | p90 low |
| HOSPITALITY | 1 | 14th | 6317 | **None Found** | Electrical - Electrical Distribution conduits | -- | -- | -- | ?? | -- | -- | None Found | 0.6 |
| HOSPITALITY | 1 | 14th | 6317 | **None Found** | Electrical - Electrical Distribution – cable trays | -- | -- | -- | ?? | -- | -- | None Found | 0.0 |
| HOSPITALITY | 1 | 14th | 6317 | **D4011.021a** | D4011.021a Fire Sprinkler Water Piping - Horizontal Mains an | 1000 LF | -- | 1.39 | NO | 1389.7 | LF | Each | 0.1 |
| HOSPITALITY | 1 | 14th | 6317 | **D4011.031a** | D4011.031a Fire Sprinkler Drop Standard Threaded Steel - Dro | 100 EA | -- | 0.76 | NO | 75.8 | EA | Each | 0.1 |

*Table 5. 11 Pacific Tower Translation Periods in Each Direction (from building model) Adapted from [41]*

| Translation Period Mode | East-West Direction (s) | North-South Direction (seconds) |
|---|---|---|
| First | 3.3(72% mass participating) | 4.0 (65% mass) |
| Second | 1.1(13% mass) | 1.3(13% mass) |
| Third | 0.5(4% mass) | 0.7 (2.5% mass) |

*Table 5. 12 Opensees Modal Analysis Results*

| Translation Period | N-S direction (s) |
|---|---|
| First | 4.356 |
| Second | 1.199 |
| Third | 0.596 |

*Table 5. 13 Ground motion record stations*

| | Recorded Site | Site Code | Distance to Pacific Tower( in Km) |
|---|---|---|---|
| 1 | Canterbury Aero Club | CACS | 10.112 |
| 2 | Christchurch Botanic Gardens | CBGS | 1.392 |
| 3 | Christchurch Hospital | CHHC | 1.168 |
| 4 | Christchurch Cashmere High School | CMHS | 4.064 |
| 5 | Hulverstone Drive Pumping Station | HPSC | 3.92 |
| 6 | Heathcote Valley Primary School | HVSC | 7.904 |
| 7 | Lyttelton Port Company | LPCC | 3.472 |
| 8 | Christchurch North New Brighton School | NNBS | 6.064 |
| 9 | Pages Road Pumping Station | PRPC | 6.128 |
| 10 | Christchurch Resthaven | REHS | 7.856 |
| 11 | Shirley Library | SHLC | 3.344 |

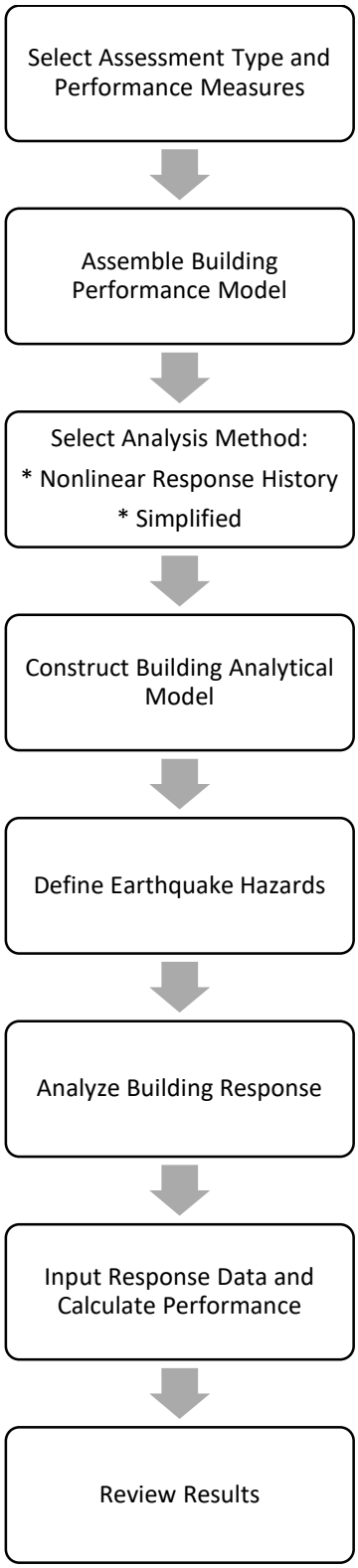


*Figure 5. 1 Performance assessment process Adapted from FEMA P-58 [16]*

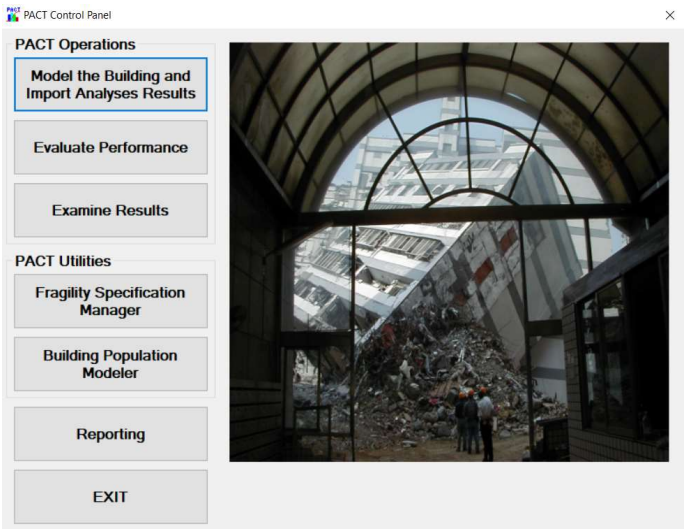


*Figure 5. 2 PACT Control Panel*

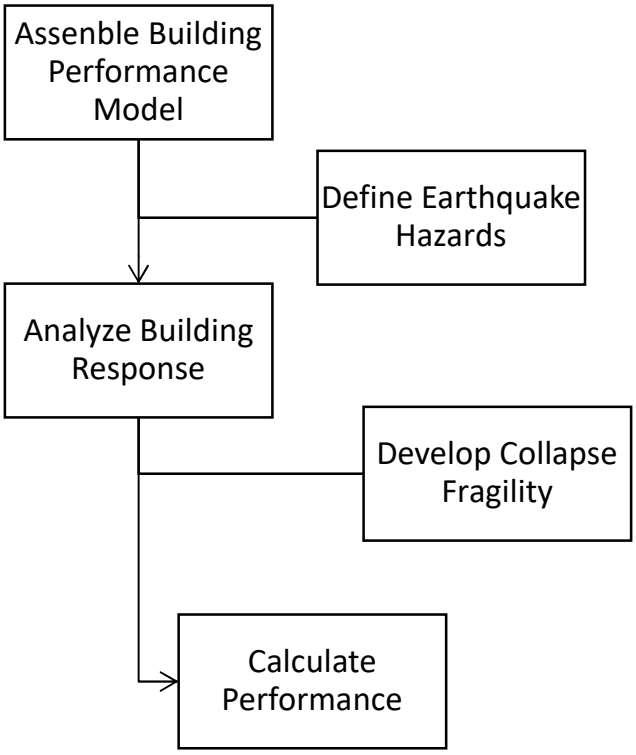


*Figure 5. 3 Flowchart of the performance assessment methodology Adapted from FEMA P-58 [16]*

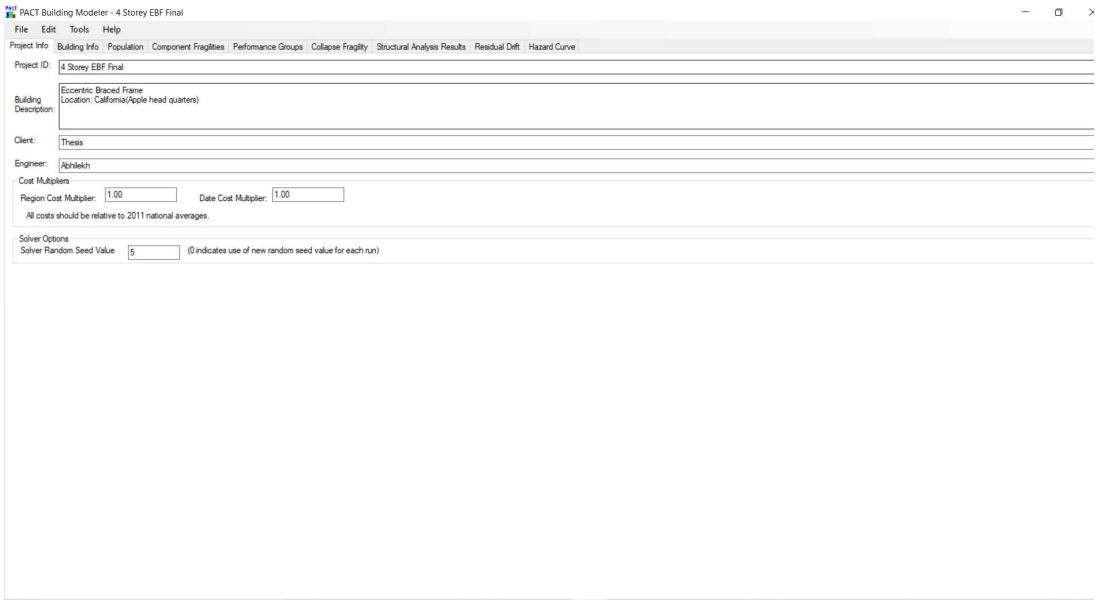


*Figure 5. 4 PACT- Project Information Tab*

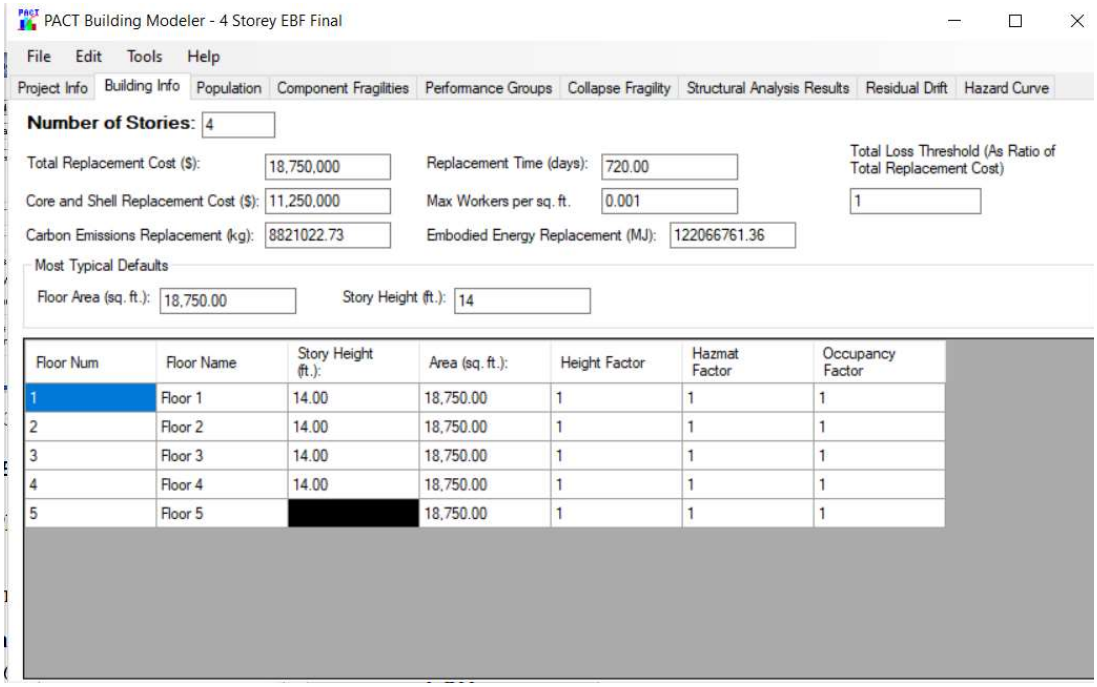


*Figure 5. 5 PACT-Building Information Tab*

| Building Information | | | | | | |
|---|---|---|---|---|---|---|
| | | | | | | |
| Length | 150 | feet | | | | |
| Breadth | 125 | feet | | | | |
| No of Stories | 4 | | | | | |
| Typical Floor Area | 18,750.00 | ft2 | | | | |
| Total Area | 75,000.00 | ft2 | | | | |
| Typical Floor Height | 14 | feet | | | | |
| Total Replacement Cost/sq ft | 250 | dollars/sq ft | | | | |
| Total Shell Replacement Cost/sq ft | 150 | dollars/sq ft | | | | |
| | | | | | | |
| Total Replacement Cost | $18,750,000.00 | dollars | | | | |
| Total Shell Replacement Cost | $11,250,000.00 | dollars | | | | |
| | | | | | | |
| Building replacement time | 720 | days | | Replacement time/story | 180 | days/sto |
| | | | | | | |
| Carbon Emissions Replacement | 8,821,022.73 | kg | | Inflation factor from 2013 to 2011 | | |
| Embodied Energy Replacement (MJ) | 122,066,761.36 | MJ | | | | |

*Figure 5. 6 Building Information Calculation*

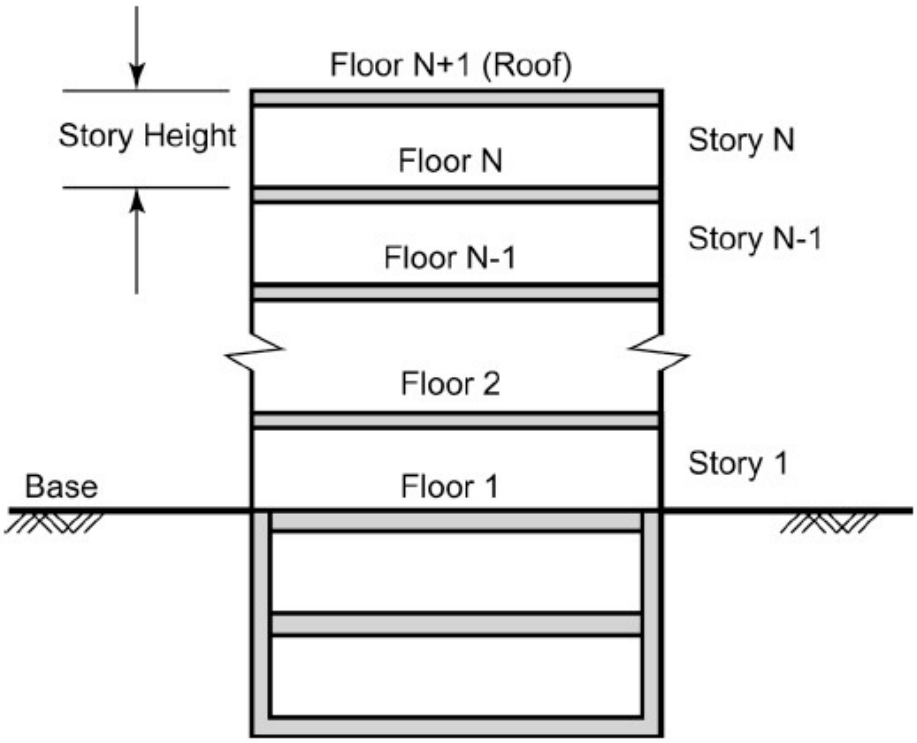


*Figure 5. 7 Definition of floor number, story number, and story height [16]*

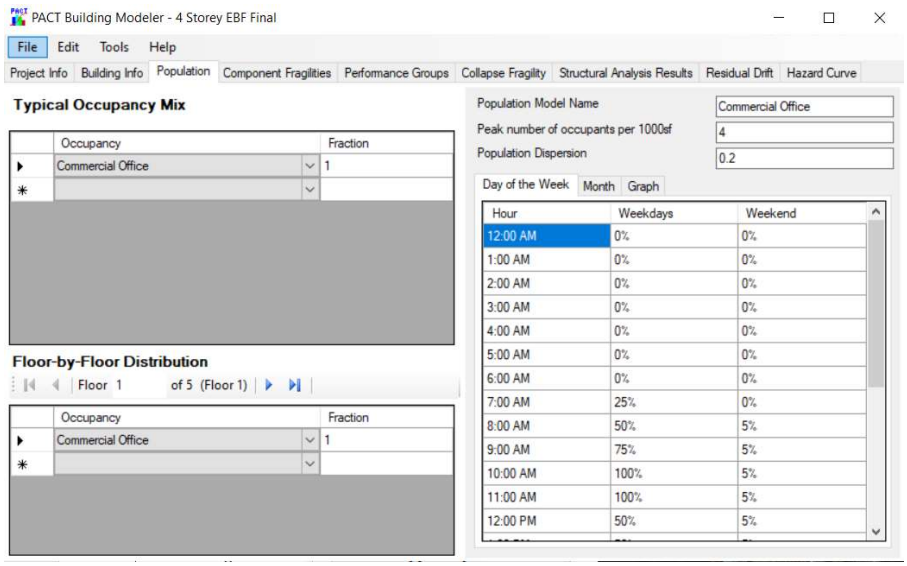


*Figure 5. 8 PACT-Population Tab*

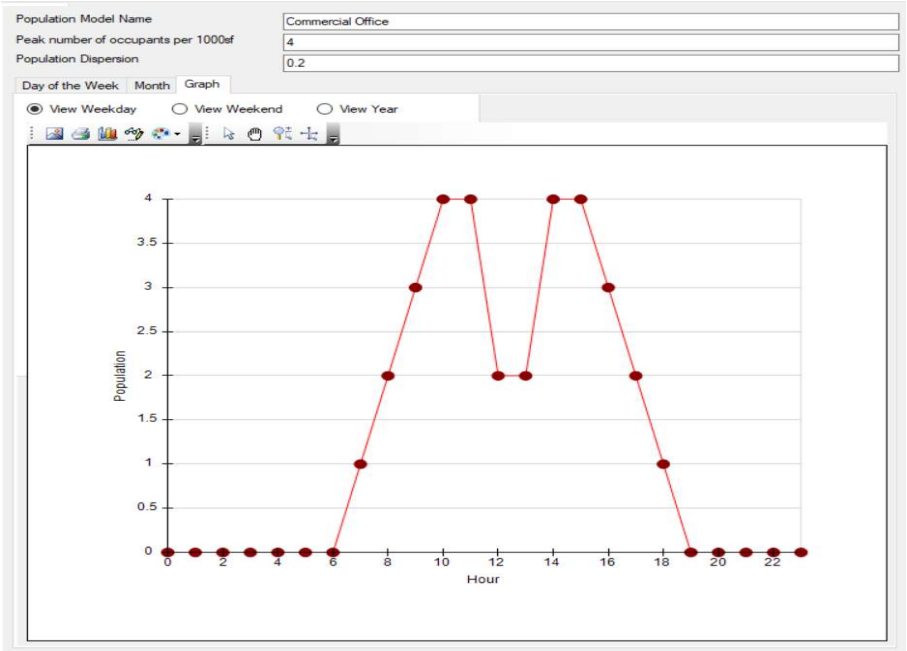


*Figure 5. 9 Default Weekday Population Distribution for Commercial Occupancy*

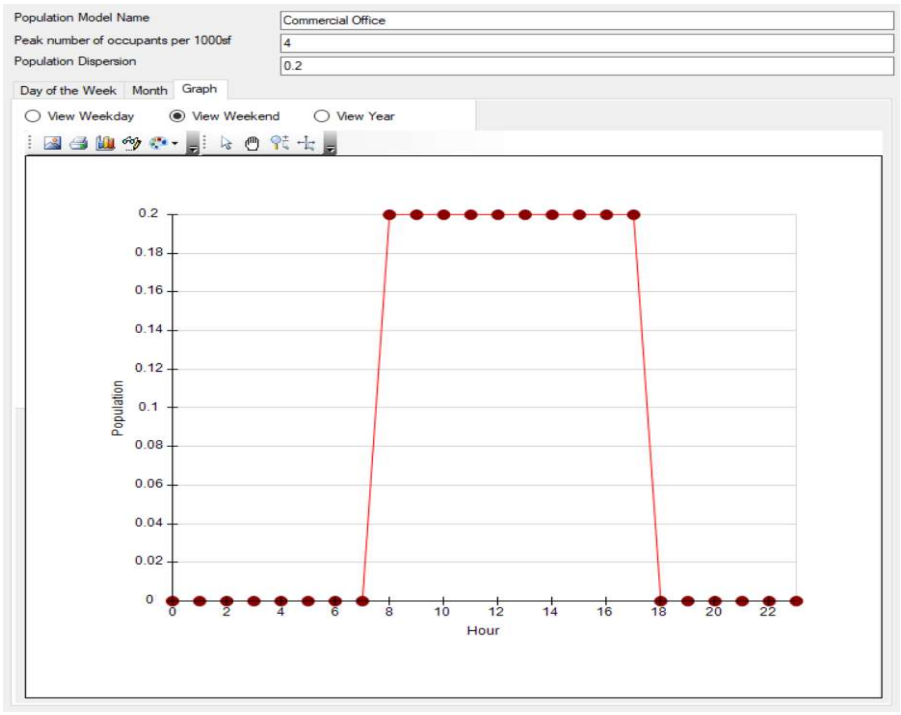


*Figure 5. 10 Default Weekend Population Distribution for Commercial Occupancy*

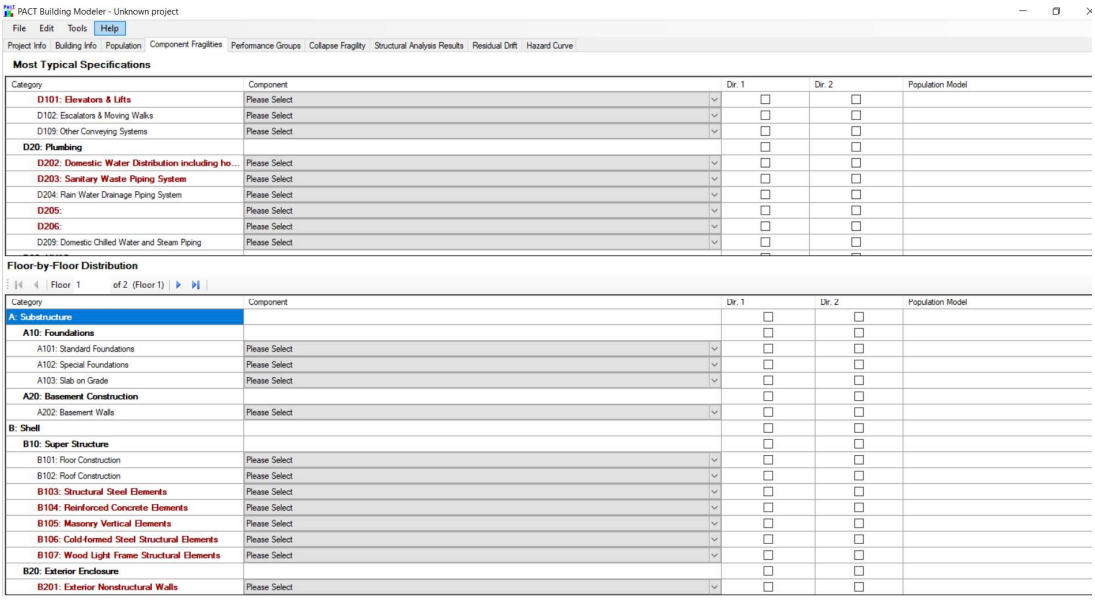


*Figure 5. 11 PACT- Component Fragilities Tab*

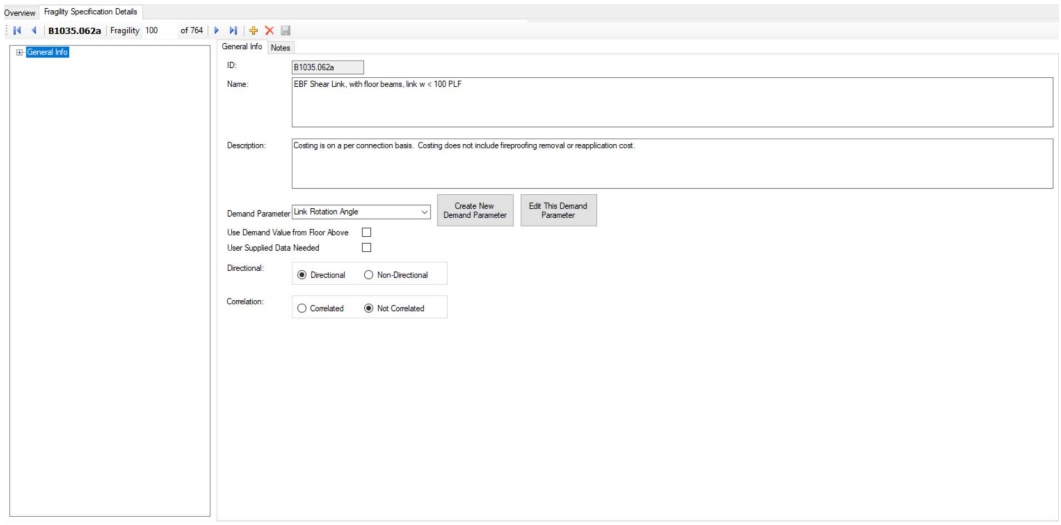


*Figure 5. 12 PACT- Fragility Specification Details*

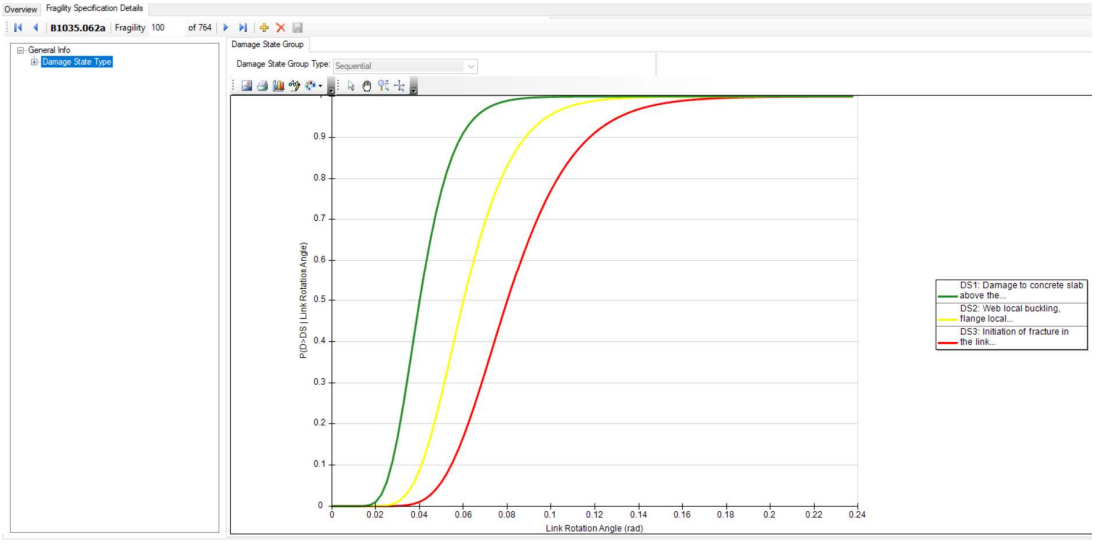


*Figure 5. 13 PACT Shear Links Fragility Functions*

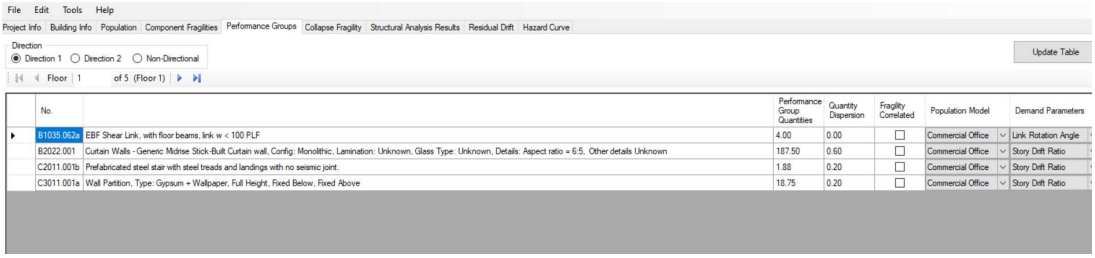


*Figure 5. 14 PACT Directional Performance Groups*

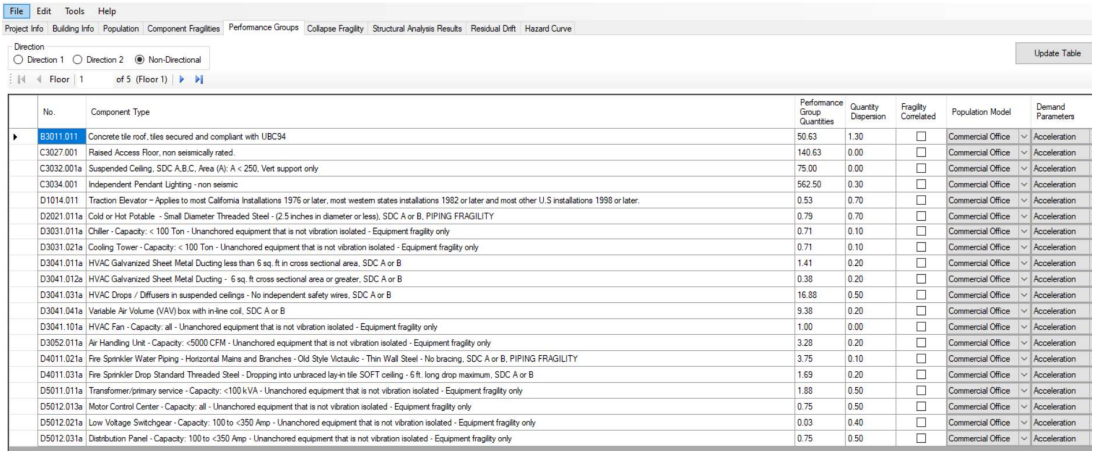


*Figure 5. 15 PACT Non-Directional Performance Groups*

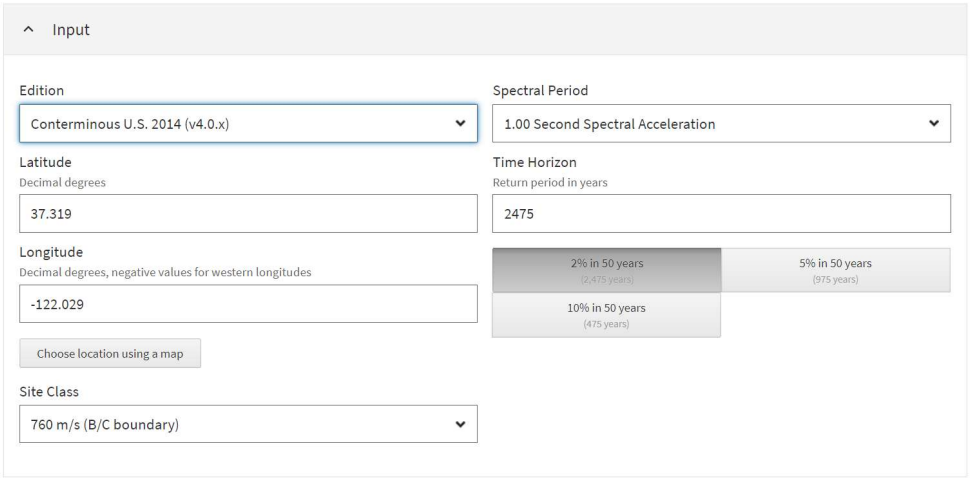


*Figure 5. 16 Unified Hazard Tool- Hazard Curve (California)*

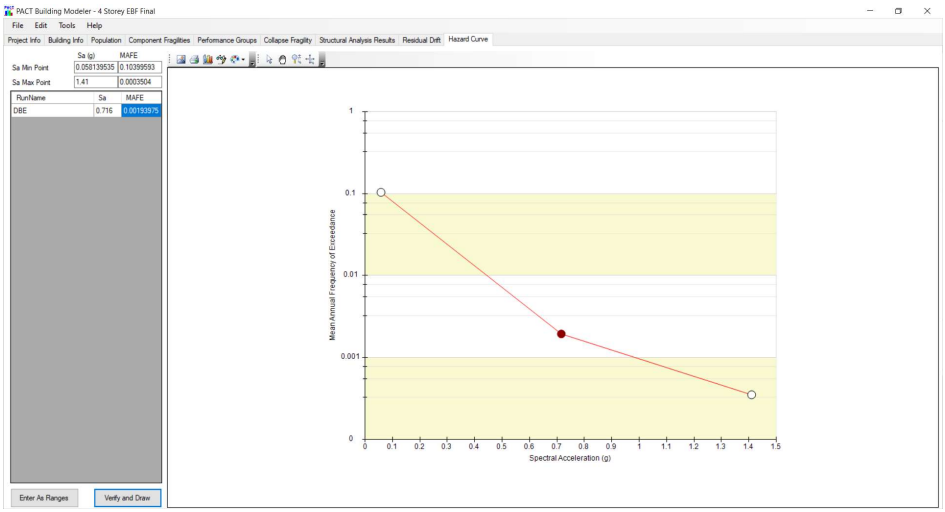


*Figure 5. 17 PACT Hazard Curve Tab*

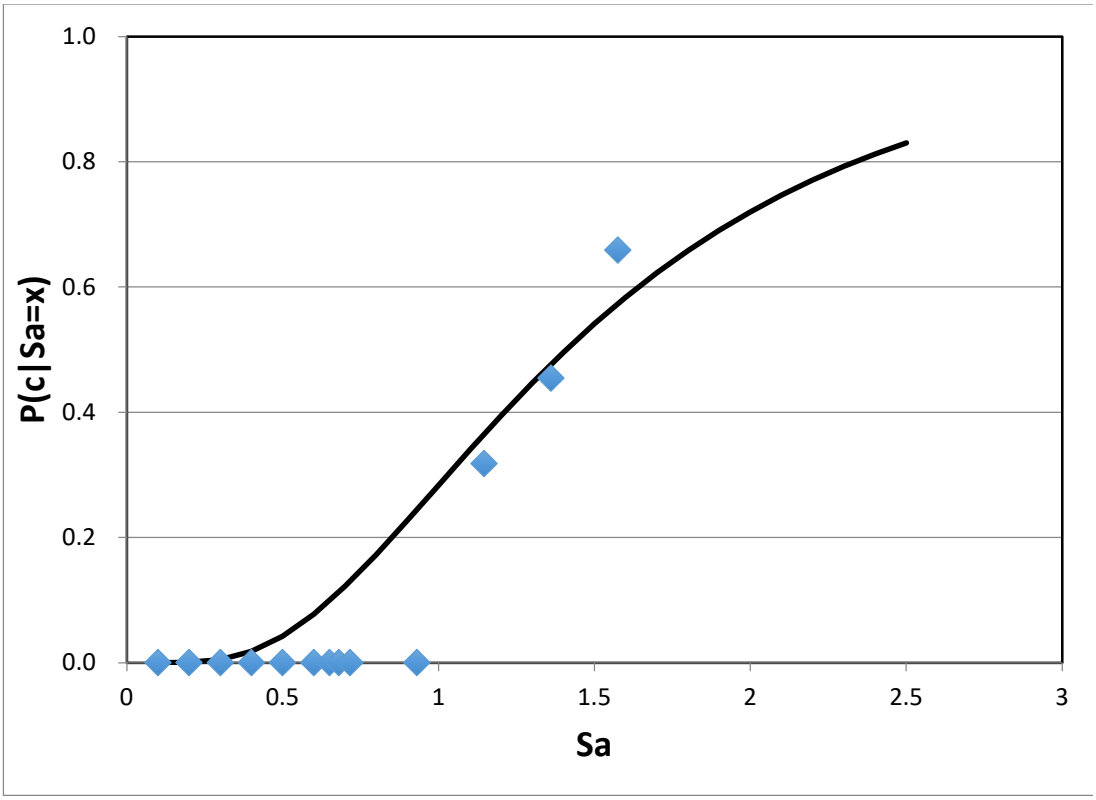


*Figure 5. 18 Collapse Fragility for 4 story EBFs (California)*

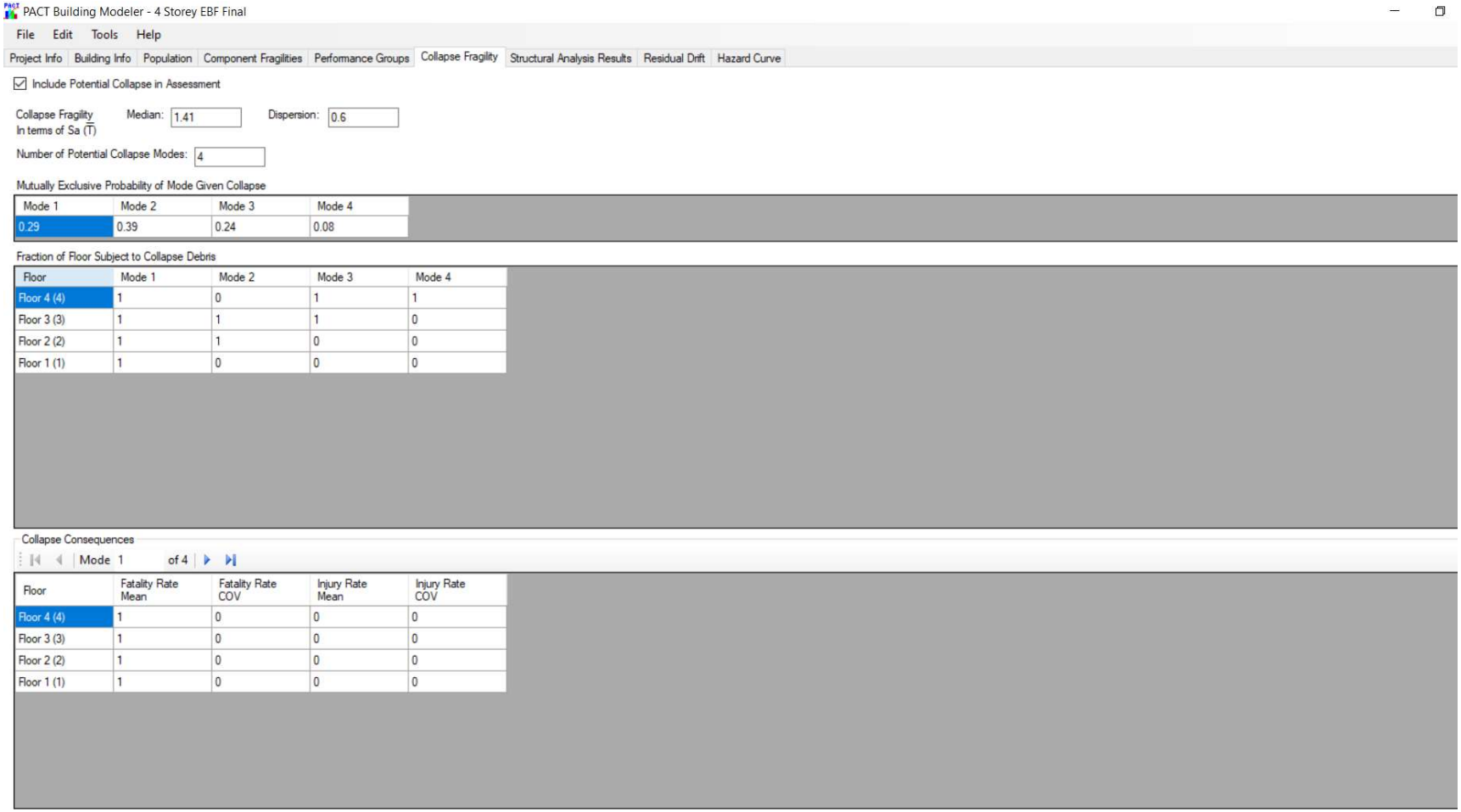


*Figure 5. 19 Collapse Fragility Tab*

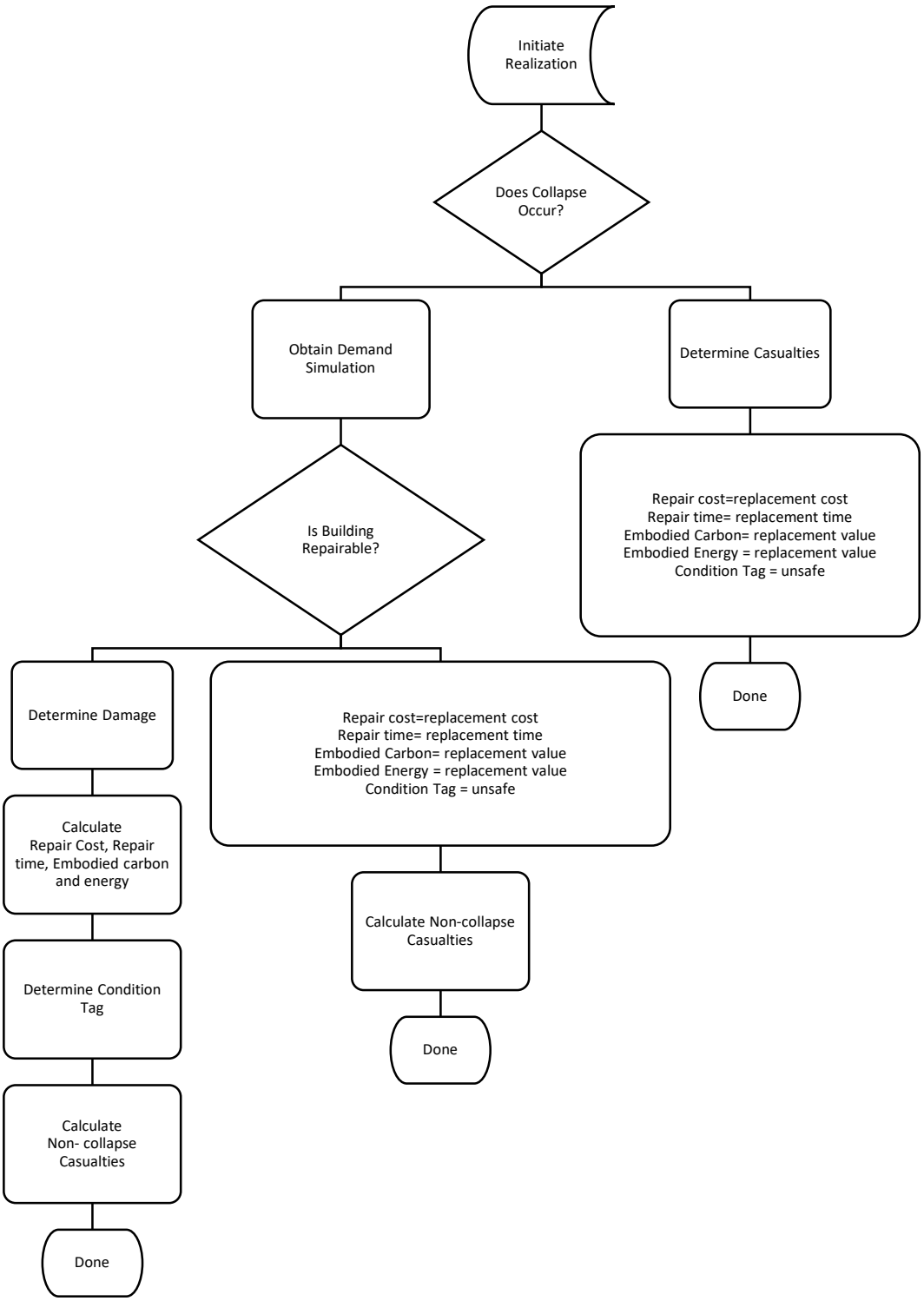


*Figure 5. 20 Flowchart for performance calculation in each realization Adapted from FEMA P-58 [16]*

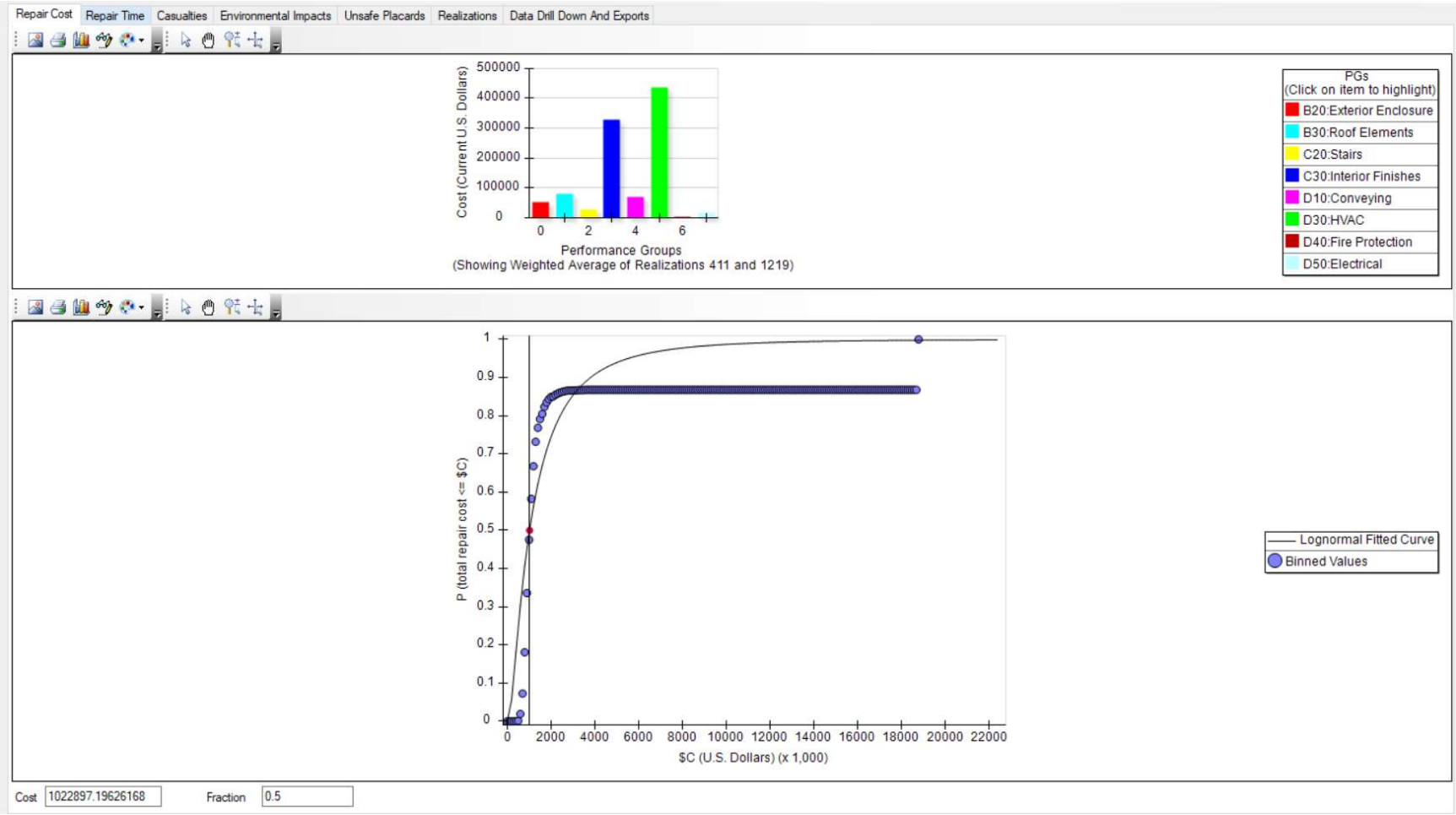


*Figure 5. 21 PACT results- Repair Cost (4 story EBFs California)*

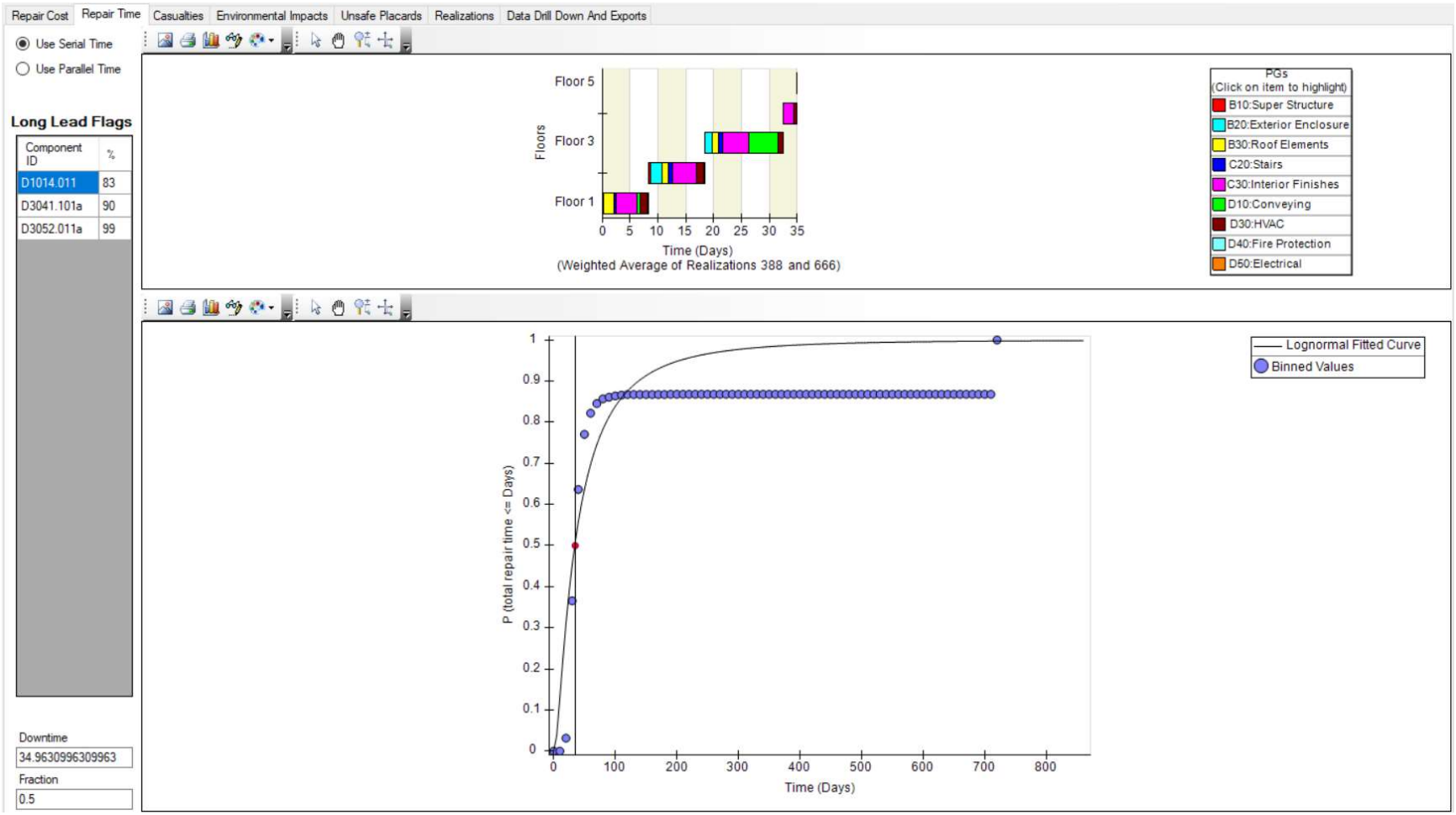


*Figure 5. 22 PACT results- Serial Repair Time (4 story EBFs California)*

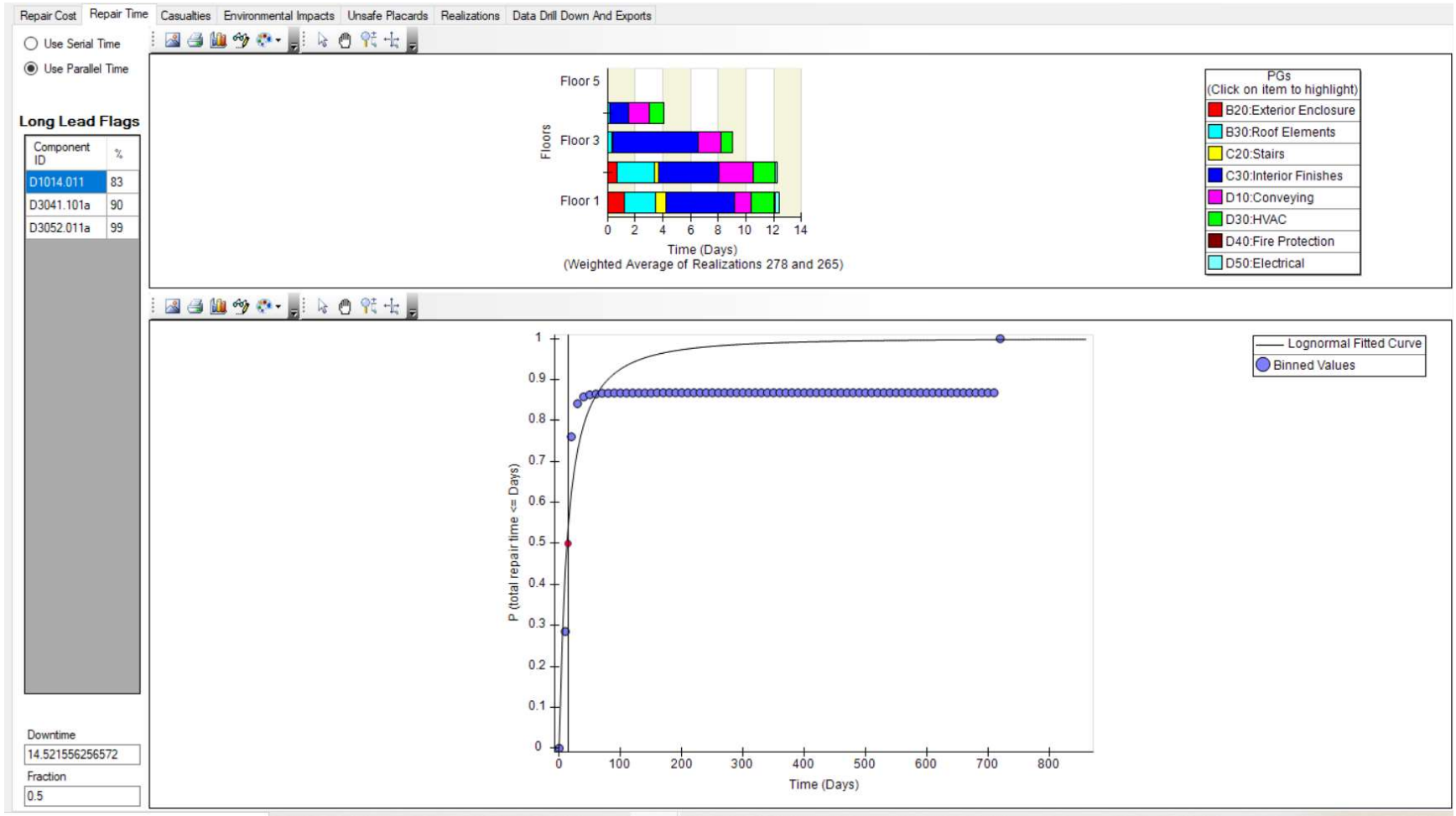


*Figure 5. 23 PACT results- Parallel Repair Time (4 story EBFs California)*

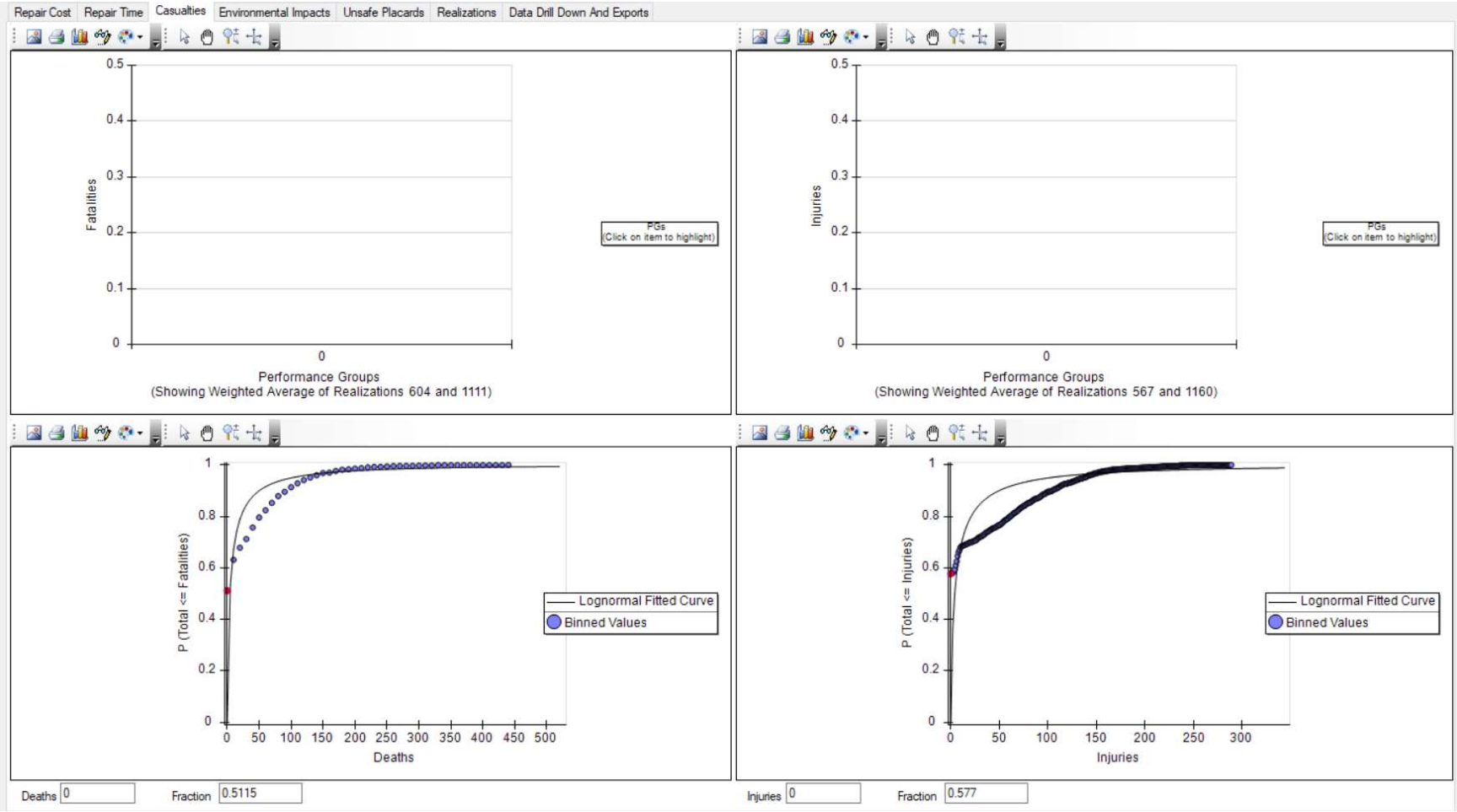


*Figure 5. 24 PACT results- Casualties (4 story EBFs California)*

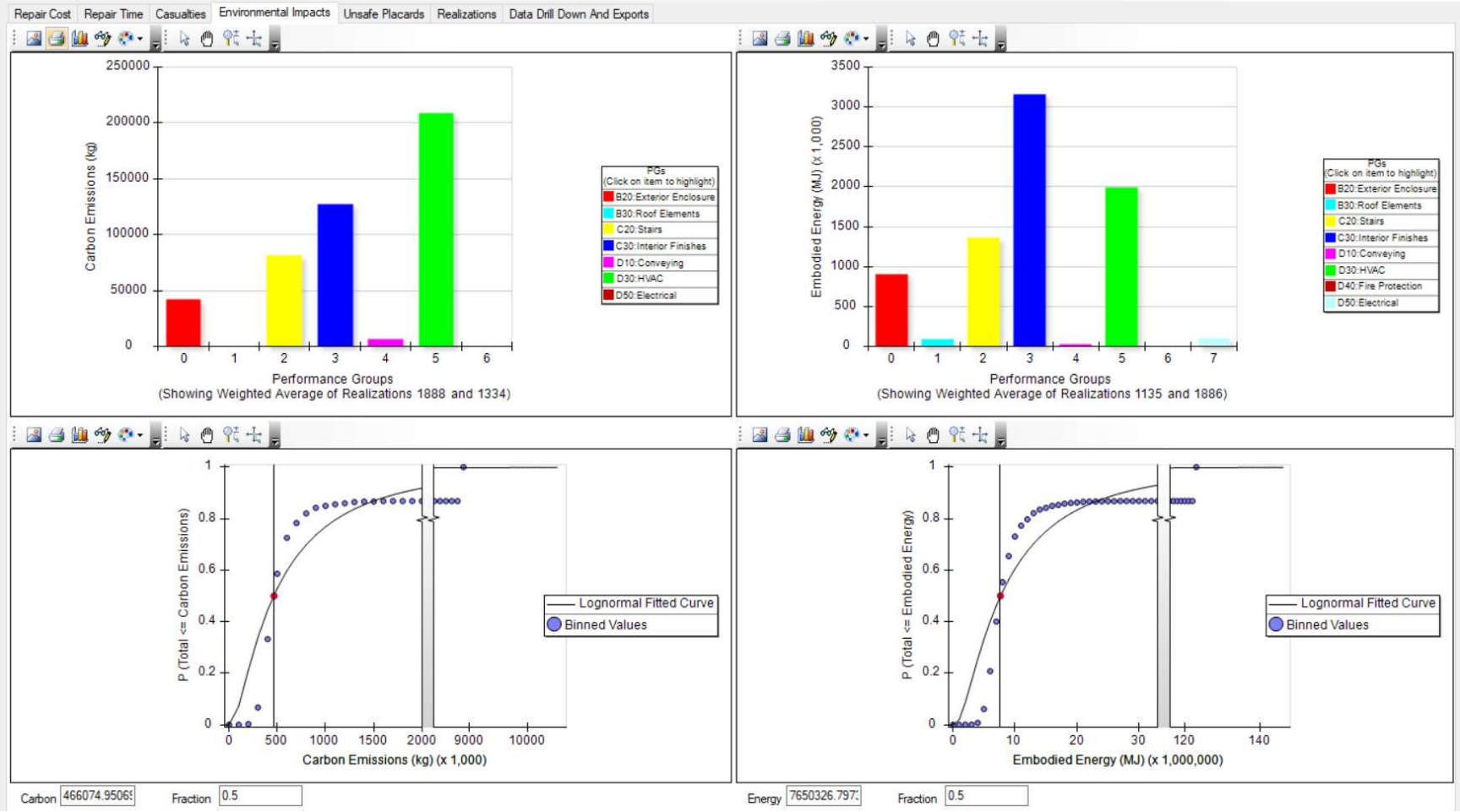


*Figure 5. 25 PACT results-Environmental Impacts (4 story EBFs California)*

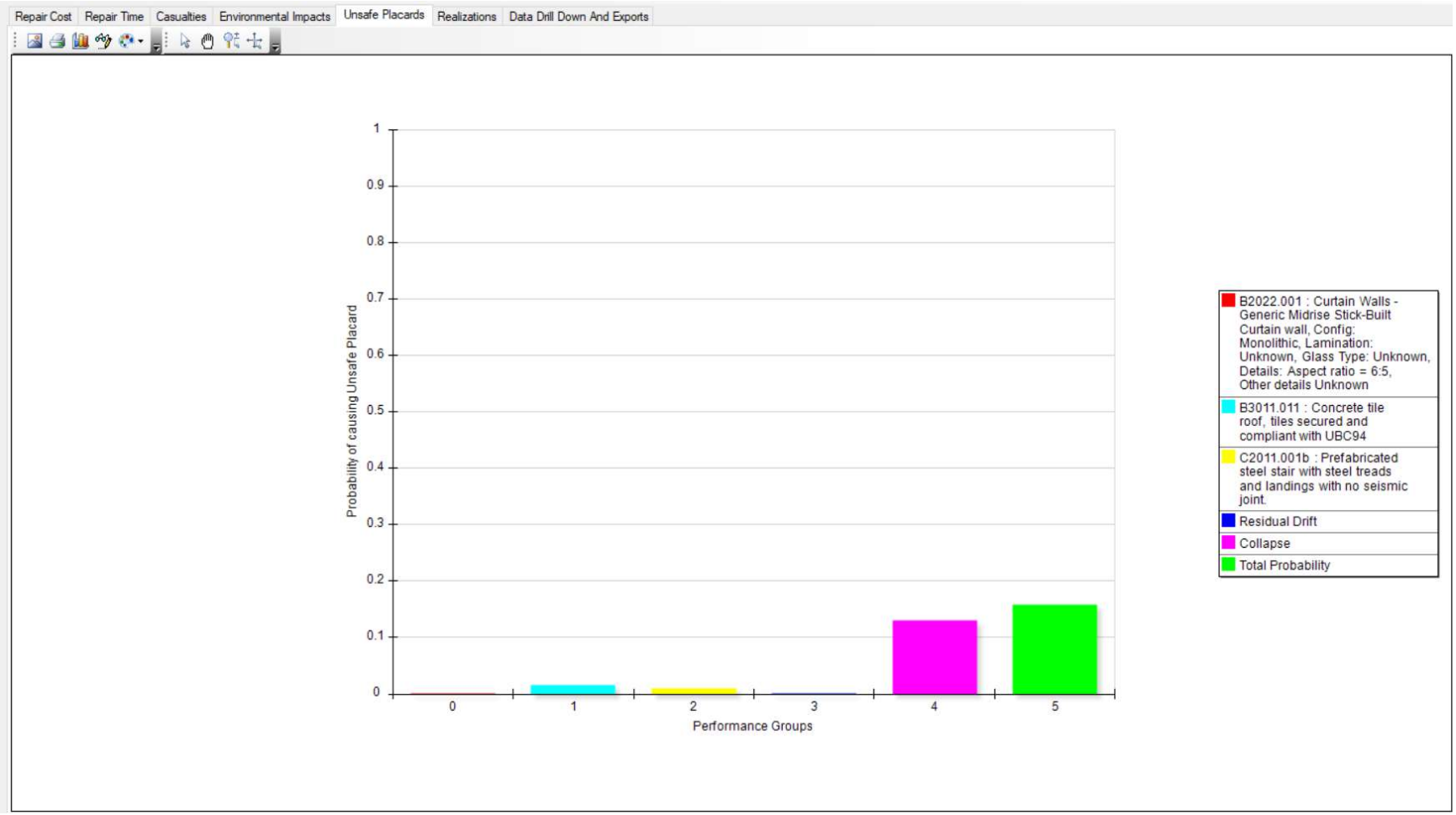


*Figure 5. 26 PACT results- Unsafe Placards (4 story EBFs California)*

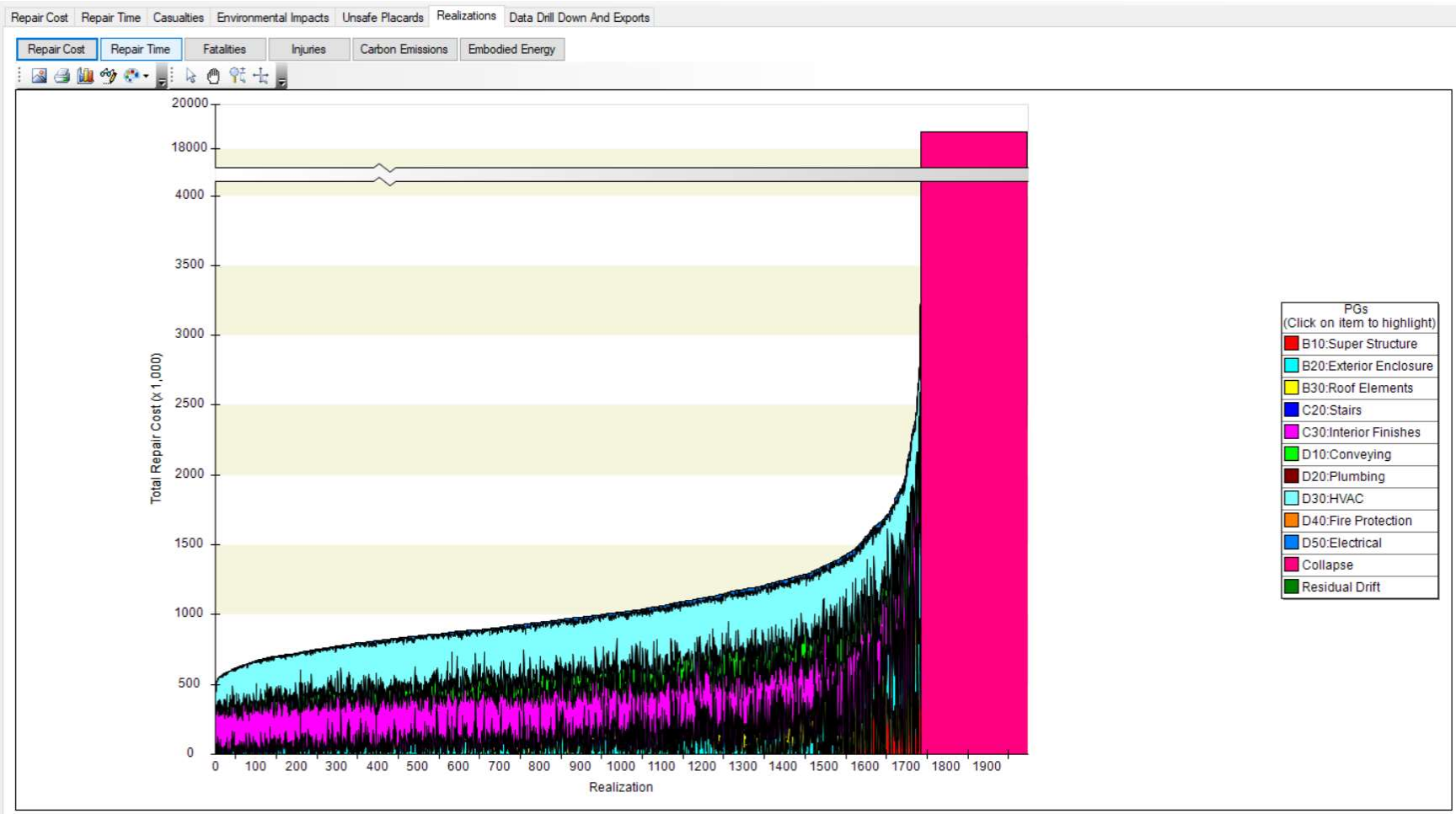


*Figure 5. 27 PACT results- Repair Cost- Realizations (4 story EBFs California)*


*Figure 5. 28 Pacific Tower Location [43]*


*Figure 5. 29 Pacific Tower [43]*

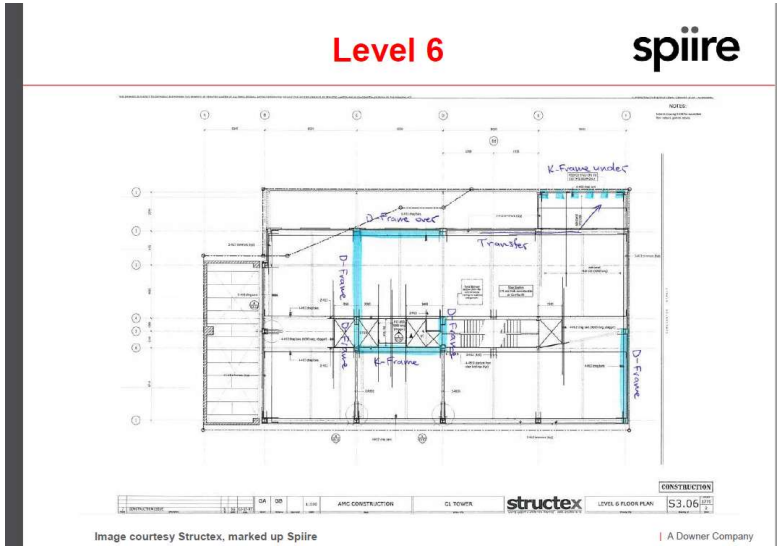


*Figure 5. 30 Pacific Tower- Level 6 [43]*

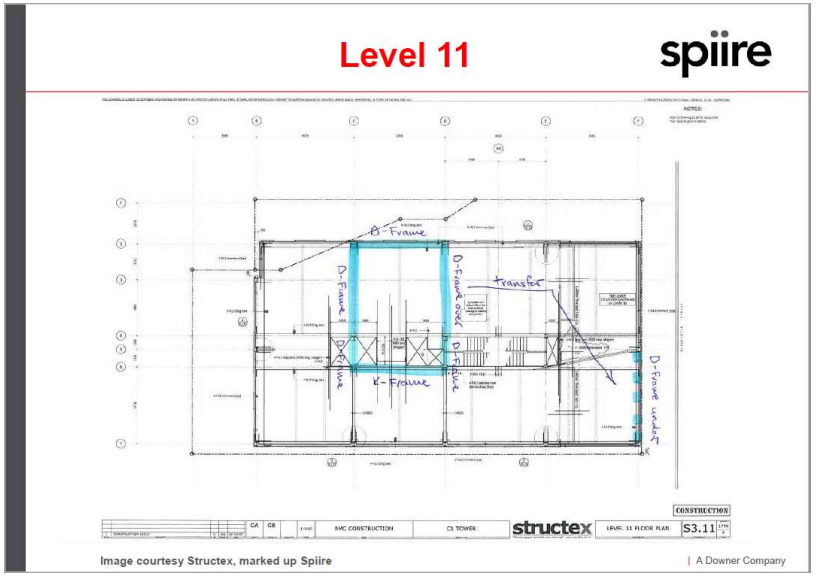


*Figure 5. 31 Pacific Tower - Level 11 [43]*

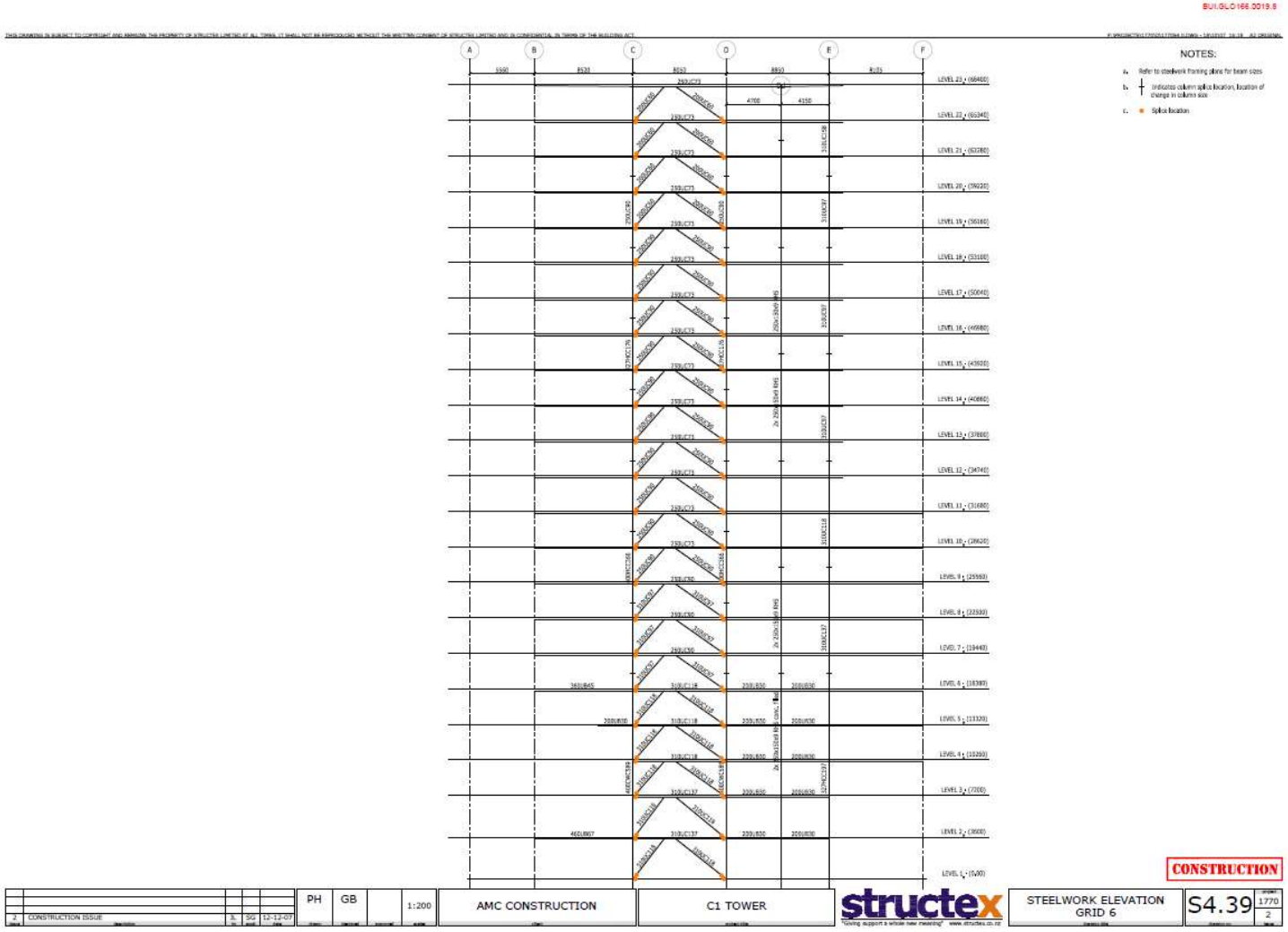


*Figure 5. 32 Pacific Tower- Elevation View (Grid 6-6) [43]*

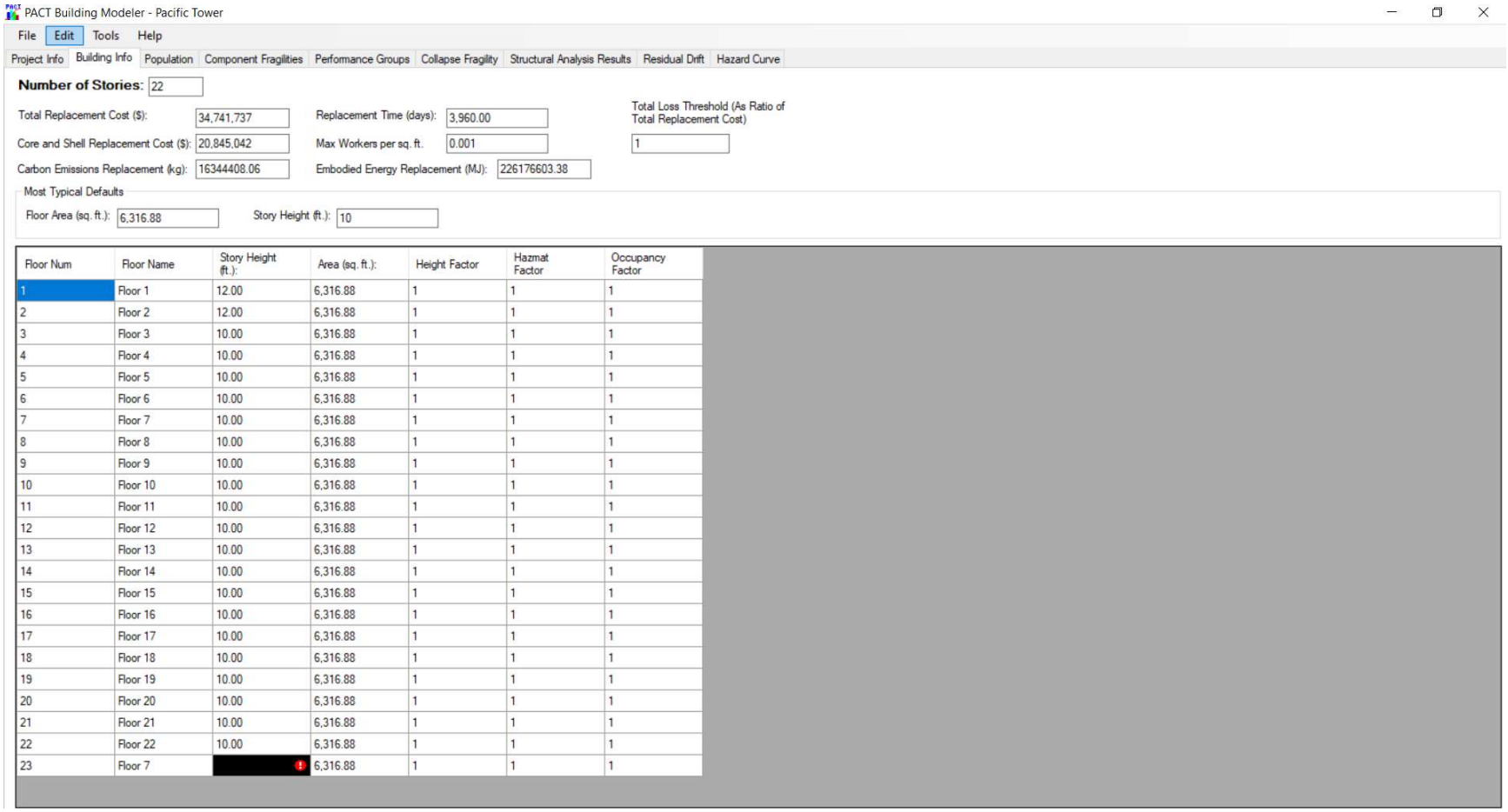


*Figure 5. 33 Building Information Tab (Pacific Tower)*

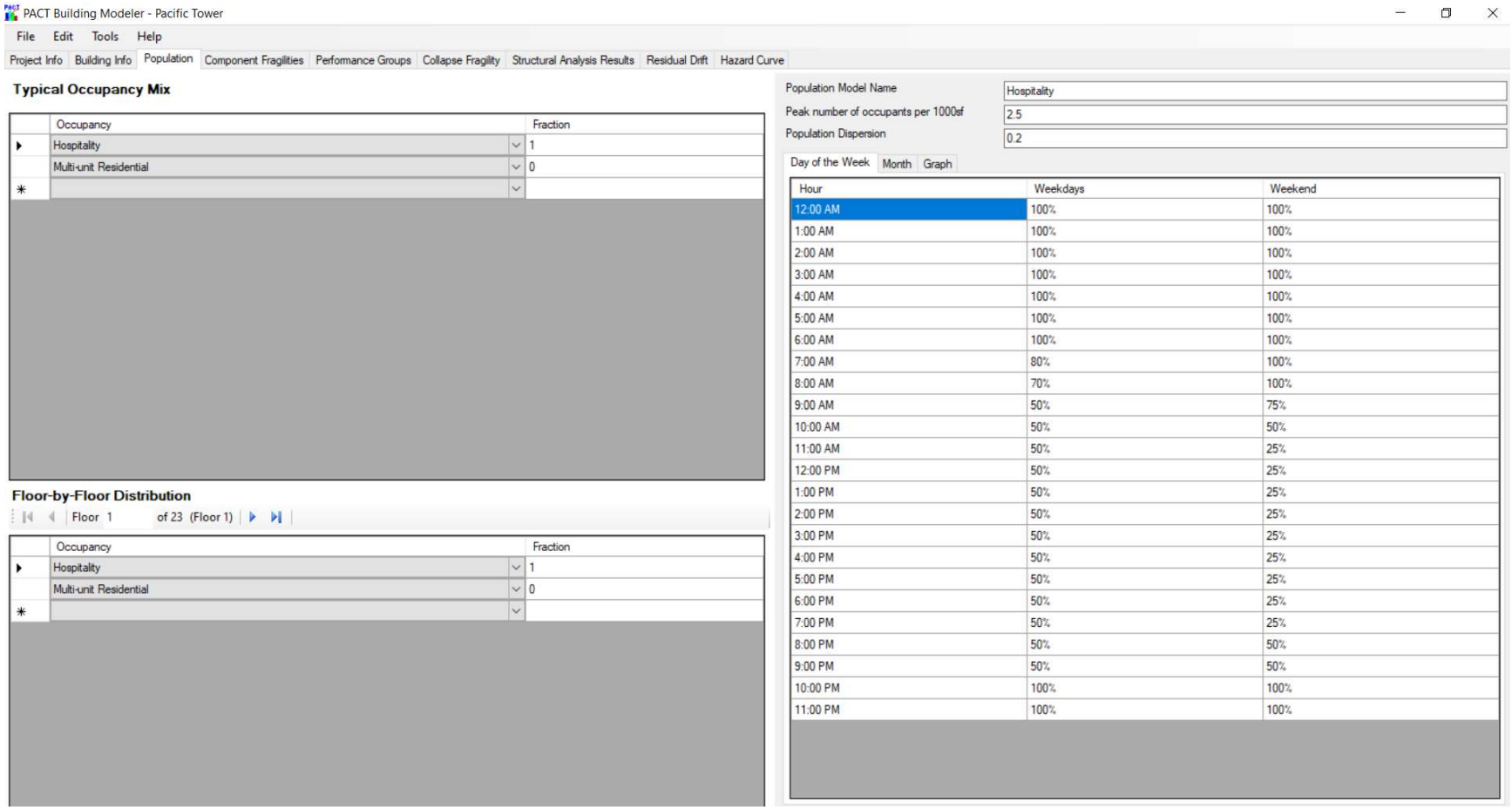


*Figure 5. 34 PACT population model (Pacific Tower)*

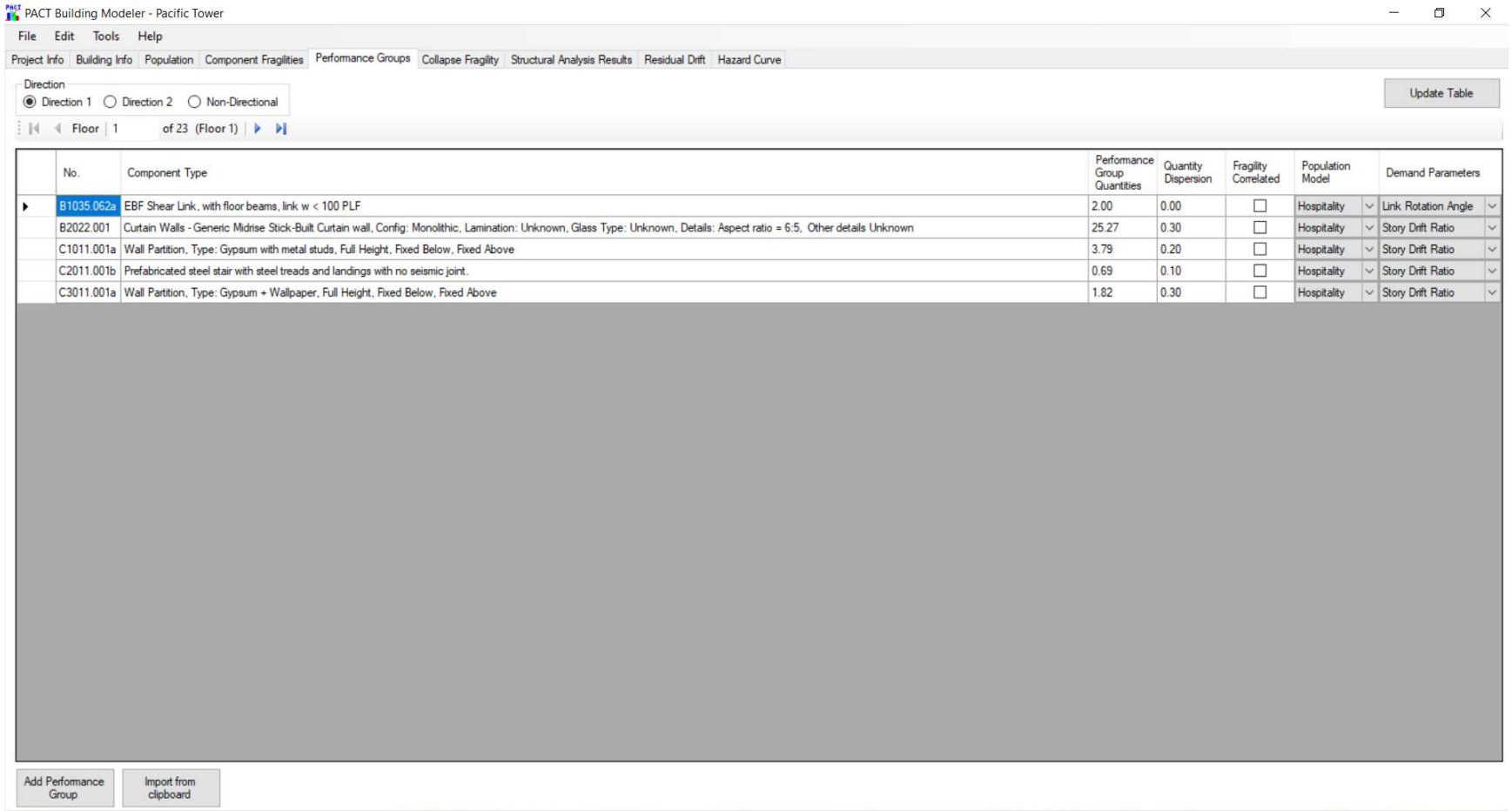


*Figure 5. 35 Performance Groups- Directional (Hospitality Occupancy)*

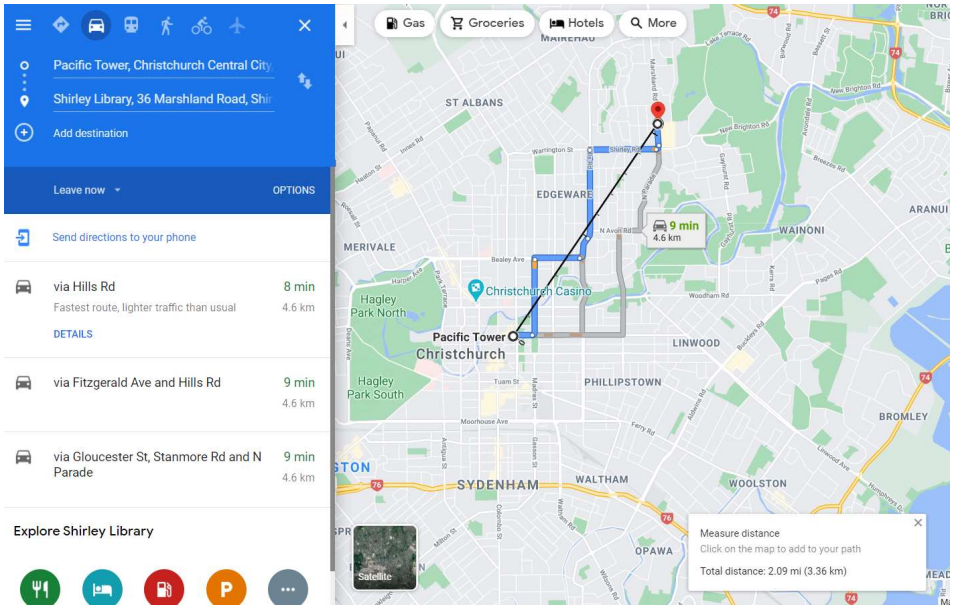


*Figure 5. 36 Example Distance Calculation between Pacific tower and Shirley Library Station using google maps*

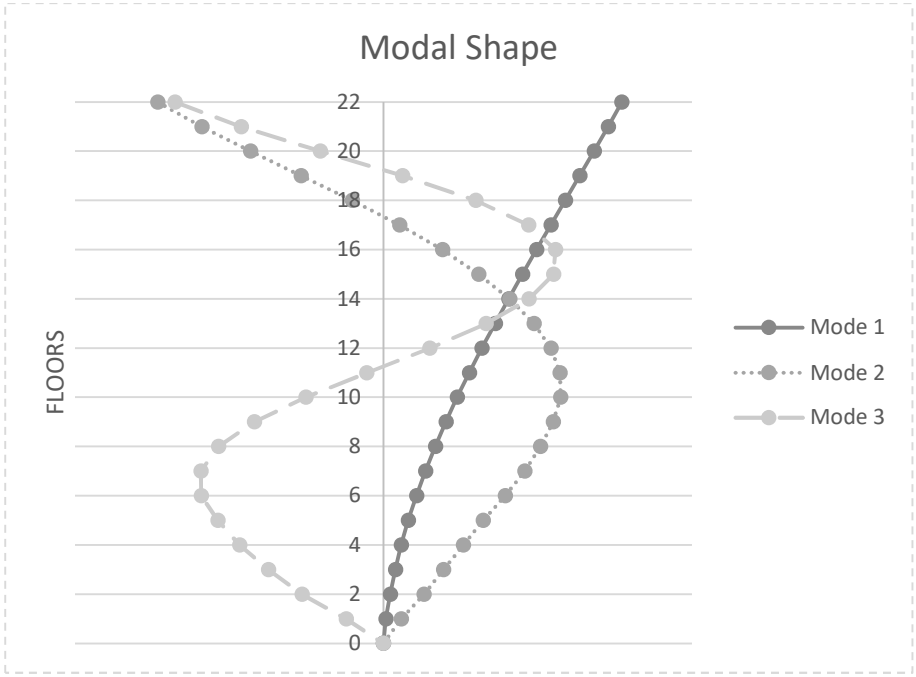


*Figure 5. 37 First three Modal shapes of Pacific Tower (OpenSees)*

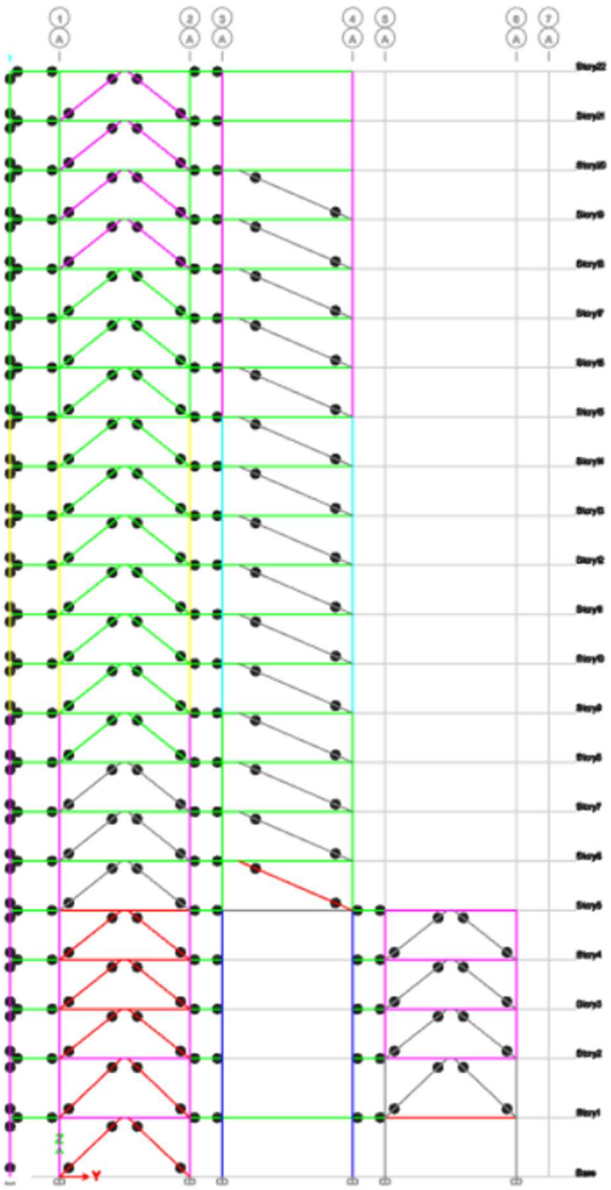

*Figure 5. 38 Pacific Tower- Relative rigidity*

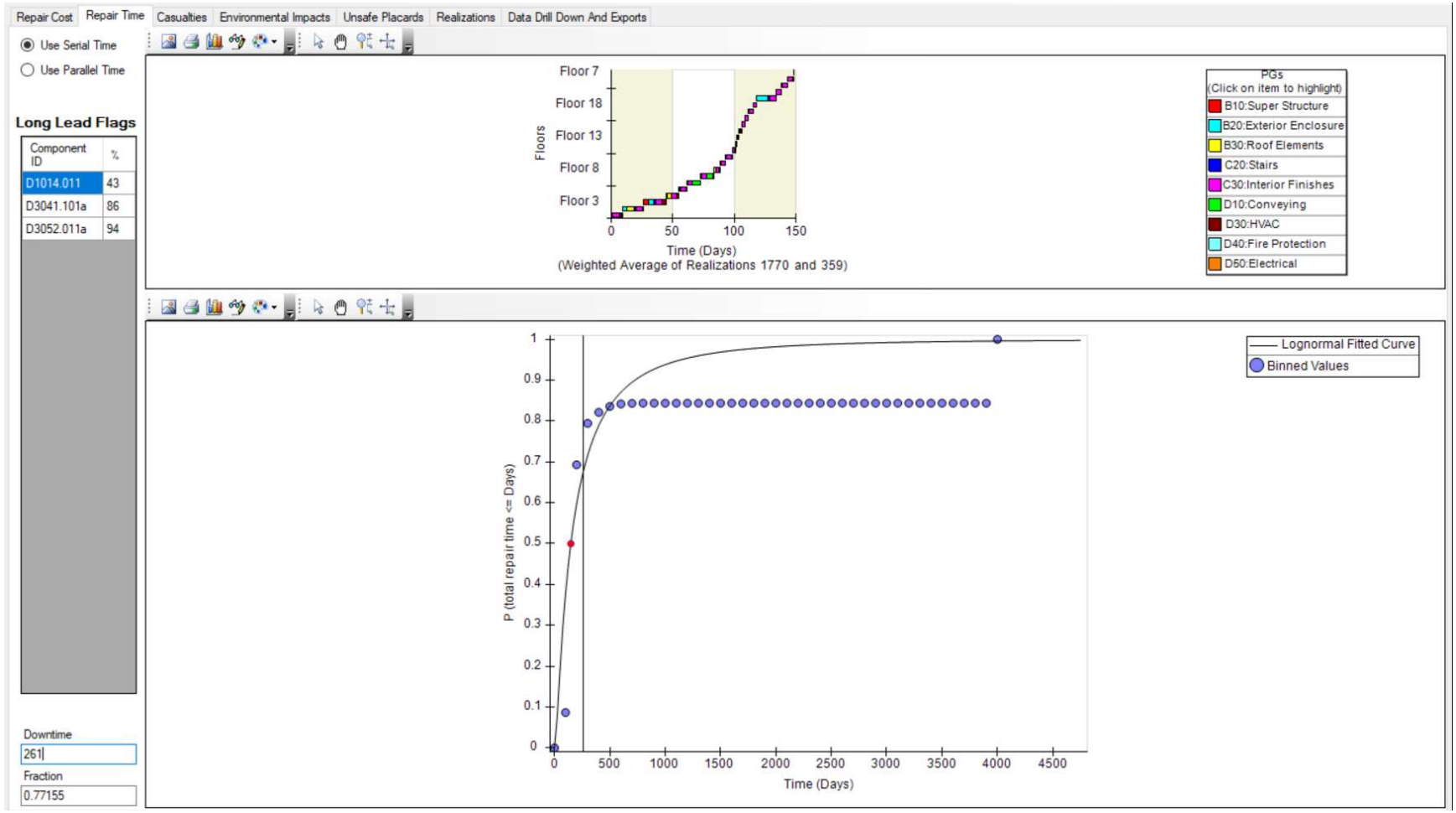


*Figure 5. 39 PACT- Repair Time (Pacific Tower)*

# Chapter 6: Conclusion

In summary, this study designed and assessed the seismic performance and resilience of nine EBFs using ASCE 7, nonlinear time history analysis and FEMA P-58 procedure. The assessment was carried out using a tool developed by FEMA known as PACT. Additionally, an existing EBF building structure located in Christchurch, New Zealand, having actual performance data from the 2011 Christchurch earthquake, was also assessed using the same procedure. Next, the existing structure's real performance data and the PACT generated performance data were compared to validate this study's performance assessment process. This study used the Pacific Tower, Christchurch New Zealand, to validate the results for the EBFs. Although the repair time of this building is about 26 months, considering this study uses replaceable links and focuses primarily on EBFs the repair time was adjusted to 261 days. It is notable that this building was retrofitted by field cut and replace all damaged EBF link beams with replaceable bolted link beam. Therefore, the repair time of 261 days can be viewed as the value predicted for the next earthquake of similar intensity. Also, PACT assessment determined a probability of 77.15% that the repair time will be equal to or less than 261 days, Figure 72. Due to the high confidence level of the repair time being equal to or less than 261 days, the assessment process used in this study is verified. Additionally, As can be seen in Table 34, there is a 75% chance that the repair cost would be almost 8.37% or less than the total replacement cost for all the newly designed EBFs. Likewise, there is a 75% chance that the repair time would be nearly 7.97% or less than the total replacement time for all the newly designed EBFs. From these results, it can be

concluded that the EBFs designed using the AISC specifications have high seismic resilience if replaceable link beams are installed.

For future studies, the use of the full back bone curve to represent material non-linearity is recommended. As a result of using the full back cone curve, Incremental dynamic analysis (IDA) can be performed to determine the collapse fragility of the structure. Additionally, connections should also be incorporated in modelling to closely predict the actual behavior of the real structure.

# References


[1] Munich Re, "NatCatSERVICE," 2020. [Online]. Available: https://www.iii.org/fact-statistic/facts-statistics-earthquakes-and-tsunamis.

[2] H. Ritchie, "Natural Disasters," 2014. [Online]. Available: https://ourworldindata.org/natural-disasters.

[3] W. C. Roeder and P. E. Popov, "Inelastic Behaviour of eccentrically braced steel frames under cyclic loadings," University of California, Berkeley, California, 1977.

[4] J. R. Libby, "Eccentrically Braced frame construction- A case history," *AISC Journal,* 1981.

[5] A. T. Merovich, J. P. Nicoletti and E. Hartle, "Eccentic Bracing in tall buildings," *ASCE,* p. 108, 1982.

[6] G. C. Driscoll and L. S. Beedle, Suggestions for Avoiding Beam-to-Column Web Connection Failure, vol. 19, AISC Engineering Journal, 1982.

[7] E. P. Popov, K. Kasai and M. D. Engelhardt, Advances in Design of Eccentrically Braced Frames, Auckland, 1986.

[8] E. P. Popov and M. D. Engelhardt, Seismic Eccentrically Braced Frames, Berkeley, California: Journal of Constructional Steel Research, 1988.

[9] K. d. Hjelmstad and E. P. Popov, "Seismic Behaviour of active beam links in eccentrically braced frames," Earthquake Engineering Research Center, Berkeley, USA, 1983.

[10] K. Kasai and E. P. Popov, "A study of seismically resistant eccentrically braced frames," Earthquake Engineering Research Center, Berkeley, 1983.

[11] ASCE, "ASCE committee on critical infrastructure," 2015.

[12] B. M. Ayyub, "Practical Resilience Metrics for Planning, Design, and Decision Making," *ASCE- ASME J.Risk Uncertainty Eng. Syst,* 2015.

[13] O. N. Attoh, A. R. Cooper and S. A. Mensah, "Formulation of resilience index of urban infrastructure using belief functions," *IEEE Systems Journal,* pp. 147-153, 2009.

[14] American Institute of Steel Construction, Specification for Structural Steel Buildings (ANIS/AISC 360-16), AISC, 2016.

[15] ASCE/SEI, Minimum Design Loads for Buildings and Other Structures (ASCE 7-10), SEI, 2010.

[16] FEMA, Seismic Performance Assessment of Buildings (FEMA P-58), FEMA, 2018.

[17] FEMA, Quantification of Building Seismic Performance Factors( FEMA P695), FEMA, 2009.

[18] AISC, Seismic Design Manual, AISC, 2018.

[19] A. Ghobarah, "Performance-based design in earthquake engineering: state of development," vol. 23, no. 2001, 2001.

[20] SEAOC VISION 2000, "Performance based seismic engineering of buildings, vols I and II: Conceptual framework," 1995.

[21] ATC 40, "Seismic evaluation and retrofit of exisiting concrete buildings," 1996.

[22] FEMA 273; FEMA 274, "NEHRP guidelines for the seismic rehabilitation of buildings; Commentary," 1996.

[23] M. J. N. Priestley, "Performance Based Seismic Design," 2000.

[24] R. O. Hamburger, "Implementing Performance based Seismic Sesign in Structural Engineering practice," 1996.

[25] J. Moehle and G. G. Deierlein, "A Framework Methodology for Performance-based earthquake engineering," 2004.

[26] R. O. Hamburger, "Development of Next- Generation Performance Based Seismic Design Guidelines," *Performance-Based Seismic Design Concepts and Implementation,* vol. PEER 2004/2005, 2004.

[27] AISC, *STEEL CONSTRUCTION MANUAL,* FIFTEENTH EDITION ed., 2017.

[28] USGS, "Design Maps," [Online]. Available: http://earthquake.usgs.gov/designmaps.

[29] BENTLEY SYSTEMS, *STAAD PRO CONNECT EDITION V22,* 2018.

[30] F. McKenna, G. L. Fenves and M. H. Scott, *Open System for Earthquake Engineering Simulation,* Berkeley: University of California, 2000.

[31] S. Mazzoni, M. H. Scott and G. L. Fenves, *OpenSees Command Language Manual,* 2006.

[32] G. J. O'Reilly and T. J. Sullivan, *Direct Displacement-Based Seismic Design of Eccentrically Braced Steel Frames,* 2016.

[33] N. Mansour, "Development of the design of eccentrically braced frames with replaceable shear links," 2010.

[34] T. Okazaki and M. D. Engelhardt, "Cyclic loading behavior of EBF links constructred of ASTM A992 Steel," pp. 751-765, 2007.

[35] ATC-63, "Quantification of Building Seismic Performance Factors," 2009.

[36] Chicago metal rolled products, "Exploring the Stress/ Strain Curve for Mild Steel," [Online]. Available: https://www.cmrp.com/blog/faq/analysis-design/exploring-stress-strain-curve-mild-steel.html.

[37] Z. yu, H.-S. Gu, H. Wang and P.-Y. Yi, "Crash simulation of the fuselage section with centra wing box for a regional jet," 2013.

[38] NIST, "UNIFORMAT II Elemental Classification for Building Specifications," Gaithersburg, Maryland, 1999.

[39] USGS, "Unified Hazard Tool," USGS.

[40] New Zealand Standard, NZS 1170.5:2004 Earthquake actions- New Zealand, Standards New Zealand, 2004.

[41] G. C. Clifton, G. Ferguson, M. Hodgson and C. K. Seal, "Performance of Eccentricall Braced Framed Buildings in the Christchurch Earthquake Series of 2010/2011," Researchgate, 2012.

[42] wikipedia, "Wikipedia," [Online]. Available: https://en.wikipedia.org/wiki/Pacific_Tower,_Christchurch.

[43] S. Gardiner, G. C. Clifton and G. A. MacRae, "Performance, damage assessment and repair of a multistorey eccentrically braced framed building following the Christchurch earthquake series," spiire, 2013.

[44] D. N. Manheim, On the design of eccentrically braced frames, Berkeley, California: University of California, 1982.

[45] ASCE/SEI, Seismic Rehabilitation of Exisiting Buildings, ASCE, 2006.

[46] PPD-21, "Critical infrastructure security and resilience," PPD (Presidential Policy Directive), 2013.